

https://dspace.org/

The effect of microwave heating on manganese promoted iron based Fischer-Tropsch catalysts

Mohiuddin, Ebrahim

2012-01-18
http://hdl.handle.net/10539/11077

Downloaded from a DSpace repository. https://dspace.org/

The effect of microwave heating on manganese promoted iron based Fischer-Tropsch catalysts

By

Ebrahim Mohiuddin

A dissertation submitted in fulfillment of the requirements for the degree of

Masters of Science in the Faculty of Science

School of Chemistry

University of the Witwatersrand

Private Bag X03

WITS

2050

Supervisors:

Prof. M. S. Scurrell and Prof. N. J. Coville

Declaration

I declare that "**The effect of microwave heating on manganese promoted iron based Fischer-Tropsch catalysts**" is my own, unaided work submitted for the degree of Masters of Science at the University of Witwatersrand, Johannesburg. It has not been submitted for any degree or examination in any other University, and all sources I have used or quoted have been indicated and acknowledged by means of complete references.

Name: Ebrahim Mohiuddin(Mr.) Date:25 July 2011

Signature:.....

Acknowledgements

I would like to thank the following people whom without this work would not have been a success.

To my supervisors, Prof. Mike Scurrell and Prof. Neil Coville for their assistance and advice throughout this project. A special thank you to Prof. Neil Coville for the proof reading of this dissertation and for being available when Mike was unable to.

Basil Chassoulas for teaching me the basics of FT and for all the help and advice in the lab, in setting up the rig and being available whenever something went wrong. None of this would have been possible without your help.

To the CATOMAT group for creating a welcoming environment and for your assistance over the last two years.

The NRF for finanancial support throughout this project.

Publications and presentations arising from this work

Publications

- The effect of microwave heating on manganese promoted iron based Fischer-Tropsch catalysts (to be published)

Poster presentations

- The effect of microwave heating on manganese and potassium promoted iron based Fischer-Tropsch catalysts, CATSA conference Bloemfontein (2010)

Oral Presentations

- Microwave treatment and incorporation manner of manganese on iron Fischer-Tropsch catalysts, FT Symposium, School of Chemistry and COMPS, university of the Witwatersrand (2010)

Abstract

A study was performed in order to investigate the effect of preparation method and the effect of microwave heating on a manganese promoted iron based Fischer-Tropsch catalyst. The effects of preparation method and microwave heating on the structure and morphology of the catalyst, its surface area and reduction behavior were investigated using various techniques such as Transmission electron microscopy (TEM), Powder x-ray diffraction (PXRD), surface area measurements (BET) and temperature programmed reduction (TPR). The FTS performance of the catalysts were also studied using a fixed bed reactor with Fischer-Tropsch Synthesis conditions (270 °C, flow rate of 30 ml/min, H_2/CO ratio = 2, pressure of 10 bar). Characterization of the catalysts calcined at 350 °C revealed that manganese enriched the surface of impregnated Mn/Fe catalysts and suppressed the reduction of the iron catalyst. However, the Mn acted as a structural promoter in the co-precipitated catalysts and also promoted the reduction of Fe_2O_3 as the manganese content increased. The co-precipitated catalyst calcined at 650 °C suppressed the reduction of iron. The impregnated catalysts showed similar conversion (~ 70%) for catalysts with Mn loadings 5%, 10% and 20%. This suggests Mn promotes the activity of the iron catalyst since less iron is present in the catalyst as the manganese loading is increased. The co-precipitated catalysts showed a 10 wt% Mn loading to be the optimum amount for increased activity and selectivity to $C_2 - C_4$ hydrocarbons, lower molecular weight olefins and a lower selectivity to heavier molecular weight hydrocarbons relative to Mn loadings of 5, 20 and 50 wt%. Mn loadings in excess of 10 wt% showed a slight increase in selectivity to heavier weight hydrocarbons. The impregnated catalysts showed very little difference in activity and selectivity but the co-precipitated catalyst showed a decrease in activity after the catalyst was microwave heated. A slight increase in selectivity to lower weight olefins and heavier molecular weight hydrocarbons was noted after microwave heating. The TPSR (Temperature programmed surface reaction) results revealed that this may be due to the stronger adsorption of CO on the surface of the catalyst after microwave heating. A similar trend was observed for catalysts promoted

with 0.1 wt% potassium i.e. a slight increase in selectivity to heavier weight hydrocarbons after microwave heating.

Table of contents

Contents

Acknowledgements……..1
Publications and presentations arising from this work……....2
Abstract……3
Table of contents..... 5
List of Figures……..8
List of Tables……12
Nomenclature……14
1. Introduction..... 15
1.1 Microwave theory 17
1.2 Mechanisms of microwave dielectric heating..... 18
1.2.1 Dielectric polarization..... 18
1.2.2 Conduction losses 20
1.2.3 Interfacial polarization 21
1.3 Microwave effects..... 21
1.4 Microwaves in heterogeneous catalysis..... 23
1.5 Fischer-Tropsch Synthesis 24
1.5.1 Fischer-Tropsch catalysts..... 25
1.5.2 Effect of promoters 27
1.5.3 Preparation of catalysts 29
1.6 Objectives of this study..... 30
1.7 Aims of Project 33
1.8 References..... 35
2. Experimental 38
2.1 Materials 38
2.2 Catalyst preparation 38
2.2.1 Preparation of impregnated catalysts 38
2.2.2 Preparation of co-precipitated catalysts 39
2.2.3 Microwave pre-treatment of catalysts..... 39
2.3 Catalyst characterization 40
2.3.1 Transmission electron microscopy (TEM) 40

2.3.2 Powder X-ray diffraction (PXRD) 40
2.3.3 Surface area measuements (BET) 41
2.3.4 Temperature programmed reduction (TPR) 41
2.3.5 Scanning electron microscopy (SEM) 41
2.3.6 Temperature programmed surface reaction (TPSR) 42
2.4 Fischer-Tropsch reactions 42
2.4.1 Reactor set-up 42
2.4.2 Experimental procedure 45
2.5 Product analysis 45
2.5.1 Online analysis 45
2.5.2 Offline analysis 49
2.6 Mass balance calculations 49
2.7 References 54
3. Results and Discussion 55
3.1 Study of unsupported iron catalyst 55
3.1.1 Transmission electron microscopy 55
3.1.2 Powder X-ray diffraction 56
3.1.3 Surface area measurements (BET) 57
3.1.4 Temperature programmed reduction 58
3.2 Addition of Mn promoter - Incipient wetness impregnation method (IWIM) 60
3.2.1 Transmission electron microscopy 60
3.2.2 Surface area measurements (BET) 61
3.2.3 Powder X-ray diffraction 62
3.2.4 Temperature programmed reduction (TPR) 65
3.3 FT Performance of impregnated catalysts 68
3.3.1 Effect of Mn loading on the activity of impregnated catalysts 68
3.3.2 FT selectivity of the impregnated catalysts 69
3.3.3 Methane selectivity 71
3.3.4 Olefin formation 71
3.4 Addition of Mn promoter - Co-precipitation (co-ppt) method 73
3.4.1 Transmission electron microscopy 73
3.4.2 Surface area measurements (BET) 75
3.4.3 Powder X-ray diffraction 76
3.4.4 Temperature programmed reduction 77

3.5 FT Performance of co-precipitated catalysts 79
3.5.1 Effect of Mn loading on the activity of co-precipitated catalysts 79
3.5.2 Selectivity of co-precipitated catalysts: effect of Mn loading 80
3.5.3 Methane selectivity 82
3.5.4 Olefin formation 82
3.6 Effect of preparation method: Comparison of impregnated and co-precipitated catalysts 84
3.7 Characterization of microwave heated catalysts 87
3.7.1 Characterization of microwave heated impregnated catalysts 87
3.7.2 FT performance of the microwave heated impregnated catalysts 91
3.7.3 Characterization of microwave heated co-precipitated catalysts 96
3.7.4 FT performance of microwave heated co-precipitated catalysts 101
3.8 Effect of microwave heating on manganese and potassium promoted iron catalysts 106
3.8.1 Characterization of catalysts 106
3.8.2 FT performance of potassium promoted catalysts 112
3.9 References 117
4. Conclusions 119

List of Figures

Chapter 1

Figure 1.1: Region of the electromagnetic spectrum showing microwave frequencies used in microwave heating..... 16

Figure 1.2: Comparison of the temperature gradient that exists within a sample for the two heating methods, a) conventional heating and b) microwave heating. 17

Figure 1.3a: Oscillating electric field for ideal dielectric (top) with induced displacement current 90° out of phase with electric field (bottom). 20

Figure 1.3b: Graph showing component of displacement current in phase with oscillating electric field. 20

Chapter 2

Figure 2.1: Schematic representation of the rig used for FTS. 44

Figure 2.2: A trace of the calibration gas using the FID-GC 46

Figure 2.3: A trace of the calibration gas using a TCD-GC to indicate peak positions... 47

Figure 2.4: A trace showing calibration with syngas using a TCD-GC 47

Figure 2.5: A typical trace of the products detected using a TCD-GC during a reaction 48

Figure 2.6: A trace showing hydrocarbon products $C_1 – C_7$ detected using a FID-GC... 48

Chapter 3

Figure 3.1: TEM images (a) and (b) showing morphology of iron particles and particle size distribution. 55

Figure 3.2: Bar graph showing the wide particle size distribution of the iron ctalyst. 56

Figure 3.3: Powder pattern showing presence of haematite phase in iron catalyst. 56

Figure 3.4: Graph showing pore size distribution 58

Figure 3.5: TPR profile of pure haematite catalyst. 59

Figure 3.6: TEM images showing Mn/Fe catalysts prepared using IWIM a) 5 wt% Mn, b) 10 wt% Mn, c) 20 wt% Mn and d) 50 wt% Mn on Fe_2O_3 after calcination at 350 °C for 6.5 hours..... 60

Figure 3.7: Powder pattern showing a mixture of manganese oxide phases. 62
Figure 3.8: Powder patterns showing effect of manganese loading on Fe_2O_3. Note that the powder pattern of the 5% Mn catalyst has been background subtracted and smoothed. Blue lines represent the reference pattern of haematite and the pink and orange linesthe reference patterns of Mn_2O_3 and MnO_2 respectively..... 63
Figure 3.9: Powder patterns of the Mn/Fe_2O_3 (10% and 20% Mn) after being calcined at 650 °C. The red lines represent the reference pattern of haematite. 64
Figure 3.10: TPR profiles comparing pure Fe_2O_3, MnO_2/Mn_2O_3 and a 5% manganese promoted iron catalyst..... 66
Figure 3.11: TPR profiles of 10% (blue), 20% (black) and 50% (red) Mn/Fe_2O_3..... 67
Figure 3.12: Activity of catalysts with varying loadings of manganese. 68
Figure 3.13: Effect of manganese content on methane formation for impregnated catalysts. 71
Figure 3.14: Effect of manganese content on olefin selectivity of impregnated catalysts. 72
Figure 3.15: TEM images showing particle size and morphology of a) 5% Mn, b) 10% Mn, c) 20% Mn, d) 50% Mn and e) 50% Mn calcined at 650 °C..... 74
Figure 3.16: Powder patterns showing appearance of a Fe-Mn mixed oxide phase with increased loading of Mn (calcinations temperature = 350 °C; except for 50% Mn loaded sample calcined at 650 °C). The red lines represent the pure haematite pattern and the green lines a FeMn mixed oxide. These were obtained from the EVA software package database. 76
Figure 3.17: TPR profiles of the co-precipitated catalysts with Mn loadings of 5% to 50%. 78
Figure 3.18: Activity of catalysts with varying loadings of manganese. 80
Figure 3.19: Effect of manganese content on methane formation for co-precipitated catalysts. 82
Figure 3.20: Effect of manganese content on olefin selectivity of co-precipitated catalysts. 83
Figure 3.21: Activities of the catalysts prepared via the co-precipitation and impregnation methods with 5% and 10% Mn loading..... 85

Figure 3.22: TEM images comparing the 5 wt% Mn impregnated catalysts a) before microwave heating, b) after microwave heating at 450 W for 10 s. 88
Figure 3.23: Powder patterns of the impregnated catalysts (a) before and (b) after microwave heating. Note that these patterns were background subtracted and smoothed to remove noise due to the fluorescence of the iron. This was done using the EVA software package. 89
Figure 3.24: Profile of 5% Mn/Fe_2O_3 impregnated catalyst before and after microwave heating. 90
Figure 3.25: Activity of 5 wt% Mn impregnated catalysts before and after microwave heating. 91
Figure 3.26: Effect of microwave heating on methane selectivity for impregnated catalysts with 5 wt% Mn loading. 94
Figure 3.27: Effect of microwave heating on olefin formation for impregnated catalysts with 5 wt% Mn loading on Fe_2O_3. 95
Figure 3.28: a) 10% FeMn coppt before microwave heating and b) 10% FeMn coppt microwave heated at 900 W for 30s. 97
Figure 3.29: Powder patterns of the co-precipitated catalysts (a) before and (b) after microwave heating. 98
Figure 3.30: Profile of co-precipitated catalyst before and after microwave heating. 99
Figure 3.31: TPSR profiles of the 10% FeMn co-precipitated catalyst before and after microwave heating. 100
Figure 3.32: Activity of 10 wt% Mn co-precipitated catalysts before and after microwave heating at 900 W for 30 s. 101
Figure 3.33: Effect of microwave heating on methane selectivity for co-precipitated catalysts with 10 wt% Mn loading. 104
Figure 3.34: Effect of microwave heating on olefin formation in the $C_2 - C_5$ range for co-precipitated catalysts with 10 wt% Mn loading. 105
Figure 3.35: Effect of microwave heating on olefin formation in the $C_6 - C_{11}$ range for co-precipitated catalysts with 10 wt% Mn loading. 105
Figure 3.36: TEM images of iron particles in a) before microwave heating and b) after microwave heating. 106

Figure 3.37: SEM image showing morphology of iron particles at 240 000× magnification. 107
Figure 3.38: Graph showing particle size distribution of Fe-Mn catalyst promoted with potassium. 108
Figure 3.39: Comparison of potassium promoted Fe-Mn catalysts before and after microwave heating. 109
Figure 3.40: TPR profiles of potassium promoted Fe-Mn catalyst before and after microwave heating. 110
Figure 3.41: Activity of catalysts before and after microwave heating. 113
Figure 3.42: Comparison of methane selectivity before and after microwave heating. 115
Figure 3.43: Effect of microwave heating on olefin selectivity. 116

List of Tables

Chapter 3

Table 3.1: Table showing the average surface area, pore size and pore volume 57

Table 3.2: Surface areas and pore volumes for catalysts with different loadings of Mn. 61

Table 3.3: Crystallite sizes of peaks after 20% Mn/Fe_2O_3 catalyst was calcined at 350 °C and 650 °C..... 64

Table 3.4: Results showing temperatures at which reduction occurs for catalysts shown in figure 3.10. 66

Table 3.5: Results showing temperature at which reduction occurs for catalysts shown in figure 3.11. 67

Table 3.6: FTS performance of impregnated catalysts (IWIM) at iso-conversion of 67% 70

Table 3.7: Surface areas of co-precipitated FeMn catalysts..... 75

Table 3.8: data showing temperatures at which reduction occurs for the TPR profiles shown in figure 3.17 78

Table 3.9: FTS performance of co-precipitated catalysts (CO-PPT) at iso-conversion of 73.6% 81

Table 3.10: Data showing BET measurements before and after microwave heating 88

Table 3.11: Crystallite sizes of the catalyst before and after microwave heating. 89

Table 3.12: Comparison of FTS performance between microwaved and non-microwaved catalysts at iso-conversion. 93

Table 3.13: Surface area measurements before and after microwave heating. 97

Table 3.14: Crystallite sizes of certain peaks of catalysts before and after microwave heating. 98

Table 3.15: Comparison of FTS performance between microwave heated and non-microwave heated catalysts at iso-conversion. 103

Table 3.16: Surface area measurements of Fe-Mn and Fe-Mn-K catalysts 108

Table 3.17: Crystallite sizes obtained using the Scherrer equation for the given peak positions. 110

Table 3.18: Results showing the temperatures at which reduction occurs..... 111

Table 3.19: Comparison of FTS performance between microwave heated and non-microwave heated Fe-Mn-K catalysts at iso-conversion. 114

Nomenclature

Abbreviation	Description
AFROX	African Oxygen
BASF	Badishe Anilin und Soda Fabrik
BET	Brunauer-Emmett-Teller
CO conv.	Carbon monoxide Conversion
FID	Flame Ionization Detector
FT	Fischer Tropsch
FTS	Fischer-Tropsch Synthesis
GC	Gas Chromatograph
HC dist.	Hydrocarbon distribution
IWIM	Incipient wetness impregnation method
LTFT	Low temperature Fischer Tropsch
OPEC	Organisation of the Petroleum Exporting Countri
PXRD	Powder x-ray diffraction
Syngas	Synthesis gas
TCD	Thermal conductivity detector
TEM	Transmission electron microscopy
TPR	Temperature programmed reduction
TPSR	Temperature programmed surface reaction
UHP	Ultra high purity
WGS	Water gas shift
XPS	X-ray photoelectron spectroscopy

1. Introduction

Today one of the most common methods used to cook food, both domestically and industrially, is by use of microwave ovens.[1] Microwaves were first used during the Second World War for radar detection. The core component of the microwave oven, the magnetron, was built by Randall and co-workers at the University of Birmingham for radar applications. It was accidentally found that the radiation emitted by the magnetron was able to heat water.[1] Soon thereafter, microwave radiation was developed as a heating source and in the 1950's the first microwave ovens became commercially available. In the 1970's and 80's the domestic use of microwave ovens became widespread due to its popularity for the rapid heating of foods and it was during this time that researchers in fields such as chemistry began to show a great deal of interest in microwave radiation as a source of heating and activation of chemical reactions.[1] The first application of microwave chemistry was in organic chemistry, when gas-phase discharge was applied in order to decompose simple organic compounds.[2] Although microwave chemistry was predominantly used in organic synthesis, over the decades microwaves have been widely used in various other fields of chemistry, such as polymer chemistry, analytical chemistry, inorganic synthesis and heterogeneous catalysis.[2]

Microwaves are electromagnetic waves. Microwaves make up that part of the electromagnetic spectrum which lies between the infra-red region and the radiowave region as shown in Figure 1.1. Microwaves typically have wavelengths of 1 cm to 1 m i.e. frequencies of 30 GHz to 300 MHz respectively. Microwave ovens that are used domestically and industrially operate at frequencies of either 915 MHz (32.8 cm wavelength) or 2.45 GHz (12.2 cm wavelength) with most domestic microwave appliances operating at 2.45 GHz. This is to avoid any interference with radar or telecommunication services which make use of the remaining frequencies.[4] One should not mistake microwave dielectric heating with microwave spectroscopy as they are different. In microwave spectroscopy reactions take place in the gas phase. Molecules show sharp peaks in the microwave spectrum. This is caused by excitation of molecules

and transitions between discrete rotational energy levels take place. Due to the sharp bands that occur for small molecules, microwave spectroscopy can be used as a fingerprinting technique to identify molecules and many molecules in outer space have been identified using microwave spectroscopy.[2, 5] In dielectric heating, however, molecules are not excited to higher energy levels. This is because dielectric heating occurs when molecules are present in the liquid and solid phases which have peaks that are too broad to be observed in microwave spectroscopy and dielectric loss heating effects occur instead of microwave spectroscopy effects. This is because molecules in these phases are not able to rotate separately. Therefore the two should not be confused as microwave spectroscopy effects stem from discrete energy states whereas dielectric heating effects are more of a bulk phenomenon.

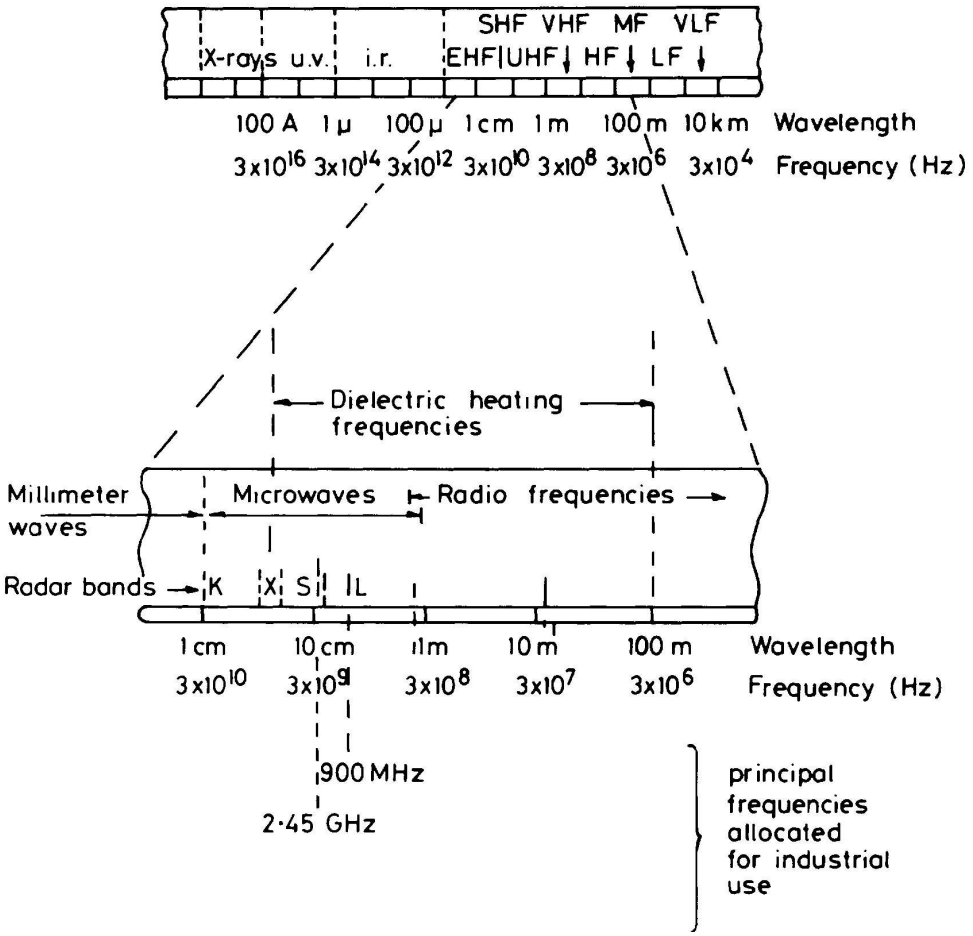


Figure 1.1: Region of the electromagnetic spectrum showing microwave frequencies used in microwave heating.[5]

1.1 Microwave theory

Microwave heating is significantly different from conventional heating. Using a microwave a sample material is irradiated with electromagnetic waves and this energy is converted directly to heat within the sample. In conventional heating the sample is heated via thermal conduction. Generally in thermal heating a temperature gradient exists where the temperature at the surface is greater than that at the centre of the material because heat must travel from the surface to the interior. For microwave heating, in an ideal situation the temperature of the material is uniform throughout but in reality a temperature gradient also exists. In this case the interior is hotter than the surface thus leading to increased heating rates and contrasting conventional heating.[4] A comparison of the two heating methods is shown in Figure 1.2.

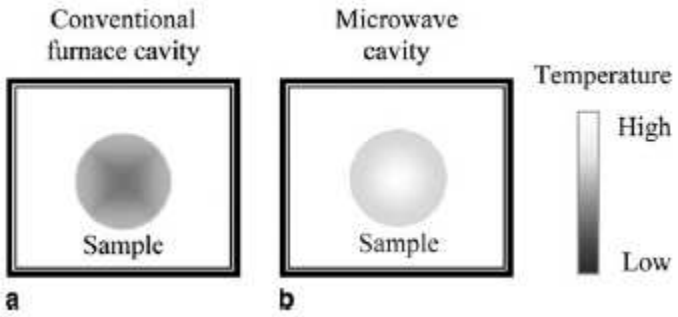


Figure 1.2: Comparison of the temperature gradient that exists within a sample for the two heating methods, a) conventional heating and b) microwave heating.[4]

"A dielectric is one which contains either permanent or induced dipoles which when placed between two electrodes acts as a capacitor."[6] In microwave heating, the heating effect arises when the material being irradiated with electromagnetic energy in an electric field causes a force to be exerted on charged particles. If particles are free to move a current is established but if they are restricted to certain areas they move until they are balanced by an opposing force. This results in dielectric polarization.[5] The average power dissipated in a dielectric is dependent on the volume of the dielectric and the materials dielectric property and therefore microwave heating is said to be volumetric in nature.[4]
The microwave absorption power generated, P_{abs}, is defined by

$$P_{abs} = 2\pi f \varepsilon_0 \varepsilon''_{eff} E^2_{rms} V \quad (1)$$

Equation 1 shows the relationship between the microwave absorption power and the electromagnetic field for a dielectric with a particular volume. Here ε_0 is the permittivity of free space i.e. the permittivity of a material which describes the ability of the material to store charge relative to free space, ε''_{eff} is a component of ε_0 or the relative dielectric loss factor, f is the frequency of radiation and E_{rms} the root mean square of the electric field. In solids the microwaves only penetrate a certain depth below the surface. At this penetration depth the power is half that at the surface and D_p, the penetration depth is given by the following equation:

$$D_p = \lambda_0/2\pi . \sqrt{\varepsilon'}/\varepsilon'' \quad (2)$$

where, λ_0 is the wavelength of the microwave radiation, ε' the dielectric constant and ε'' the dielectric loss factor. These two dielectric parameters describe the properties of a dielectric material and are explained in the following section.

1.2 Mechanisms of microwave dielectric heating

Three types of microwave heating methods exist i.e. dielectric polarization, conduction losses and interfacial polarization. The first two are the primary methods of heating while the third is of less importance.

1.2.1 Dielectric polarization

Dielectric polarization results from an electric field causing polarization of charges in a material and the inability of the polarization to follow rapid oscillations of the electric field. The total polarization α_t is made up of four different components namely α_e – electronic polarization which is the polarization of electrons around nuclei, α_a – atomic polarization i.e. displacement of nuclei due to irregular distribution of charge within the molecule, α_d – dipolar polarization caused by permanent dipoles being re-orientated by an electric field and α_i – interfacial polarization or the build up of charge at the interfaces.[5] The atomic and electronic polarizations do not contribute to dielectric heating because the response time for the polarization and depolarization of α_a and α_e is much faster than microwave frequencies i.e. they respond to the rapid reversals of an electric field which

are caused by electromagnetic radiation that have a frequency similar to its timescale for polarization and depolarization. However the time taken for permanent dipoles to be polarized is comparable to microwave frequencies. This indicates that the orientations and polarizations are frequency dependent.[5] It is generally noted that for a polar liquid the ability for it to be polarized decreases as the frequency increases from 10^6 (radio frequencies to 10^{12} (infra-red frequencies).The re-orientation of the dipoles and displacement of charge is like an electric current. This is known as the Maxwell displacement current.[6] When the electric field oscillates at a low frequency the molecules rotate and match the pace of the electric field. The displacement current that occurs is $\pi/2$ out of phase with the electric field as shown in Figure 1.3a. Therefore there is no lag between the two and no heating occurs. At higher frequencies the electric field oscillates much faster than the response time of the molecules and molecules cannot vibrate before the electric field is reversed, therefore no heating occurs. At the microwave frequency the molecules are able to vibrate but lag behind the electric field reversals. Therefore there is a shift in the displacement current by δ degrees and a component of the displacement current, $I \times \sin\delta$ (as shown in Figure 1.3b) that is in phase with the electric field is obtained. This is known as dielectric loss which is responsible for the heating that occurs due to the energy that is transferred from the electric field to the sample.[6]

The dielectric loss factor ε'' and the dielectric constant ε' are fundamental parameters used to understand the dielectric heating ability of materials. The dielectric loss factor is a measure of the efficiency with which electromagnetic radiation is converted into heat and the dielectric constant measures the ability of a material to be polarized by an electric field. These parameters are frequency dependent and show that the dielectric constant reaches a maximum at low frequencies as maximum energy can be stored. As the frequency increases ε' drops while simultaneously ε'' rises.[5] The ratio of the dielectric constant and loss factor which is given by $\tan\delta = \varepsilon''/\varepsilon'$, known as the loss tangent, is used as a measure of the ability of a material to convert electromagnetic radiation into heat energy at a given frequency and temperature. Therefore for materials with similar dielectric constants the loss tangent can be used to determine which materials are more likely to be heated by microwave radiation.

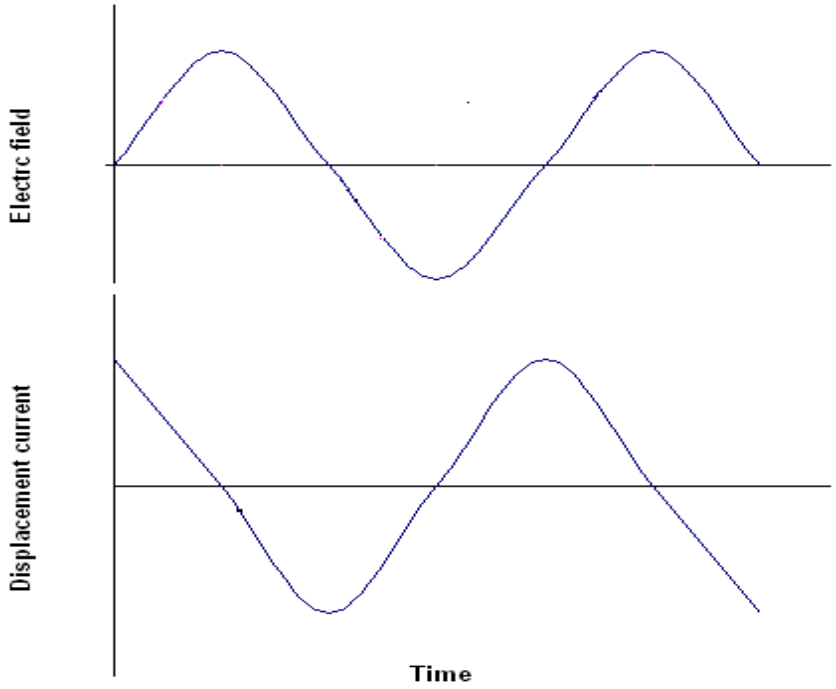


Figure 1.3a: Oscillating electric field for ideal dielectric (top) with induced displacement current $\pi/2$ out of phase with electric field (bottom).[6]

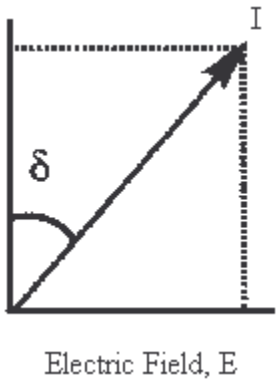


Figure 1.3b: Graph showing component of displacement current in phase with oscillating electric field.[6]

1.2.2 Conduction losses

When a conducting material is irradiated with microwave radiation, the electric field causes charge carriers such as electrons and ions to move through the sample and results

in polarization. The heating that takes place is due to the induced currents facing some electrical resistance. For highly conducting materials such as metals most of the microwave energy is not absorbed but reflected, although some of the large surface voltages may be induced. This results in arcing which is observed when metals are placed in a microwave.[7] Liquids that contain ions experience much greater heating rates than pure liquids due to both dipolar polarization and conduction mechanisms.

Conduction losses also occur as a function of temperature. At room temperature conduction losses are only significant at low frequencies but as the temperature increases conduction losses increase and may become equivalent to dipolar relaxation at microwave frequencies.[5]

1.2.3 Interfacial polarization

Interfacial polarization is seen as a combination of the dipolar polarization and conduction properties. It is caused by the build up of charges at the interfaces. It usually occurs when a conducting medium is placed in a non–conducting medium, for example when a good microwave absorber such as a metal is placed in a poor microwave absorber like sulphur.[7] For powdered metals where the surface layer is much larger than for a bulk metal the microwaves may be absorbed and the induced currents cause heating. However, the polarization of a conducting material (metal) may be retarded by the surrounding non–conducting material and the polarization of the metal particles then lags behind the oscillating electric field similar to that in the dipolar polarization mechanism. Thus the frequency dependency of the heating properties of the sample is similar to dipolar polarization although it happens through a conduction mechanism.[7]

1.3 Microwave effects

Many chemical reactions have been carried out under microwave heating instead of conventional heating since the method provides a faster heating rate, shorter residence times, greater selectivity and better yields. These attributes are said to be due to the

"microwave effect".[1] The microwave effect may be divided into two types: thermal and non – thermal effects. Thermal effects are those which are caused by dielectric heating i.e. the heat generated. The thermal gradient which may exist inside a sample is the cause of the attributes mentioned above. Non thermal effects are due to the microwaves themselves i.e. the frequency and power of the electromagnetic radiation and not the dielectric heating that takes place. Thermal and non thermal effects can be distinguished by comparing microwave heating to classical heating. If the same effects occur for classical and microwave heating, the effect is a thermal one. Non thermal effects rarely occur in conventional heating. They have been shown to exist for example by Klimov[8] and co-workers in their investigation of ethylene epoxidation on Ag/Al_2O_3 catalysts and by Roussy *et al.*[9] for the isomerization of 2-methylpentane on Pt/Al_2O_3 catalysts. Non thermal effects may lead to changes in selectivity but rate enhancements are strictly caused by thermal effects as conclusively shown by Stuerga *et al.*[10]. Previously it was believed that microwave radiation interacted directly with the reactants and caused the effect.[4]

Thermal effects that have been observed when reactions are carried out by dielectric heating are rapid heating effects, the formation of hot spots and pressure cooker effects.[4] It has been suggested by some researchers that rapid heating may lead to better yields in polymer curing. In the case of solids a thermal effect is observed, which is the formation of hot spots. Hot spots are regions which have a higher temperature than the surroundings because of a greater interaction with microwave radiation. These effects may lead to increased heating rates and shorter reaction times. In the case of heterogeneous catalysis these hot spots may be very small i.e. in the nanometer range for materials that contain small metal particles and the temperatures of these areas is difficult to measure and cannot be done directly.[4] For example, organic reaction performed by Gedye *et al.*[11] was heated at high pressures and temperatures. During microwave heating, rate enhancements were observed. When the reactions were carried out in sealed tubes under classical heating, similar results were obtained. This indicates that the thermal effect that occurred is due to the build up of pressure in the sealed tube and this phenomenon is responsible for the effects seen during microwave heating.[4]

1.4 Microwaves in heterogeneous catalysis

Microwave chemistry has been extensively used in organic chemistry for the synthesis of organic compounds where short reaction times and can give high yields of product. Two types of reactions exist; these are the solid state and non-solid state reactions. In the case of heterogeneous catalysis to which microwave radiation technology has been applied it is the former reaction that is of importance.[3] In solid state reactions a highly microwave active reagent i.e. one which is polar, may be supported on a poor microwave absorber such as alumina or silica. Alternatively a strongly microwave active support can be used in which the reactants do not need to be microwave active.[12] By coupling a material that strongly absorbs microwaves to one which is microwave transparent it is possible to drive a localized solid state chemical reaction.[5] This method can be used for the preparation of catalysts for heterogeneous systems such as Fischer-Tropsch Synthesis.

Domestic ovens are usually used in academic and industrial research laboratories due to their low cost and availability. However, these ovens have to be modified before they can replace conventional furnaces. Other components of heterogeneous catalytic systems such as reactors also have to be modified for use in microwave reactions. For example, reactors made out of steel have to be made out of quartz so that the solid catalyst absorbs most of the microwave power while the quartz reactor and reactant gas are microwave inactive.[4] Microwave ovens can be modified so that reactors fit into the microwave cavity. Methods for temperature measurements must also be adapted because ordinary thermocouples cannot be used in the microwave field without shielding and therefore fibre optic sensors are used.[1]

A lot of work has been performed on different heterogeneous catalytic reactions by Zhang *et al.*, these reactions include carbon dioxide reforming of methane,[13] reduction of sulphur dioxide with methane,[14] the decomposition of hydrogen sulphide[15] and the oxidative coupling of methane[16]. However, to our knowledge there have been very few studies on the use of microwave heating in Fischer-Tropsch Synthesis. Microwave effects are elucidated by comparing the catalytic reactions operating under both microwave

heating and conventional heating. What researchers have found is that although temperature measurements are difficult, most of the microwave effects are thermal effects. However, it has also been noted that because the two heating methods are significantly different, a comparison cannot only be made on the basis of temperature.[1] Other parameters such as conversion, selectivity, catalyst and distribution of microwave active materials are also important.

1.5 Fischer-Tropsch Synthesis

Fischer-Tropsch Synthesis (FTS) is the conversion of synthesis gas (syngas) which is a mixture of CO and H_2 into hydrocarbons via the use of a heterogeneous transition metal catalyst. The FTS reaction occurs when the adsorbed CO is hydrogenated to form CH_2 monomers which polymerize on the metal surface to form linear hydrocarbons. This mechanism of the FTS reaction was proposed by Franz Fischer and Hans Tropsch in 1926.[20] Fischer-Tropsch synthesis is an environmentally friendly way of producing liquid fuels and high value chemicals from coal and natural gas.[21,22]

Fischer-Tropsch Synthesis can be said to have begun in the early 1900's when Sabatier and Senderens discovered that the hydrogenation of CO to give methane occurred when using Co, Ni and Fe catalysts.[23] In 1913 Badishe Anilin und Soda Fabrik (BASF) reported the production of liquid hydrocarbons.[24] The catalyst used was a cobalt catalyst. Fisher and Tropsch in 1923 reported the production of hydrocarbons using an alkalised iron catalyst.[25] Major catalyst developments began in Germany after the Second World War by Ruhrchemie and Lurgi and in the United States by Kellog Co. This led to the opening of the Sasol plant in South Africa in 1955. Due to the realization of shortages in petroleum and the oil embargo in 1973 by OPEC which led to increases in the price of oil, there was a renewed interest in research of FT process after 1973.[26] Now Sasol runs a series of plants and is the largest scale implementer of F-T technology. Other large-scale operations that have been recently commissioned are the Shell Middle Distillate Synthesis in Bintulu, Malaysia and the Low Temperature Fischer-Tropsch (LTFT)

facility in Ras Laffan, Qatar. The Shell plant converts natural gas into low sulphur diesel fuels and produces 12000 barrels/day. Qatar is based on Sasol technology and uses a cobalt catalyst at 220°C producing petroleum from natural gas at an average of 140000 barrels/day.[27]With the discovery of large coal reserves and the fact that petroleum reserves are rapidly diminishing FTS is expected to play a major role in the future.

1.5.1 Fischer-Tropsch catalysts

The most commonly used metal catalysts for CO hydrogenation or FTS are nickel, iron, cobalt and ruthenium. Generally Ni catalysts are very active but lead to a large production of methane relative to other hydrocarbon products. They are also more selective to methane than the Fe, Co and Ru catalysts. The activity for the different metal catalysts is shown to have the following order[28]:

Ru > Fe > Ni > Co > Rh > Pd > Pt > Ir

Of these only Ru, Ni, Fe and Co have the appropriate activity for commercial FT application. The Ni catalysts are mainly used when the principal product required is methane. Supported Ru catalysts are good catalysts for study since they neither oxidise nor carburize during FT synthesis. However, Ru catalysts are too expensive to be used for commercial applications. Fe and Co catalysts have been widely used in many industrial applications throughout the years due to the low cost and availability of Co. Co catalysts show greater stability than Fe catalysts and can be used at lower temperatures and pressures.[29] Fe and Co catalysts are the only feasible catalysts for commercial FT application.

Iron catalysts

Iron catalysts have been developed for industrial applications. For example, Sasol uses an alkalised iron based catalyst in a commercial slurry reactor. Thus Fe is considered to be a most important FT catalyst.[26] Fe is obtained at a relatively low cost and therefore it is

more feasible to use Fe than Co or Ru catalysts. Fe has a high FTS activity as well as a high Water Gas Shift (WGS) activity as compared to Co catalysts which are more active than Fe for FTS, but have a low WGS activity. Thus Fe catalysts are useful for the conversion of syngas with a H_2 deficit since the WGS reactivity makes up for this. Iron catalysts tend to produce more olefins and have a lower selectivity to methane than Co catalysts over a wide range of temperatures and H_2/CO ratios.[30] The activity and selectivity of Fe can be increased by the addition of promoters which are mainly alkali metals. Potassium has been shown to increase selectivity to olefins and reduce methane production.[31] It has also been shown to increase FTS and WGS activity.[22] Copper promoters lead to reduction of Fe oxides to metallic Fe at lower temperatures. Metal oxides such as Al_2O_3, TiO_2 and SiO_2 as well as manganese can be added as structural promoters to increase stability and dispersion of Fe catalysts. Mn can also lead to the production of more olefins. Fe catalysts are activated by reduction with H_2 or CO gas. Fe catalysts can lose activity due to sintering as well a chemical poisoning for example by sulphur.[26]

Cobalt catalysts

Co based catalysts were the first to be used in industrial FT applications. With the development of superior Fe based catalysts and the high cost of Co, interest in Co as the most important FT catalyst did decline. However, it is known that Co based catalysts are more active than Fe based catalysts and also have a longer catalyst life.[32] Co catalysts are used mainly at low temperatures because selectivity to C5+ hydrocarbons and the quality of diesel range products are poor at high temperatures. It also leads to a large production of methane at high temperatures. At low temperatures Co catalysts have the highest turnover number of FT catalysts. It has also been shown that the metal surface area is directly related to the activity despite the presence of a structural promoter. Cobalt catalysts produce more linear hydrocarbons and have very low selectivity towards alcohols with water being the most predominate oxygenate. Co catalysts have a very low WGS activity compared to iron catalysts but similarly to Fe, Co is also poisoned by sulphur.

1.5.2 Effect of promoters

Addition of promoters plays an important role in catalyst preparation, especially for iron catalysts. Alkali metals are mostly used as promoters for iron catalysts. Promoters cause an increase in the selectivity and activity of the iron catalyst.[33,34] Li *et al.*[34] reported that iron-based catalysts used for the Fischer-Tropsch synthesis often prepared from iron nitrate incorporate promoters such as calcium, manganese, zinc, potassium and copper. Some of the promoters are described below.

Copper promoter

Addition of copper as a promoter into the catalyst improves the reduction of the metal oxide to the active metal in H_2. It decreases the reduction temperature and the reduction time. Bukur *et al.*[35] reported that small amounts of copper promote the formation of hydrocarbons in the Fischer-Tropsch synthesis due to hydrogenation of olefins and isomerization in secondary reactions. Studies have also shown that a doubly copper promoted iron catalyst proved to be more active than a singly promoted catalyst.[33]

Potassium promoter

The effect of potassium as a promoter has been greatly studied. Studies reveal that potassium influences the adsorption of CO and H_2. This is due to the fact that potassium has a strong basicity. This leads to the enhancement in olefin selectivity and suppresses the formation of methane.[36,37] A study on the effect of potassium on the surface properties of supported iron and precipitated Fe-Cu-SiO_2 catalysts showed that the addition of potassium to a precipitated iron catalyst elevated CO chemisorptions.[31] They described this as Fe having a tendency of withdrawing electrons from potassium which results in strengthening of the Fe-CO bond and weakening the Fe-H bond, since hydrogen can donate electrons to iron. However, the mechanism of potassium as a promoter is uncertain and there is still much room for debate. The CO chemisorption enhancement resulted in the improvement of selectivity towards olefins, an increase in

Water-Gas Shift activity and enhanced the Fischer-Tropsch synthesis activity.[38,39] However excessive potassium can facilitate carbon deposition and induce catalytic deactivation.[40] The effect of potassium on Fe-Mn catalysts has been studied as well. A study done by Jiang *et al.*[41] reported that potassium species interact with the surface of iron species and promote iron oxide reduction to form fine metallic iron clusters. On the contrary, other researchers have reported that potassium suppresses reduction of the iron catalyst. Addition of potassium results in a decrease in surface area of fused magnetite catalyst. Furthermore, the carbonization of iron during the Fischer-Tropsch synthesis occurs more rapidly when the catalyst is promoted with potassium.[36]

Manganese promoter

Studies done by Li *et al.*[34], have shown that the addition of manganese as a promoter increases the selectivity and activity of Fe-based catalysts and produces lower olefins. Similar studies have been done by others. Manganese can be a chemical or a structural promoter, the former resulting to changes in chemisorption behaviour of the catalyst, and the latter improving the dispersion of active iron and stabilizing the catalyst in FT synthesis.[40] When manganese acts as a chemical promoter, it is an electron donating promoter. Thus it promotes dissociative adsorption of CO, hence increasing olefin selectivity. Studies done by Jaggi *et al.*[42] have shown that using the co-precipitation method a single phase solid solution of Mn in hematite, α- $(Fe_{1-x}Mnx)_2O_3$ was formed after the catalyst was calcined at 773 K. Mn can migrate to the catalyst surface during the process of calcination and reduction. Furthermore, an increase in Mn content suppresses the crystal growth of hematite and the catalyst reduction from FeO to Fe in H_2.[34] However, it is to be noted that appropriate amounts of Mn are required to improve FTS activity. If excess Mn has been added, it results in the hindrance of catalyst carburization in CO and syngas due to the high Mn enrichment on the surface of the catalysts. It also results to the shift of selectivity to heavy hydrocarbons.[43,44] Manganese has been incorporated with the iron catalyst using two methods: the incipient wetness impregnation method and the co-precipitation method. These preparation methods play a role in the physicochemical properties of the catalyst.

1.5.3 Preparation of catalysts

The co-precipitation method

The co-precipitation method involves addition of manganese nitrate into an iron solution i.e. iron nitrate before precipitation. During the co-precipitation method, a solid solution of manganese in hematite (α-Fe_2O_3) is formed. This method enhances the interaction between the manganese ions and the iron ions which improves the dispersion of iron and suppresses the agglomeration of iron oxides. Manganese migrates from the surface and enters the crystal lattice of the iron during calcination and reduction processes. The presence of manganese reduces the crystallite size of the iron and it reduces the iron oxide carburization.[37,45] Incorporation of manganese has an effect on the textural properties, reduction, and on the bulk phase and surface composition of the catalyst as prepared, after reduction and after reaction.[37,45]

The incipient wetness impregnation method

This method involves firstly the precipitation of an iron solution (iron nitrate) with the appropriate base to form the support. After drying and calcination a manganese solution is added to the iron precipitate via incipient wetness. In this method the manganese promoter is mainly concentrated on surface of the catalyst.[45] A concentration of manganese on the surface of the catalyst inhibits H_2 chemisorption significantly.[45] This is due to the fact that this method yields a large iron oxide crystallite size compared to the co-precipitation method. An increase in the crystallite size suppresses the catalyst reduction.[45] The incipient wetness impregnation method is reported to inhibit carburization of the iron catalyst in CO is due to enrichment of manganese on the iron catalyst surface, thus reducing the iron concentration on the surface.[19] Furthermore, the surface basicity of the manganese impregnated catalyst is much stronger than that of the co-precipitated catalyst.[37] This can also be attributed to higher enrichment of manganese on the surface catalyst.

1.6 Objectives of this study

In heterogeneous catalysis, researchers strive to increase the activity of catalysts, enhance the selectivity of products and conserve energy by attempting to perform reactions at lower temperatures. Since the 1980's the application of microwave heating has been investigated precisely for this purpose.[16] Studies carried out by Bond *et al.*[17] on the oxidative coupling of methane show that microwave heating results in the formation of C_2 hydrocarbons at lower temperatures with greater selectivity as compared to the reaction being carried out under conventional heating. Roussy *et al.*[18] have also reported increased selectivities to higher hydrocarbons from the oxidative coupling of methane when the catalyst was heated by microwave radiation. Zhang *et al.*[16] showed that under microwave heating, C_2 hydrocarbon products converted from methane were obtained at a temperature approximately 250°C lower than that in conventional heating in the absence of oxygen. They also reported that reaction occurred in the gas phase and rates increased in the absence of oxygen possibly due to the localised heating of methane. However, it was also found that in the presence of oxygen there was no difference in selectivities between the classical and microwave heating procedures.

Enhancements in reaction rates have also been reported in other heterogeneous catalytic reactions such as in the catalytic reduction of sulphur dioxide with methane using a MoS_2 catalyst on an activated alumina support. Chemat *et al.*[19] has reported that the reactions can be enhanced by heating the catalyst with microwave irradiation because the strong microwave absorbing sites have a greater temperature than that of the bulk catalyst i.e. "hot spots" are created in the catalyst. Zhang *et al.*[14] showed that when using a MoS_2/Al_2O_3 catalyst and microwave irradiation, SO_2 was reduced at a temperature 200°C lower than required in conventional heating. They claimed that this was due to the formation of hot spots within the catalyst.

Some other microwave assisted heterogeneous catalytic reactions carried out by Zhang *et al.* include the carbon dioxide reforming of methane[13] carried out over platinum catalysts supported on alumina. Their results showed that the conversions of CO_2 and CH_4 and

product selectivity in terms of H_2/CO ratio increased with increasing temperature using both microwave and conventional heating methods and that conversions and selectivities were higher under microwave heating than under conventional heating at the same measured temperature. The microwave effects seen were attributed to the formation of hot spots within the catalyst bed. When they compared the microwave dielectric heating effects of the endothermic decomposition of H_2S to the exothermic hydrodesulphurization of thiophene[15] they found that there was a shift in the reaction equilibrium, although in opposite directions for the endothermic and exothermic reactions. In addition there was also an increase in reaction rate under microwave dielectric heating and this was also proposed to be due to the presence of hot spots in the catalyst.

From the literature reports it is noticed that for the many different heterogeneous catalytic reactions investigated the use of microwave dielectric heating has been successful in enhancing the reaction rates and selectivities of reactions. However, not much has been mentioned about the use of microwave dielectric heating in Fischer-Tropsch Synthesis (FTS). To the best of our knowledge the only research carried out on this subject is by Linda Linganiso on the solid state interactions induced by microwaves on Fischer-Tropsch catalysts.[45] Work was done on unsupported iron and silica supported iron as well as potassium promoted iron catalysts. Linganiso[46] reported increases in activity of the Fe/SiO_2 catalyst after microwave pre-treatment. This was attributed to the presence of OH groups on the surface of the catalyst which are good absorbers of microwaves and this lead to enhanced activity of the catalysts. Increases in selectivity of the catalyst were also reported, in particular increased olefin selectivity after microwave pre-treatment of potassium promoted Fe/SiO_2 catalysts. This was described as being due to an iron and potassium interaction being enhanced by the microwave pre-treatment.[46] These positive results are encouraging and it would be worthwhile to further investigate the effect of microwave heating on catalysts for Fischer-Tropsch Synthesis.

Controlling selectivity in Fischer-Tropsch Synthesis is an important aspect for catalyst development. By choosing the right catalyst (iron or cobalt) and the addition of promoters

it may be possible to enhance the selectivity to a particular type of product. Cobalt catalysts generally lead to the production of more linear alkanes whereas iron with the correct promoters may be manipulated to give alkenes, oxygenates and branched hydrocarbons.[22] Many researchers have shown that addition of optimum amounts of potassium to iron catalysts leads to increases in activity of the catalyst and selectivity towards olefins. Moskovits *et al.*[47] have shown that increasing potassium from 0.9 wt% to 2.7 wt% caused an increase in the activity of the catalyst as well as suppressing the dissociative adsorption of H_2 thus retarding the reduction of the iron catalyst. Similar results have been obtained by Wan *et al.*[48] for 5 wt% K in which reduction by H_2 of Fe was suppressed and CO adsorption facilitated thus leading to more olefinic products. Manganese has been revealed to be a promoter that increases selectivity to lower olefins i.e. in the range of C_2 to C_4 products which are important as feed-stocks in the petrochemical industry. Das *et al.*[49] have reported increased olefin selectivity, especially selectivity towards C_3, using supported Fe – Mn catalysts. Li *et al.*[34] also reported enhanced olefin to paraffin ratios and also increased selectivity to heavy (C_{12}+) hydrocarbons on silica supported catalysts. Even greater selectivities to olefins may be obtained with doubly promoted iron catalysts such as Fe-Mn-K catalysts. Das *et al.*[50] have shown that using Fe-Mn-K catalysts good activity and selectivity to lower alkenes ($C_2 – C_4$) was obtained with 70-80% formation of lower alkenes.

In this project Mn/Fe_2O_3 and $K/Mn/Fe_2O_3$ catalysts will be used to selectively produce olefins. It would therefore be interesting to observe whether microwave dielectric heating would further promote the selectivity of these catalysts. It is important to note that for the heterogeneous catalytic reactions mentioned in the literature, in which microwave dielectric heating was used and increases in selectivity and reaction rate were observed, the reactions took place when the reactor which contained the catalyst was placed in a microwave cavity and the reagent gas was passed through it. In this project the reactor will not be placed in a microwave cavity. Microwave radiation of the solid state catalyst will be performed. The catalyst will be pre-treated with microwave radiation using a domestic microwave oven. Only after microwave pre-treatment will the catalyst be used in Fischer-Tropsch Synthesis. In heterogeneous catalysis the structure of the catalyst can

determine the behaviour of the catalyst in a chemical reaction. The structure of the catalyst may also be related to the performance of the catalyst. The method of preparation and manner in which promoters are incorporated into the catalyst are significant as different methods may lead to different physicochemical properties of a catalyst. In this project two methods i.e. the co-precipitation method and incipient wetness impregnation method will be used to prepare the catalyst. Catalysts prepared by the co-precipitation method and its performance in FTS have been studied extensively but not much has been reported on catalysts prepared by the incipient wetness method. Also as far as we know there has been no investigation on the effects of microwave heating on these types of catalysts i.e. supported and unsupported Mn/Fe_2O_3 and Mn/Fe_2O_3 catalysts. The structure and textural properties of the catalysts will be studied before microwave treatment, after microwave treatment and after Fischer-Tropsch Synthesis to determine the effects of microwave heating on the performance of the FT catalyst.

1.7 Aims of project

Previous researchers have embarked mostly on investigating the effect of promoters such as potassium and manganese on the selectivity towards lower olefins and catalytic activity of F-T iron catalysts. Limited studies have been reported on the effect of microwave pre-treatment on Mn/Fe_2O_3 based catalyst.

The present study aims to:

1. Investigate the effect of microwave pre-treatment on structure and the morphology of a promoted iron catalyst.
2. To investigate the effect of the preparation method on the structure of the catalyst using both the wetness impregnation method and co-precipitation methods.
3. To characterize the unsupported Mn/Fe_2O_3 and $K/Mn/Fe_2O_3$ catalysts
4. To study the textural properties, reduction behaviour, composition and morphology of the catalysts using BET surface area measurements, Powder x-

ray diffraction (PXRD), Transmission electron microscopy (TEM) and Temperature Programmed Reduction (TPR).

5. To study the effects of microwave pretreatment on the performance of the catalyst i.e. on the activity and selectivity of the catalysts in Fischer-Tropsch Synthesis.

1.8 References

1. H. Will, P. Scholz, B. Ondruschka, *Chem. Eng. Technol.* 27 (2004) 113-122.
2. S.A Galema, *Chem. Soc. Rev.* 26 (1997) 233-235.
3. X. Wang, T. Zhang, C. Xu, X. Sun, D. Liang, L. Lin, *Chem. Commun.* (2000) 279-280
4. X. Zhang, D. O. Hayward, *Inorganica Chimica Acta*. 359 (2006) 3421–3423.
5. D. M. P. Mingos, D. R. Baghurst, *Chem. Soc. Rev.* 20 (1991) 1-47.
6. C. Gabriel, S. Gabriel, E. H. Grant, B. S. J. Halstead, D. M. P. Mingos, *Chem. Soc. Rev.* 27 (1998) 213-223.
7. G. Whittaker, 1997, A basic introduction to microwave chemistry
8. A. Y. Klimov, B. S. Balzhinimaev, L. L. Makarshin, *Kinet. Catal.* 39 (1998) 511.
9. G. Roussy, J. M. Thiebaut, M. S. Medjram, *Catal. Lett.* 21 (1993) 133.
10. D.A.C. Stuerga, P.J. Gaillard*, J. Microwave Power Electromagn. Energy* 31 (1996) 87.
11. R. N. Gedye, W. Rank, K. C. Westaway, *Can J Chem*. 69 (1991) 706.
12. S. Caddick, *Tetrahedron* 51 (1995) 10403-10432.
13. X. Zhang, C. S-M. Lee, D. M. P. Mingos, D. O. Hayward, *Catal. Lett.* 88 (2003) 129-139.
14. X. Zhang, D. O. Hayward, C. Lee, D. M. P. Mingos, *Appl. Catal. B* 33 (2001) 137-148.
15. X. Zhang, D. O. Hayward, D. M. P. Mingos, *Catal. Lett.* 88 (2003) 33-38.
16. X. Zhang, C. S-M. Lee, D. M. P. Mingos, D. O. Hayward, *Appl. Catal. A-Gen.* 249 (2003) 151-164.
17. D. Bond, R. B. Moyes, D. A. Whan, *Catal. Today* 17 (1993) 427.
18. G. Roussy, E. Marchal, J. M. Thiebaut, A. Kiennemann, G. Maire, *Fuel Process Technol.* 50 (1997) 261.
19. F. Chemat, D. C. Esveld, M. Poux, J. L. Di-Martino, *J. Microwave Power Electromagn. Energy* 33 (1998) 88.
20. R. C. Brady, R. Pettit, *J. Am. Chem. Soc.* 103 (1981) 1287-1289.
21. L. Guczi, New trends in CO activation, Elsevier, vol. 64, (1991) 225

22. R. J. O'Brien, L. Xu, R. L. Spicer, S. Bao, D. R. Milburn, B. H. Davis, *Catal. Today* 36 (1997) 325.
23. P. Sabatier, J. B. Senderens, *C. R. Acad. Sci.*, Paris, 134 (1902) 514
24. BASF: German Pat. 293,787 (1913)
25. F. Fischer, H. Tropsch, *Brennst.-Chem.*, 4 (1923) 276.
26. M. C. Bahome, Synthesis and use of carbon nanotubes as a support for the Fischer-Tropsch Synthesis, PhD Thesis, University of the Witwatersrand, 2007
27. http://en.wikipedia.org/Fischer-Tropsch Process. Accessed 24/11/2010.
28. E. M. Mokoena, Synthesis and use of silica materials as support for the Fischer-Tropsch reaction, PhD Thesis, University of the Witwatersrand, Johannesburg, 2005.
29. D.J. Duvenhage, The preparation, Characterization and Evaluation of Titania Supported Fe:Co Bimetallic Catalysts for the Hydrogenation of CO, PhD Thesis, University of the Witwatersrand, Johannesburg, 1994
30. S. Li, S. Krishnamoorthy, A. Li, G. D. Meitzner, E. Iglesia, *J. Catal.* 206 (2002) 202-217.
31. Y. Yang, H-W. Xiang, Y-Y. Xu, L. Bai, Y-W. Li, *Appl. Catal.,A* 266 (2004) 181-194.
32. A. A. Mirzaei, M. Faizi, R. Habibpour, *Appl. Catal.,A* 306 (2006) 98-107.
33. T.H. Dlamini, Precipitated Fe-based Fischer-Tropsch Catalysis, Thesis (1998) 2-10.
34. T. Li, Y. Yang, C. Zhang, X. An, H. Wan, Z. Tao, H. Xiang, Y. Li, F. Yi, B. Xu, *fuel* 86 (2007) 921-927.
35. D. B. Bukur, D. S. Mukesh, A. Patal, *Ind. Eng. Chem. Res.*29 (1990) 194.
36. Y. Yang, H. Xiang, Y. Xu, L. Bai, Y. Li, *Appl. Catal.* 266 (2004) 181-182.
37. T. Li, Y. Yang, C. Zhang, Z. Tao, H. Wan, X. An, H. Xiang, Y. Li, *Journal of Natural Gas Chemistry* 16(2007) 278-282.
38. T. Herranz, S. Rojas, F.J. Pérez-Alonso, M. Ojeda, P. Terreros, J.L.G. Fierro, *Appl. Catal.* 311 (2006) 66-67
39. K.M. Kreitman, M. Baerns, J.B. Butt, *J.Catal.* 105 (1987) 319-320.

40. Z. Tao, Y. Yang, M. Ding, T. Li, H. Xiang, Y. Li, *Catal. Lett.*, 117, (2007) 130-135.
41. M. Jiang, N. Koizumi, M. Yamada, *Appl. Catal. A:Gen*., 204 (2000) 58.
42. N.K. Jaggi, L.H. Schwartz, J.B. Butt, *Appl. Catal.*, 13 (1985) 347-348.
43. J.B Butt, *Catal.Lett.* 7 (1990)83-84.
44. T. Grzybek, H. Papp, M. Baerns, *Appl. Catal.*, 29 (1987) 335-336.
45. T. Li, Y. Yang, C. Zhang, Z. Tao, H. Wan, X. An, H. Xiang, Y. Li, *Journal of Natural Gas Chemistry* 16(2007) 244-250.
46. L. Z. Linganiso, Microwave induced solid-state interactions for the synthesis of Fischer-Tropsch catalysts, PhD Thesis, University of the Witwatersrand, Johannesburg, 2008.
47. D. G. Miller, M. Moskovits, *J. Phys. Chem.* 92 (1988) 6081-6085.
48. H. Wan, B. Wu, C. Zhang, H. Xiang, Y. Li, *Journal of Molecular Catalysis A: Chemical* 283 (2008) 33-42.
49. D. Das, G. Ravichandran, D. K. Chakrabarty, *Catal. Today* 36 (1997) 285-293.
50. C. K. Das, N. S. Das, D. P. Choudhry, G. Ravichandran, D. K. Chakrabarty, *Appl. Catal. A-Gen.* 111 (1994) 119-132.

2. Experimental

In this chapter the materials and methods used to prepare the catalysts used in the study are described. Several techniques such as PXRD, BET surface area measurements, TPR and TEM have been used to characterize the catalyst and a description of their use is explained in detail. The FT reactor setup for testing the performance of the catalyst is described as well as the analysis of the FT products produced in the catalytic reactions.

2.1 Materials

Iron nitrate [$Fe(NO_3)_3.9H_2O$] (Sigma Aldrich purity 98%) was used as the metal precursor for the synthesis of the unsupported catalyst. Manganese nitrate [$Mn(NO_3)_2.4H_2O$] (Merck purity 98%) was used as the metal precursor for catalyst promotion and as a co-catalyst. Potassium carbonate (K_2CO_3) (Saarchem purity 99.5%) was used as the source for potassium promotion. Syngas (60% hydrogen, 30% carbon monoxide and 10% nitrogen) cylinders were obtained from AFROX. All chemicals were used without further analysis and purification.

2.2 Catalyst preparation

2.2.1 Preparation of impregnated catalysts

The unsupported iron catalyst was prepared using the precipitation method. The required amount of $Fe(NO_3)_3.9H_2O$ to prepare a 4 M solution was accurately weighed out and dissolved in deionized water. This was stirred continuously at room temperature for approximately 30 minutes. A 15% NH_4OH solution was prepared and used to precipitate the iron. The ammonia solution was added to the iron nitrate solution while stirring until a pH of 7.2 was attained. Thereafter the precipitate was

filtered and washed with deionized water and left to dry at room temperature overnight. It was then oven dried at 120 °C for approximately 12 hours. After drying the catalyst was calcined at 350 °C for 6.5 hours to remove nitrates and convert the iron to the oxide form. The catalyst was promoted with different loadings of manganese. A $Mn(NO_3)_2.4H_2O$ solution was prepared by dissolving the crystals in approximately 2 ml of deionized water and the iron was impregnated with the solution, for example, with a loading of 5 wt% of Mn. This was then dried in an oven overnight and then re-calcined at 350 °C for 6.5 hours. Those catalysts that were promoted with potassium were impregnated with a K_2CO_3 solution (2 ml) to give a 0.1 wt% loading of K and then calcined for a third time. The catalysts were then characterized.[1]

2.2.2 Preparation of co-precipitated catalysts

The 4 M $Fe(NO_3)_3.9H_2O$ solution and $Mn(NO_3)_2.4H_2O$ crystals dissolved in approximately 2 ml of deionized water were mixed together and stirred continuously at room temperature. A solution of NH_4OH was used to precipitate the catalyst until a pH of 7.2 was achieved. The precipitate was filtered and washed with deionized water and left to dry at room temperature overnight. It was then further dried in an oven at 120 °C for 12 hours and calcined at 350 °C for 6.5 hours. Some co-precipitated catalysts were calcined at 650 °C for 6.5 hours.

2.2.3 Microwave pre-treatment of catalysts

The catalysts were irradiated with microwaves by using an LG (900 W) domestic microwave oven. The sample (approximately 5 g) was uniformly distributed in a glass petri dish and microwaved at 450 W for 10 seconds.[2]

2.3 Catalyst characterization

Different methods of preparation of the catalyst affect the structure of the catalyst. The catalyst preparation method affects the structure of the catalyst. The characterization techniques used in this study such as Transmision Electron Microscopy (TEM), Powder X-ray diffraction (PXRD), N_2 physisorption (BET) and Temperature programmed reduction (TPR) allowed us to study the structure and morphology of the catalyst, its surface area and the reduction behaviour of the catalyst.

2.3.1 Transmission electron microscopy (TEM)

Unsupported iron-manganese catalysts were studied using the JEOL-100s transmission electron microscope operating at 80 keV. Samples were prepared by dispersing the catalyst in methanol and sonicating for 15 minutes. The sample was loaded onto a copper grid for viewing. The sample morphology and particle size were studied before and after microwave heating.

2.3.2 Powder X-ray diffraction (PXRD)

Powder X-ray diffraction was used to determine the phase of the catalyst and calculate the crystallite size. This was done for both microwaved and non-microwaved samples. Approximately 1 g of sample was used for analysis. The powder patterms were obtained using the advanced D8 Bruker X-ray diffractometer as well as the Bruker D2 phaser diffractomoeter using a Cu source (1.5418 Å) and a LynxEye detector. The scan was within a 2θ range of 5-90° with 0.03° steps at 25 °C.

2.3.3 Surface area measuements (BET)

BET analysis was used to determine the surface area and pore sizes of the catalysts. This was done using the Micromeritics TRISTAR 3000 analyser. All catalysts were degassed by purging with N_2 gas while being heated at 150 °C for 4-5 h in order to remove moisture. The average surface area, pore diameter and pore volume were obtained and reported.

2.3.4 Temperature programmed reduction (TPR)

The effects of promoters and microwave heating on the catalyst reduction behaviour were studied using TPR. Approximately 0.1 g of sample was loaded into a quartz U-tube reactor containg quartz wool and heated from room temperature to 900 °C at a ramping rate of 10 °C/min. Hydrogen 5%, balance argon, was used as the reducing gas and was pumped through the U-tube at a constant flow rate of 30 ml/min. The consumption of hydrogen was measured by analysing the effluent gas using a thermal conductivity detector (TCD) and the outputs recorded on a computer.

2.3.5 Scanning electron microscopy (SEM)

Scanning electron microscopy (SEM) was used to study the surface structure and morphology of the catalyst. SEM differs from TEM in the way in which electrons interact with the sample. In SEM the electron beam strikes the sample at an angle and secondary electrons are backscattered from the surface atoms and hit the detector. The signal is amplified by a photomultiplier and an image is generated.

The sample was prepared a day before viewing. The sample holder was coated with graphite and the sample placed onto the graphite. The sample was then coated with gold and palladium. A FEI NOVA scanning electron microscope was used and samples were viewed at HV = 5.00 kV and 205000X magnification.

2.3.6 Temperature programmed surface reaction (TPSR)

Temperature programmed surface reaction (TPSR) is the surface characterization technique that is used to study surface reactions and adsorption of molecules on a surface. TPSR was used to study the effect of microwave irradiation of the FeMn catalysts. TPSR was also used to study the effect of manganese and potassium promoters on the adsorption of CO on the catalyst surface.

The TPSR experiments were performed in a quartz U-tube reactor containing quartz wool that was used to hold the catalyst. Typically 0.5 g of catalyst was loaded into the reactor and reduced in pure hydrogen at a flow rate of 30 ml/min at 350 °C for 6 hours. The catalyst was then allowed to cool to room temperature in flowing hydrogen. The gas was then switched to 5% CO and balance Ar and the CO was adsorbed onto the catalyst at room temperaure for 30 minutes at a flow rate of 20 ml/min. The gas was switched back to pure hydrogen and allowed to flow over the catalyst while desorption occured. The flow rate was kept constant at 30 ml/min while ramping the temperature up to 800 °C at a rate of 10 °C/min. The analysis was carried out using an FID detector and the outputs recorded on a computer.

2.4 Fischer-Tropsch reactions

2.4.1 Reactor set-up

The FTS reaction was performed using unsupported iron catalysts. A stainless steel fixed bed reactor was used and connected with a thermocouple which just touched the catalyst surface so that accurate temperature measurements are obtained. The temperature of the reactor was set using a temperature control box and the heating rate was therefore controlled. The reactor was connected to a heated wax trap which was kept at 150 °C although the heating rate was not controlled. This was connected in

series to a second trap i.e. the “cold trap” which is at ambient temperature for oil and water collection. The rig was also equipped with two gas chromatographs (GCs) in series, one with a flame ionization detector (FID) and the other with a thermal conductivity detector (TCD). Nitrogen was used as the carrier gas in the FID-GC and argon in the TCD-GC. To prevent condensation in the line between the reactor and the FID-GC, the line connecting the two GCs was heated using heating tape and temperatures were kept constant at a 100 °C. The lines and reactor were covered in quartz wool to prevent heat loss. The reactor outlet gas flow was controlled using a needle valve and the gas flow rate was measured using a bubble meter. All gases were vented via a bubble meter.

All the gases were supplied by AFROX. Syngas containing CO, H_2 and N_2 with the composition 30%, 60% and 10% respectively i.e. (H_2/CO = 2/1) was used for reaction and ultra high purity (UHP) hydrogen for reduction. The gases were fed to the reactor and controlled using pressure regulators. The gases were connected to a three way valve to enable us to switch between hydrogen and syngas. The flow of effluent gases from the reactor to the GCs were pressure regulated and set to atmospheric pressure to avoid huge fluctuations in flow rate. The schematic representation of the rig set-up can be seen in Figure 2.1:

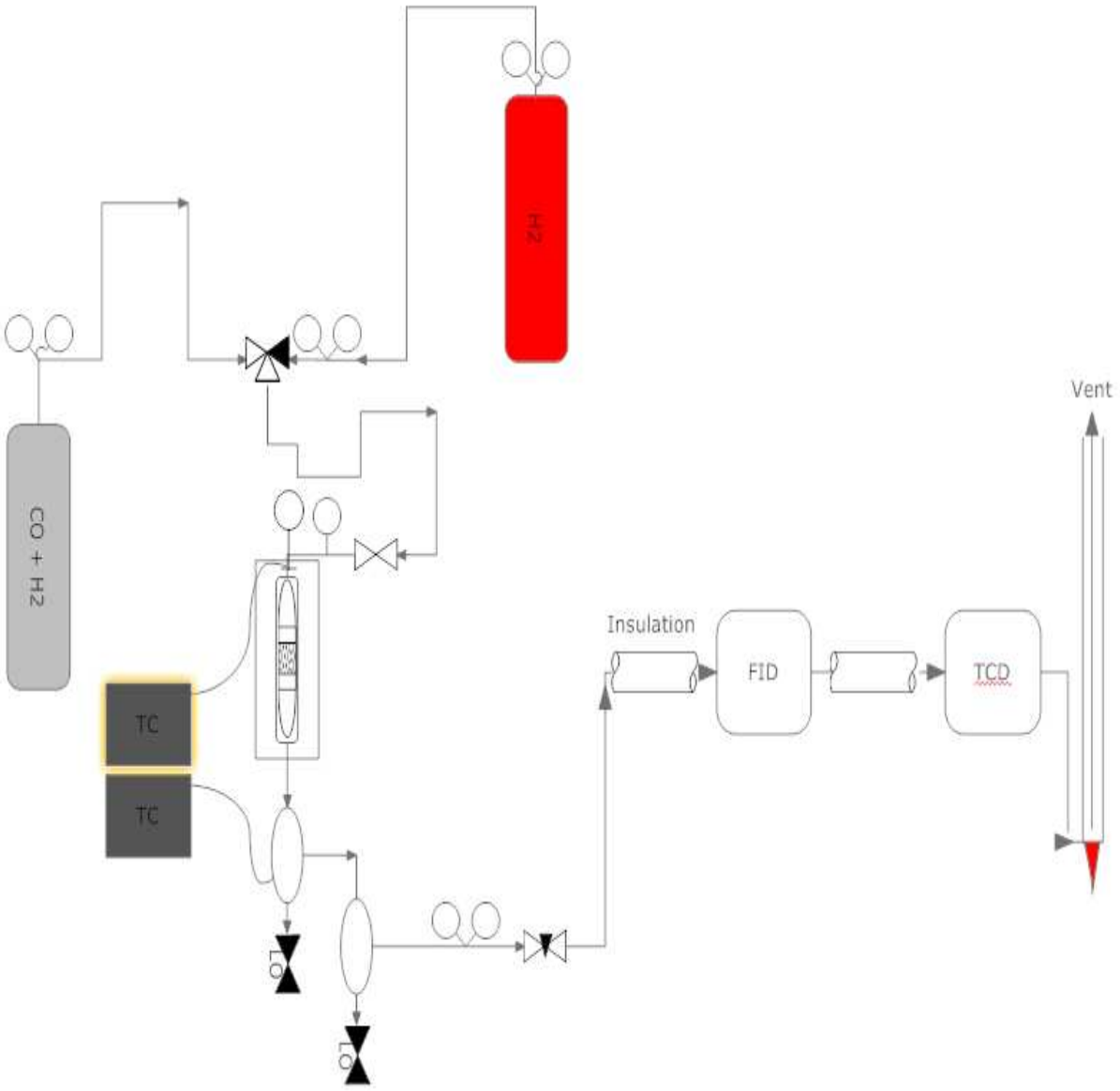


Figure 2.1: Schematic representation of the rig used for FTS.

2.4.2 Experimental procedure

The activity and selectivity of the catalysts were studied via FTS. Approximately 1 g of unsupported catalyst was loaded into the stainless steel fixed bed reactor (diameter of 16 mm). The catalyst was supported on quartz wool. The quartz wool does not interfere with the reaction. The thermocouple tip was placed on the catalyst so that accurate temperature readings were obtained. The catalyst was first reduced in pure hydrogen at 350 °C for 20 hours. Hydrogen at a flow rate of 30 ml/min at a pressure of 2 bar was used. The reactor was allowed to cool to room temperature while hydrogen flowed through it. Hydrogen was switched to syngas with a 2:1 ratio of H_2:CO and the reactor was heated up to 270 °C over 2 hours. Thereafter FTS was carried out at 270 °C at a pressure of 10 bar and flow rate of 30 ml/min. The FTS reaction was carried out for approximately 120-140 hours. The FID-GC was used for the analysis of gaseous hydrocarbon products online i.e. C_1 – C_7 and TCD-GC for detection of H_2, CO, N_2, CH_4, and CO_2. The oil and wax hydrocarbon products i.e. C_5 – C_{40} were analysed on an offline GC column. The space velocity was kept constant at 30 ml/min/g catalyst. The data was was recorded on a computer system.

2.5 Product analysis

2.5.1 Online analysis

The online analysis was performed using two GCs. The GC with a flame ionization detector was used for analysis of the hydrocarbons (C_1 – C_7) and the GC with a thermal conductivity detector for analysis of gaseous products such as H_2, N_2, CO and CO_2. A computer programme called Clarity was used to record the data. The outputs were recorded as peak areas with automatic integration. The data could then be converted to molar quantities using the appropriate calculations. The FID-GC was equipped with two 1 m 1/8 inch stainless Porapak Q packed columns joined together in order to obtain separation between α-olefin and α-paraffin products in the range C_2

– C_4. The TCD-GC was eqiupped with a 1.5 m 1/8 inch stainless Carboxen 1000 column for separation of CO, CO_2 and N_2 products. The FID-GC was calibrated every six months with a calibration gas supplied by AFROX with a composition 10% CO, 5% CO_2, 2.5% CH_4, 0.5% C_2H_6, 0.2% C_2H_4 and balance Ar. Calibration of methane, ethylene and ethane was used for the calculations of hydrocarbon product quantities. The TCD-GC was also calibrated every six months firstly with a calibration gas with known compositions of 20% CH_4, 20%, H_2, 20% N_2, 20% CO and 20% CO_2 in order to identify peak positons. The TCD was also calibrated with syngas with composition 10% N_2, 30% CO and 60% H_2 so that CO conversion could be calculated. Typical traces of the calibration and reaction analyses are shown in the following illustrations.

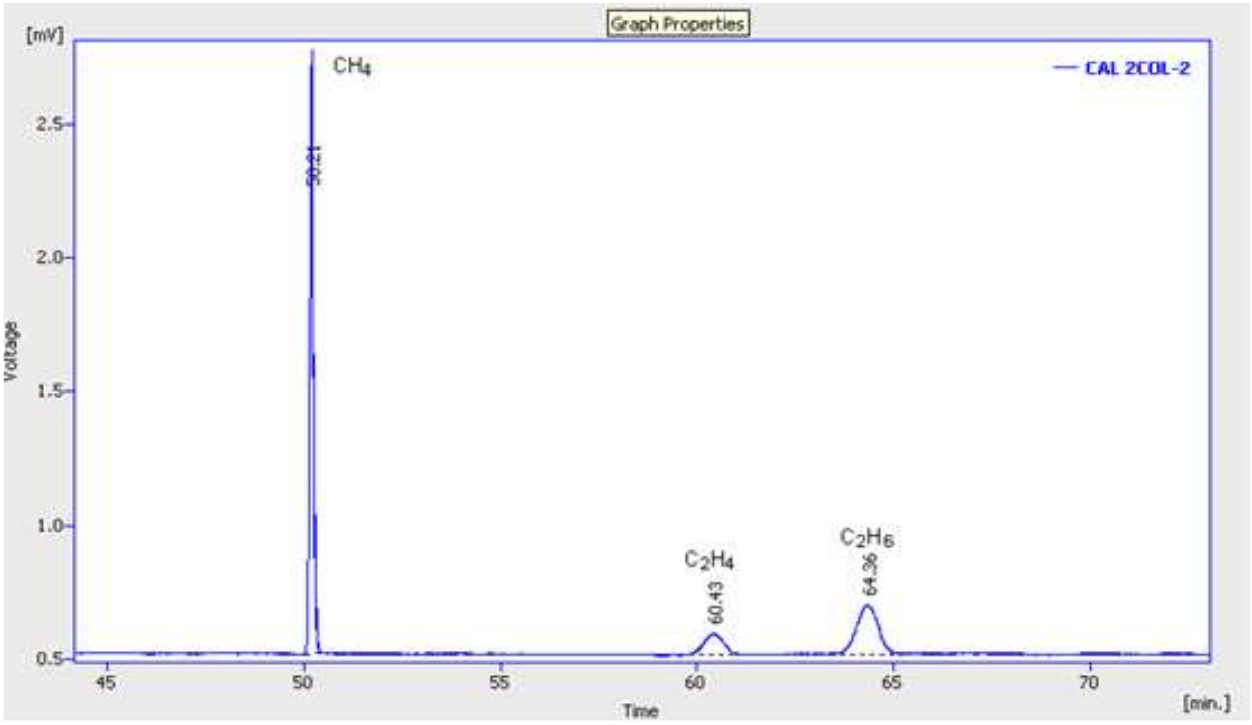


Figure 2.2: A trace of the calibration gas using the FID-GC

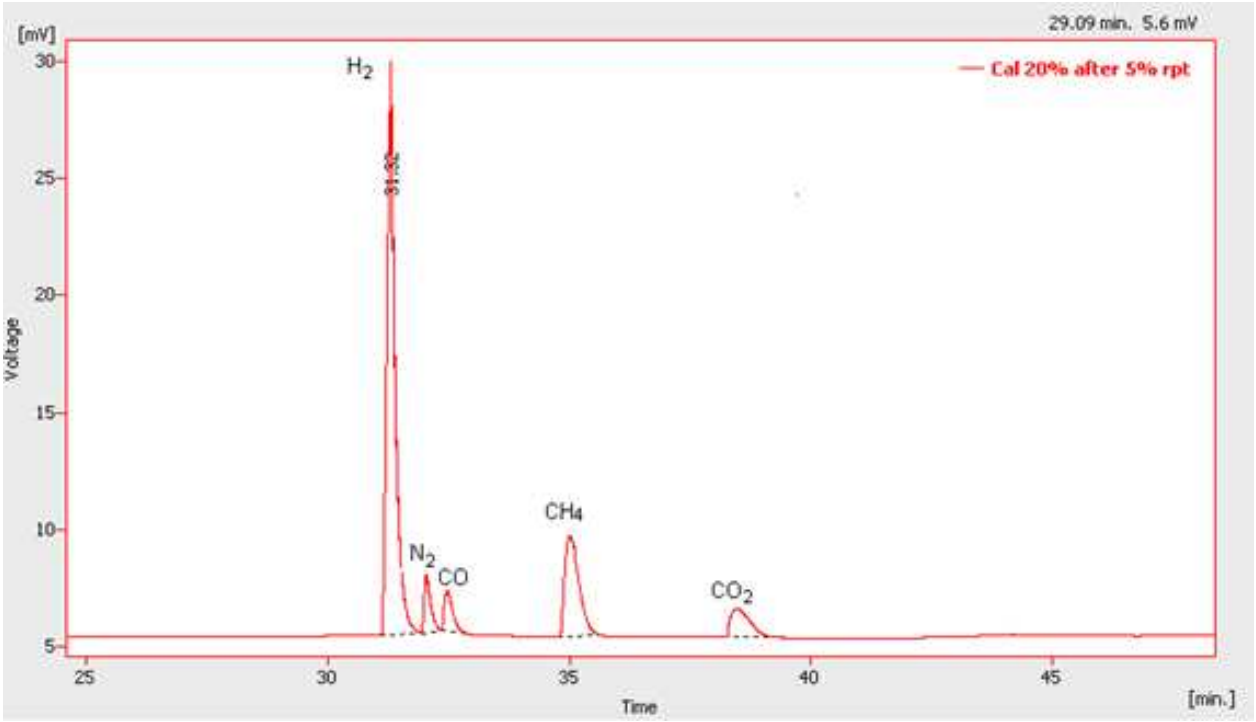


Figure 2.3: A trace of the calibration gas using a TCD-GC to indicate peak positions

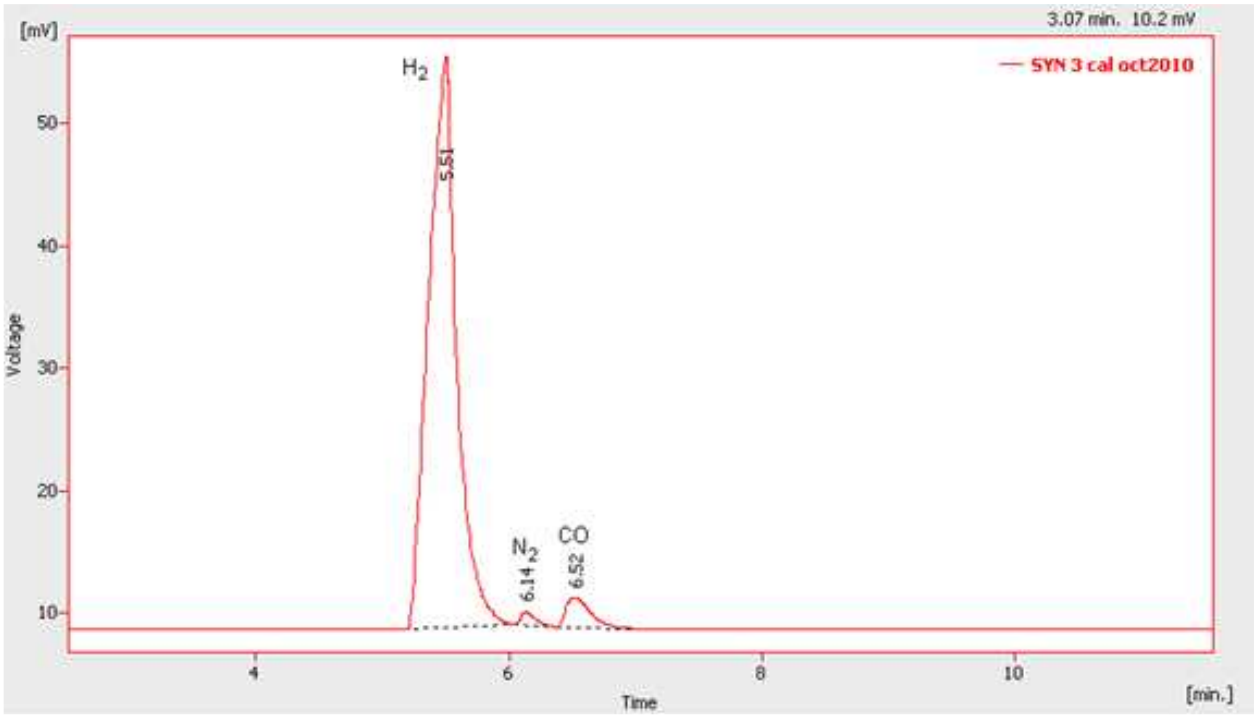


Figure 2.4: A trace showing calibration with syngas using a TCD-GC

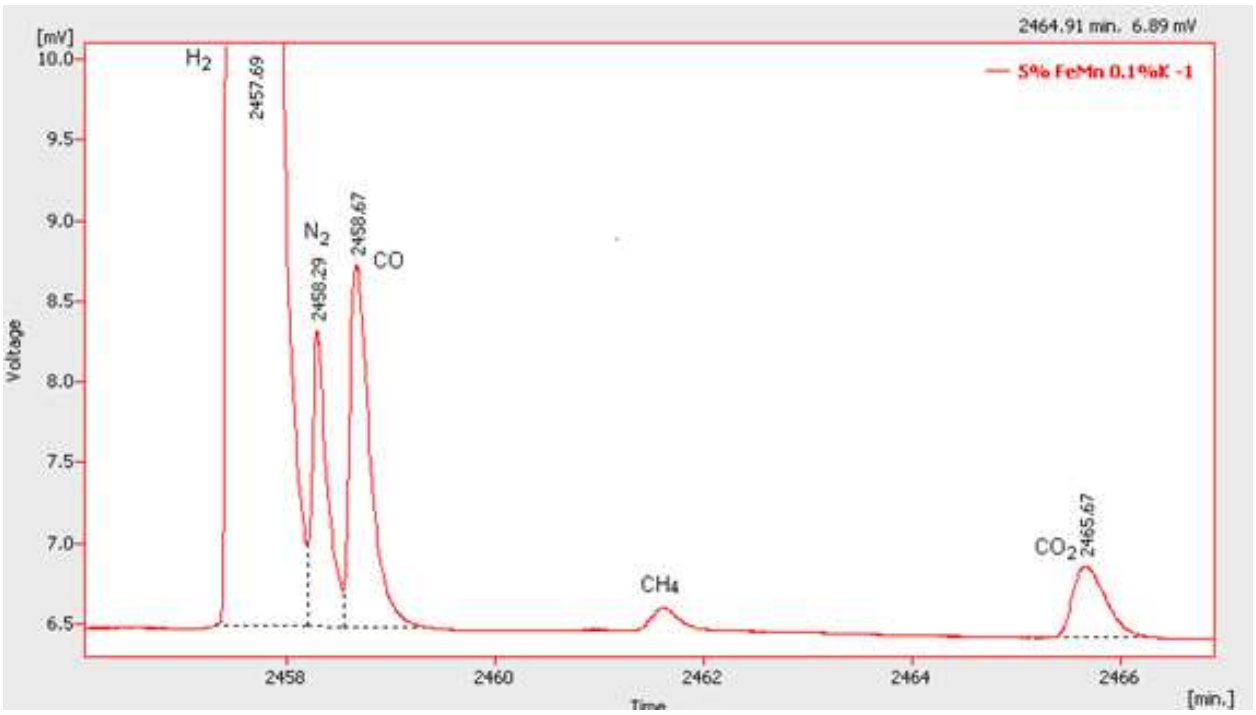


Figure 2.5: A typical trace of the products detected using a TCD-GC during a reaction

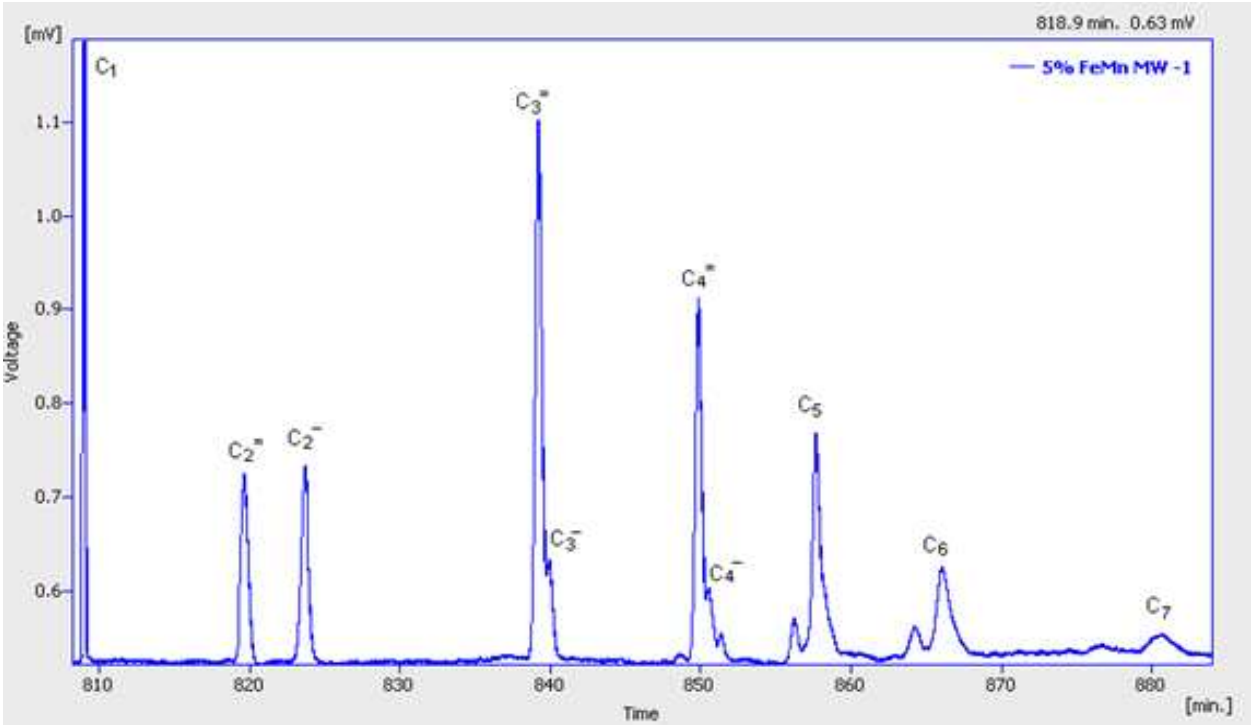


Figure 2.6: A trace showing hydrocarbon products C_1 – C_7 detected using a FID-GC

2.5.2 Offline analysis

The oil and wax products were analysed on an offline GC. The Varian 3700 gas chromatograph with a 30 m × 5 μFT column, (O.D. = 0.53 mm), with ZB-1 stationary phase and flame ionization detector at temperature = 320 °C was used to analyse hydrocarbon products C_5 – C_{40}. Nitrogen was used as the carrier gas with a flow rate of 30 ml/min. Wax and oil together with water was collected from the hot and cold traps respectively and the oil was separated from the water before analysis. Approximately 0.2 μl of both the oil and the wax samples was injected for analysis. The oven temperature programme for their analysis is given below:

Oil: Heat to 60°C at 10°C/min, heat to 300°C at 12.5°C/min and hold at 300°C for 30 minutes.

Wax: Heat to 220°C at 74°C/min, heat to 300°C at 10°C/min and hold at 300°C for 240 minutes.

2.6 Mass balance calculations

The methods used to perform the mass balance calculations were similar to those carried out by Bahome[3], Mokoena[4], Duvenhage[5], Price[6], Phadi[7] and Hexana[8]. Atom balances were performed on carbon and oxygen.

As explained in section 2.5.1 the data were recorded using a Clarity software and presented as peak areas which were automatically integrated. This was then converted to molar quantities using the equations below.

The mass balance period was recorded once the catalyst reached a steady state which was typically 24 hours after the FTS reaction was started. At this point the hot and cold traps were drained, the mass balance period began and was taken to end when the

reaction was stopped approximately after 120-140 hours. Once the reaction was stopped the oil and wax traps were drained, the products weighed and samples (0.2 µl) were analysed on the offline GC.

The outlet flow stream was measured on a daily basis using a bubbler at ambient pressure and temperature. The feed inlet flow rate to the reactor was determined using N_2 gas contained in the syngas cylinder. The equation used to determine the feed flow rate is given below:

$$F_{in} = \left[\frac{X_{N2,in}}{X_{N2,out}}\right] \times F_{out} \qquad (2.1)$$

where F_{in} is the total feed flow rate in mol/s, $X_{N_2,\,in}$ and $X_{N_2,\,out}$ are mole fractions of nitrogen in the feed (Syngas) and reactor exit streams respectively and F_{out} is the total reactor exit stream in mol/s.

The number of moles in the carbon feed stream in the total mass balance period was calculated by:

$$N_{C,in} = F_{in} . t . X_{CO,in} \qquad (2.2)$$

where $N_{C,\,in}$ is the moles of carbon in the feed, F_{in} is the total feed flow rate in mol/s, t is the total mass balance time and $X_{CO,\,in}$ is the mole fraction of CO in the feed gas.

Calibration of the components was carried out with a premixed gas of known composition containing CH_4, C_2H_6, C_2H_4, CO, CO_2, and Ar. The moles of product of each of the components present in the calibration gas were calculated using the following equation:

$$N_{c,out} = \frac{A_c}{A_{c,cal}} . X_{c,cal} . F_{out} . t \qquad (2.3)$$

where A_c is the GC integrated area of component c, $A_{c,cal}$ is the area of the component c in the calibration gas and $X_{c,cal}$ is the mole fraction of the component c in the calibration gas.

The hydrocarbon product areas were corrected for C_2H_4 (olefins) and C_2H_6 (paraffins) by using the response factors based on those presented by Bahome[3] and Phadi[7]. The mole fractions of hydrocarbons $X_{HC,i}$ were calculated using the equation below:

$$X_{HC,i} = \frac{RF_i . A_{HC,i}}{A_{C2cal}} . X_{C2,cal} \qquad (2.4)$$

Where RF_i the response factor for carbon number *i*, $A_{HC,i}$ is the integrated GC area for a hydrocarbon with carbon number *i*, $A_{C2,cal}$ and $X_{C2,cal}$ refer to peak area and mole fraction of the C_2 hydrocarbon in the calibration gas.

The mass response factors for the hydrocarbon with carbon number greater than 15 were assumed to be one[3]. The mass fractions of these hydrocarbons (i > 15) were thus determined directly from the GC integrated areas using the following equation:

$$m_i = \frac{A_{IIC,i}}{\Sigma A_{IIC,i}} \qquad (2.5)$$

The %CO conversion was calculated as follows:

$$\left[\frac{CO_{in} - CO_{out} \times gas\ contraction}{CO_{in}}\right] \times 100 \qquad (2.6)$$

where the gas contraction was determined from the $\frac{N_{2,in}}{N_{2,out}}$ calibration.

The product selectivity for hydrocarbons S_i was calculated for component x_i as follows:

$$S_i = \left[\frac{mass\ component\ x_i}{\Sigma x_i}\right] \times 100 \qquad (2.7)$$

The olefin to paraffin ratio x_2 is given by the following equation:

$$O/P\ ratio\ x_2 = \frac{Mass\ olefin\ x_2}{Mass\ total\ hydrocarbon\ x_2} \qquad (2.8)$$

Carbon and oxygen mass balances were determined using the information obtained from the above analysis and calculations.

The mass balance equations for carbon and oxygen are as follows:

$$\%mb\ C = \left[\frac{mol\ CO_{out} + mol\ CO_{2out} + mol\ {}^{C}/_{HC}}{mol\ CO_{in}}\right] 100 \qquad (2.9)$$

$$\%mb\ O = \left[\frac{mol\ CO_{out} + (mol\ CO_{2out} * 2) + mol\ H_2O_{out}}{mol\ CO_{in}}\right] 100 \qquad (2.10)$$

where mol C/HC is the sum of the moles of carbon per hydrocarbon for carbon number n.

The individual rates of reaction for FTS (r_{FTS}) and water gas shift (r_{WGS}) were calculated from experimentally obtained quantities as :

$$(r_{WGS}) = r_{CO2} \qquad (2.11)$$

$$(r_{FTS}) = r_{CO} - r_{CO2} \qquad (2.12)$$

where r_{CO} is the rate of carbon monoxide conversion and r_{CO2} is the rate of carbon dioxide formation.

2.7 References

1. T. Li, Y. Yang, C. Zhang, Z. Tao, H. Wan, X. An, H. Xiang, Y. Li, *Journal of Natural Gas Chemistry* 16 (2007) 244-250.
2. L. Z. Linganiso, Microwave induced solid-state interactions for the synthesis of Fischer-Tropsch catalysts, PhD Thesis, University of the Witwatersrand, Johannesburg, 2008.
3. M. C. Bahome, Synthesis and use of carbon nanotubes as a support for the Fischer-Tropsch Synthesis, PhD Thesis, University of the Witwatersrand, Johannesburg, 2007.
4. E. M. Mokoena, Synthesis and use of silica materials as support for the Fischer-Tropsch reaction, PhD Thesis, University of the Witwatersrand, Johannesburg 2005.
5. D.J. Duvenhage, The preparation, Characterization and Evaluation of Titania Supported Fe:Co Bimetallic Catalysts for the Hydrogenation of CO, PhD Thesis, University of the Witwatersrand, Johannesburg, 1994.
6. J. G. Price, An investigation into novel bimetallic catalysts for use in Fischer-Tropsch reaction, PhD Thesis, University of the Witwatersrand, Johannesburg, 1994.
7. T. T. Phadi, Titanates and titania coated titanates as supports in the Fischer-Tropsch synthesis, MSc Dissertation, University of the Witwatersrand, Johannesburg, 2008.
8. W. M. Hexana, A systematic study of the effect of chemical promoters on the precipitated Fe-based Fischer-Tropsch synthesis catalyst, PhD Thesis, University of the Witwatersrand, Johannesburg, 2009.

3. Results and Discussion

In this chapter we present the results obtained from the characterization of the various types of catalysts studied throughout this project. This chapter is divided into three main sections ie. Characterization of the unsuppported iron catalyst, the effect of preparation method and microwave heating of Mn/Fe_2O_3 catalysts and the study of potassium promoted Mn/Fe_2O_3 catalysts.

3.1 Study of unsupported iron catalyst

3.1.1 Transmission electron microscopy

The iron was precipitated using ammonium hydroxide as the precipitating agent. It was washed with deionized water, then dried and calcined to remove nitrates and the iron was converted to the oxide form. The unsupported iron catalyst morphology and particle size was studied using TEM (see Fig 3.1).

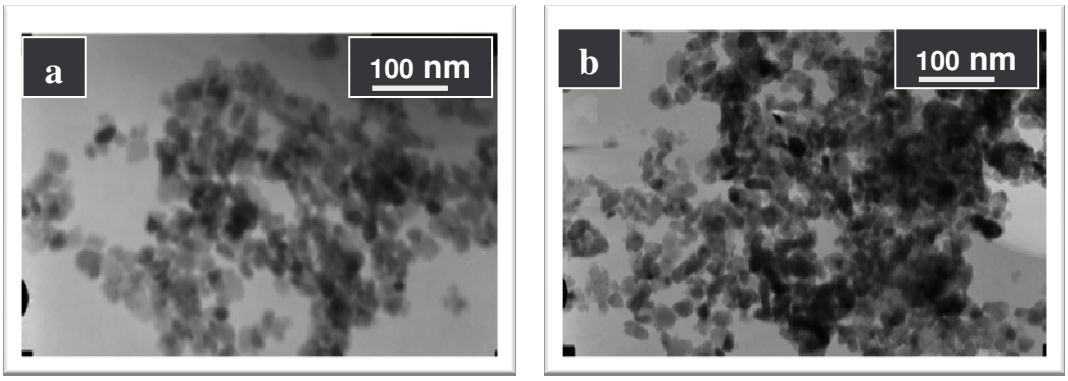


Figure 3.1: TEM images (a) and (b) showing morphology of iron particles and particle size distribution.

In the images above we see that some of the iron particles are clustered together and some are dispersed. They generally have a spherical like morphology although some

have irregular shapes. To determine the particle size distribution the diameters of the particles which exhibit a fairly spherical morphology were measured and the results showed that the particles were small (in the nanometer range) and had a wide size distribution in the range of 30-50 nm. This can be seen in Fig 3.2.

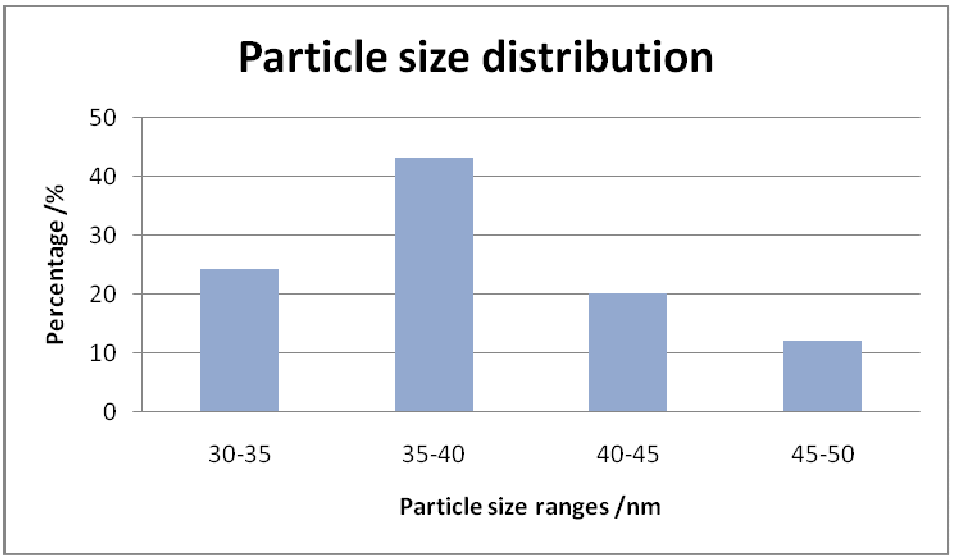


Figure 3.2: Bar graph showing the wide particle size distribution of the iron ctalyst.

3.1.2 Powder X-ray diffraction

Powder X-ray diffraction was performed in order to determine the iron phase present in the catalyst. The powder pattern is shown in Fig 3.3.

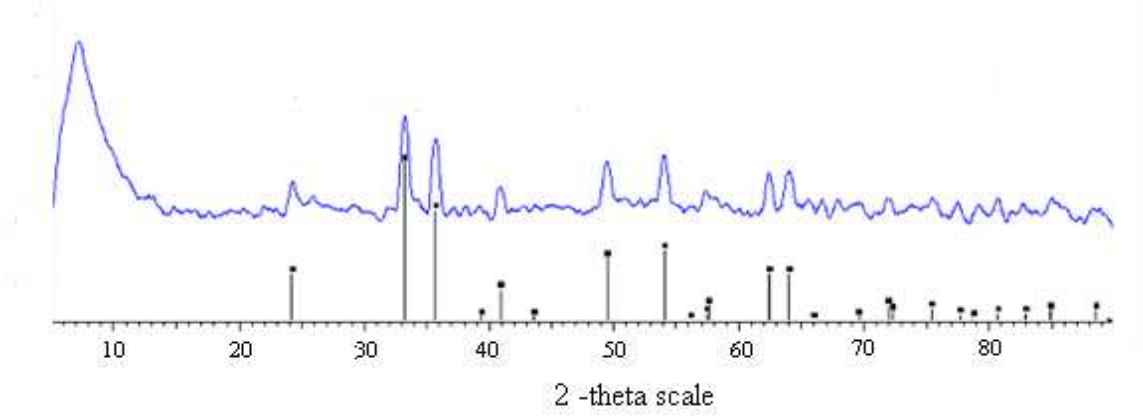


Figure 3.3: Powder pattern showing presence of haematite phase in iron catalyst.

A phase identification was carried out by comparing the powder pattern obtained with patterns from a database on the EVA software package. The powder pattern of the iron catalyst has fairly broad peaks indicating it has small crystallite sizes typically in the range of 20 – 30 nm and shows that it exists as a pure α-Fe_2O_3 haematite phase with 2θ peaks at 24.12°, 33.18°, 35.61°, 40.83°, 49.42°, 54.00°, 62.38° and 63.96°. Note that the pattern above has been smoothed and the background subtracted (using EVA) to remove the background noise caused by flouresence of the iron catalyst. Thus the peak positions could be easily identified.

The crystallite size of the catalyst was determined using PJF XRD analyser which uses the Scherrer equation:

$$d = k\frac{\lambda}{\beta}\sin\theta$$

where d is the average crystallite size, k is the Scherrer constant taken to be equal to 0.9. λ is the wavelength of the X-ray radiation, β is the full width at half-maximum and θ is the diffraction angle.

The average crystallite size was calculated to be 26.1 nm and this is similar to the data obtained from the TEM analysis.

3.1.3 Surface area measurements (BET)

The surface area and porosity of the unsupported iron catalyst was studied using N_2 physisorption (BET method). The results are expressed in the following table: (Table 3.1)

Table 3.1: Table showing the average surface area, pore size and pore volume

	Surface area (m^2/g)	Pore diameter (nm)	Pore volume (cm^3/g)
Fe_2O_3	24.7	12.1	0.074

From Table 3.1 we see that the surface area of the catalyst is quite low. In general the smaller the pore size the larger the surface area. This catalyst has a low surface area because some of the particles as shown in the TEM are clustered together and the pore diameter is probably due to the mesopores. The pore volume is also low which means that the surface area will be low. The pore diameter reported in the table is an average result and the pore size distribution can be seen in Figure 3.4:

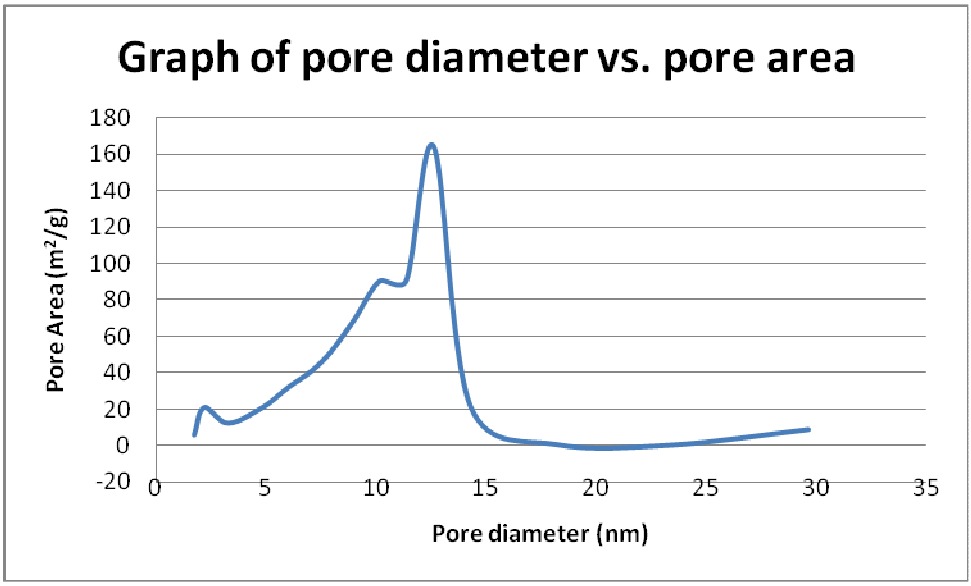


Figure 3.4: Graph showing pore size distribution

From the graph we notice that there are three peaks indicating a range of pore sizes. The bulk of the pores are in the 10-12 nm range. The very small pores (approximately 2 nm in size) are probably associated with the iron particle itself.

3.1.4 Temperature programmed reduction

A TPR study was undertaken to investigate the reduction behaviour of the catalyst in order to determine the temperature at which the catalyst could be reduced prior to FT synthesis. The temperatures at which the catalyst reduces is shown in Figure 3.5. The profile shows two distinct peaks where reduction occurs. The first reduction peak at 360 °C corresponds to the reduction of haematite to magnetite i.e. $Fe_2O_3 \rightarrow Fe_3O_4$ and

the second smaller reduction peak at 600 °C corresponds to the reduction of magnetite to metallic iron i.e. $Fe_3O_4 \rightarrow Fe$. This is a typical α-haematite TPR profile is very similar to what has been found in the literature.[1] The reduction temperature chosen for the catalyst during FTS was 350 °C. This temperature was maintained for a long period of time in order to fully reduce the catalyst.

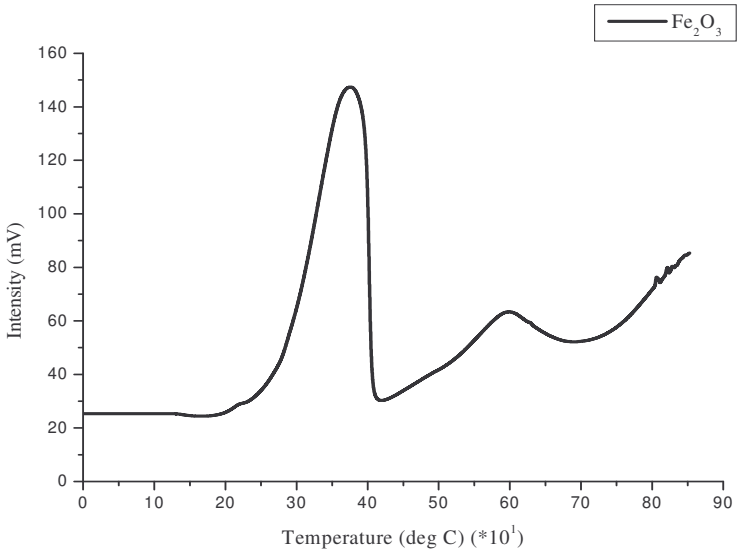


Figure 3.5: TPR profile of pure haematite catalyst.

3.2 Addition of Mn promoter - Incipient wetness impregnation method (IWIM)

Fe_2O_3 catalysts with Mn loadings of 5 wt%, 10 wt%, 20 wt% and 50 wt% were prepared using the incipient wetness impregnation method (IWIM) and the effect of manganese loadings was studied using a range of characterization techniques:

3.2.1 Transmission electron microscopy

The TEM images shown in Figure 3.6 indicate the effect of manganese addition on the strucure and morphology of the catalyst as a function of Mn loading.

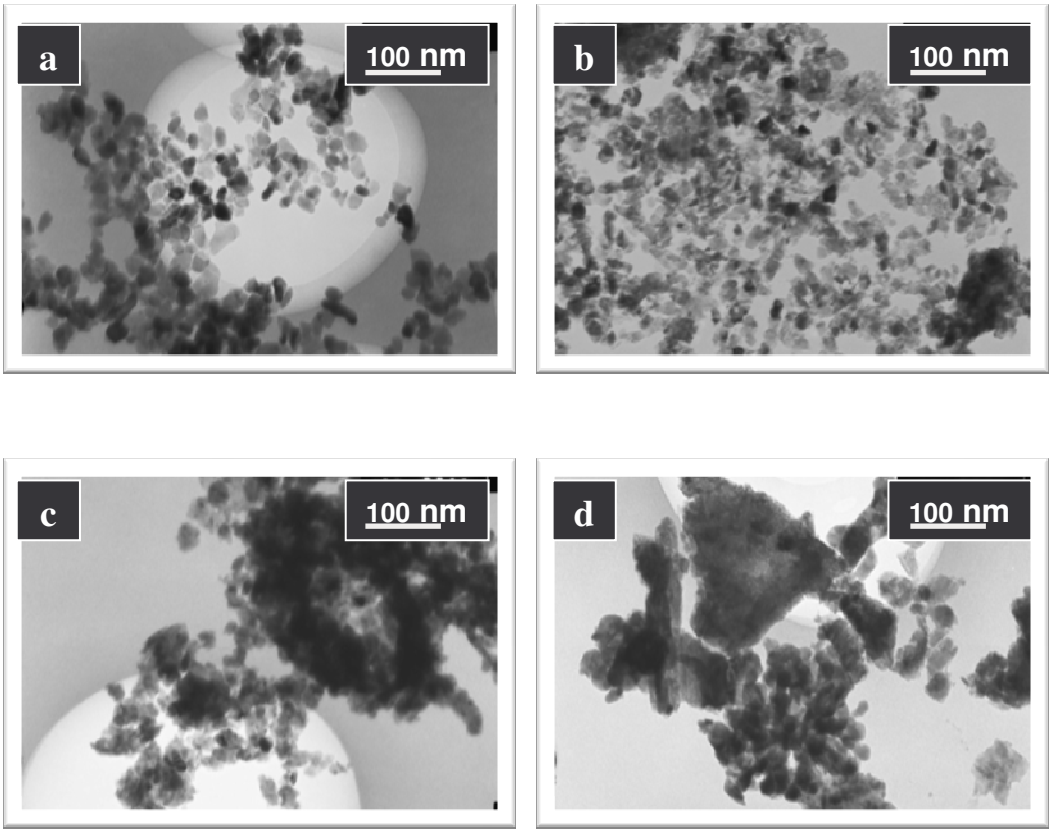


Figure 3.6: TEM images showing Mn/Fe catalysts prepared using IWIM a) 5 wt% Mn, b) 10 wt% Mn, c) 20 wt% Mn and d) 50 wt% Mn on Fe_2O_3 after calcination at 350 °C for 6.5 hours.

The TEM images were taken of the Mn/Fe_2O_3 samples after calcination at 350 °C for 6.5 hours. With low loadings of 5 wt% Mn the catalyst particles have a spherical morphology and the particle sizes average between 30-35 nm in size. However, the iron and manganese particles cannot be distinguished from each other. As the loading is increased to 10 wt% the catalyst retains its spherical morphology but clusters start to form (approximately 100 nm in size). As the loading is further increased to 20 and 50 wt% the well distributed spherical morphology of the catalyst is lost and the particle size cannot be determined because huge clusters of presumably manganese have been formed (approximately 250-300 nm in size). This occurs because the manganese is deposited directly onto the surface of the iron catalyst thereby covering the spherical particles and forming large clusters.

3.2.2 Surface area measurements (BET)

Table 3.2 shows the results of the effect of Mn loading on the surface area and pore volume of the Mn/Fe_2O_3 catalysts:

Table 3.2: Surface areas and pore volumes for catalysts with different loadings of Mn.

Mn loading on Fe Mn/Fe_2O_3	Surface area (m^2/g)	Pore diameter (nm)	Pore volume (cm^3/g)
Fe_2O_3	24.7	12.1	0.074
5%	21.5	9.6	0.052
10%	21.5	10.9	0.059
20%	20.1	10.1	0.051
50%	16.2	11.5	0.046

As the loading is increased the surface areas and the pore volume generally show a decrease. This is due to the presence of the manganese which is deposited onto the surface of the iron in the impregnation method thereby blocking pores and reducing the surface area. Li *et al.*[2] reported similar results for catalysts prepared by impregnation of Mn on $Fe/K/SiO_2$. The author found that the manganese was enriched

at the surface of the catalyst which is similar to that found in this catalyst. These results correlate with the images obtained from the TEM measurements as the larger clusters will have a lower surface area if they are non porous. The decrease in surface area is not very large as the Mn loading increases from 5% to 50%. This is because the manganese particles formed are very similar to the iron particles in terms of size and shape which they adopt. They are found next to each other in the Periodic Table and have similar atomic radii and atomic masses.

3.2.3 Powder X-ray diffraction

The XRD powder pattern shown in Figure 3.7 is that of manganese nitrate ($Mn(NO_3)_2.4H_2O$) that has been calcined to produce manganese oxides. The same conditions used to calcine the Mn/Fe_2O_3 impregnated catalyst were used here to calcine the manganese nitrate.

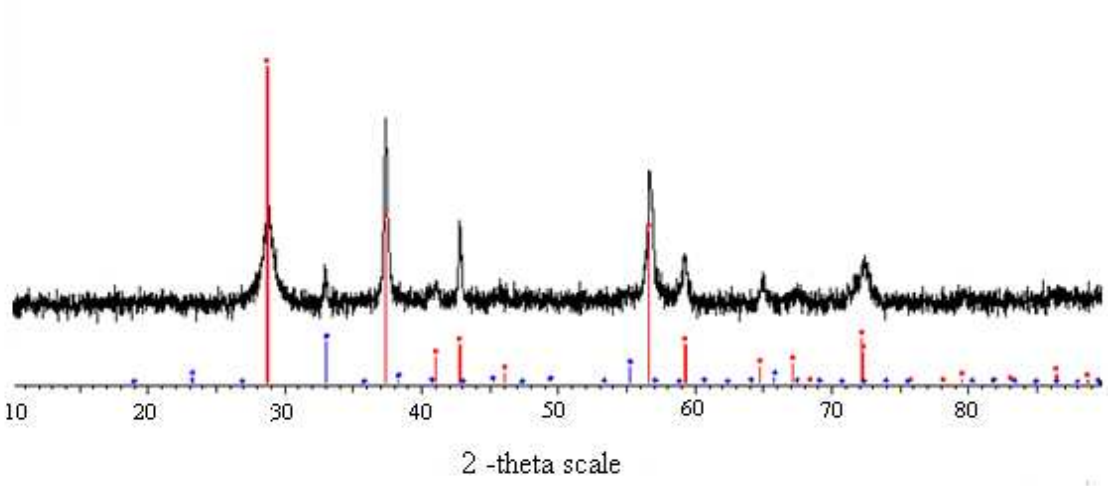


Figure 3.7: Powder pattern showing a mixture of manganese oxide phases.

The powder pattern indicates that calcination of the manganese nitrate precursor at 350 °C for 6.5 hours produces a mixture of manganese oxide MnO_2, Mn_2O_3 phases. The pattern shows the MnO_2 phase (pyrolusite) to be the dominant one i.e. the peaks corresponding to the red lines. The peak at 33° 2θ corresponds to the database structure for Mn_2O_3 (i.e. the blue lines).

The powder patterns of the impregnated Mn/Fe_2O_3 catalysts are shown in Figure 3.8. Catalysts with loadings of 5% Mn up to 20% Mn show only the presence of the haematite phase of iron. Maiti *et al.*[3] when studying co-precipitated catalysts suggested that even at low loadings of Mn, the possibility of Mn being incorporated into the haematite crystal lattice cannot be disregarded. Although manganese promotion of the catalyst by the impregnation method is known to enrich the surface of the catalyst[2], even at loadings of Mn up to 20% the Mn cannot be detected by XRD methods. A plausible explanation is that the manganese oxides exist as a poorly crystalline material or the crystallite sizes are too small. At high Mn loadings i.e. 50% loadings, the emergence of a new phase is noted. The MnO_2 phase is detected together with the haematite phase. In Figure 3.7 it was shown that the manganese exists in two phases. In the 50% loaded sample the Mn_2O_3 phase should also be present but because the peaks for Mn_2O_3 overlap with Fe_2O_3 its presence is not detected. Das *et al.*[4] reported when studying co-precipitated Fe-Mn catalysts that after calcining catalysts with Mn loadings (17-33 %) at a higher temperature of 650 °C (previously calcined at 450 °C) a Fe-Mn solid solution was formed. However, in this study the catalyst with a 20% loading calcined at 650 °C only showed the presence of the haematite phase with reasonably sharp peaks (Figure 3.9).

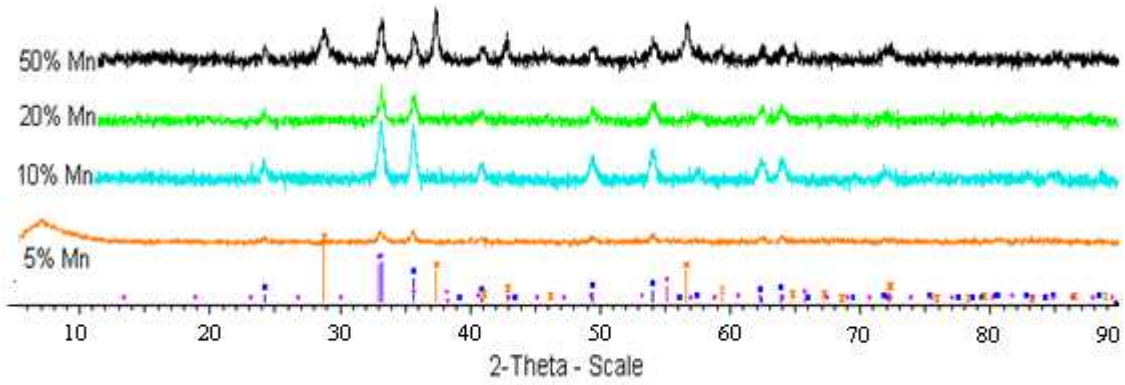


Figure 3.8: Powder patterns showing effect of manganese loading on Fe_2O_3. Note that the powder pattern of the 5% Mn catalyst has been background subtracted and smoothed. The blue lines represent the reference pattern of haematite and the pink and orange lines the reference patterns of Mn_2O_3 and MnO_2 respectively.

Calcination of the 10% andof the 10% and 20% Mn/Fe_2O_3 samples were performed at 650 °C. The higher temperature causes the particles to sinter and form larger iron crystallites. Therefore sharper peaks are observed in the XRD powder pattern (Figure 3.9) relative to the peaks detected at 350 °C. The Scherrer equation was applied to a few of the XRD peaks and the crystallite sizes are shown in Table 3.3. even at 650 °C no XRD peks due to MnO_x were detected.

Table 3.3: Crystallite sizes of peaks after 20% Mn/Fe_2O_3 catalyst was calcined at 350 °C and 650 °C.

Peak position/ 2θ	Crystallite size/ nm 350 °C	Crystallite size/ nm 650 °C
24.1	31	118
33.1	35	72
35.6	45	72
40.8	22	73

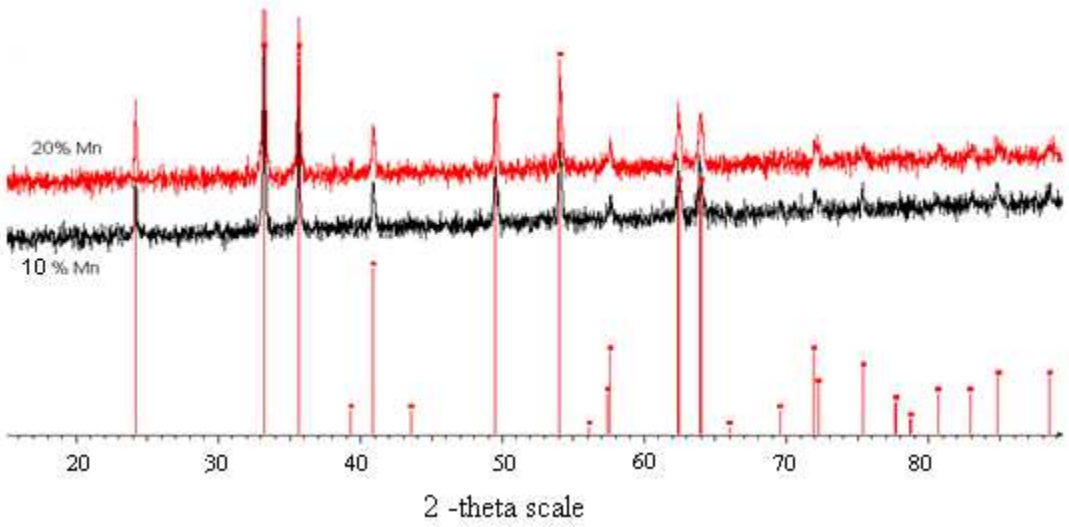


Figure 3.9: Powder patterns of the Mn/Fe_2O_3 (10% and 20% Mn) after being calcined at 650 °C. The red lines represent the reference pattern of haematite.

3.2.4 Temperature programmed reduction (TPR)

The reduction behaviour of the Fe_2O_3 sample before and after promotion with manganese was recorded using the TPR technique and data are shown in Figure 3.10. The plots compare the TPR profiles of the pure haematite, calcined manganese nitrate which produces a mixture of phases i.e. MnO_2 (the dominant phase) and Mn_2O_3 and the 5% manganese promoted iron (Mn/Fe_2O_3) catalyst. The TPR profile of Fe_2O_3 shows two peaks at 376 °C and 600 °C that correspond to the reduction of $Fe_2O_3 \rightarrow Fe_3O_4$ and $Fe_3O_4 \rightarrow Fe$ respectively as discussed earlier (chapter 3.1.4). The TPR profile for MnO_2 also shows a clear two step reduction. A similar profile was obtained by Villasenor *et al*.[5] The XRD powder pattern of the manganese oxides revealed that it exists as two phases i.e. Mn_2O_3 and MnO_2. These two phases have different reduction temperatures. Studies performed by Stobbe *et al*.[6] showed that the reduction temperature is not only influenced by the Mn oxidation state but by the amount of crystallinity of a particular Mn phase. The first peak is due to the reduction of $MnO_2 \rightarrow Mn_2O_3$ (at 487 °C) and $Mn_2O_3 \rightarrow MnO$ (at 652 °C). The final phase of MnO can be identified by its characteristic green colour. It is possible that the reduction of Mn_2O_3 goes through a Mn_3O_4 phase.

The manganese promoted catalyst shows a peak shift to higher temperatures (376 °C to 480 °C and 600 °C to 633 °C) indicating that manganese suppresses the reduction of the iron catalyst. This is due to the manganese enriching the surface of the iron catalyst thereby preventing the hydrogen adsorbing onto the iron.[2] Two extra peaks for the 5% Mn/Fe_2O_3 catalyst are observed at 240 °C and 340°C. It is suggested that these are due to the reduction of MnO_2 which is at the surface of the catalyst. The peaks occur at a much lower temperature than observed for the pure Mn oxides (487 °C, 652 °C). This suggests that the iron assists the Mn reduction.

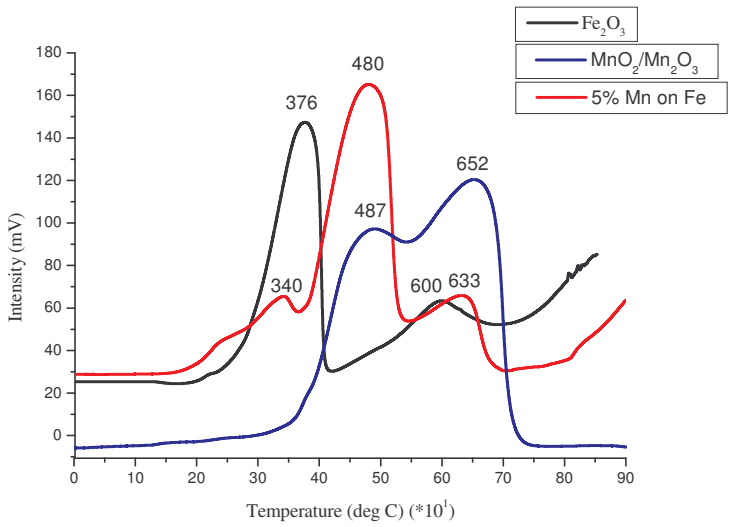


Figure 3.10: TPR profiles comparing pure Fe_2O_3, MnO_2/Mn_2O_3 and a 5% manganese promoted iron catalyst.

A summary of the peak positions obtained from the TPR profiles is shown in table 3.4.

Table 3.4: Results showing temperatures at which reduction occurs for catalysts shown in Figure 3.10.

Catalyst	Temperature/ °C	Reduction
Fe_2O_3	376	$Fe_2O_3 \rightarrow Fe_3O_4$
	600	$Fe_3O_4 \rightarrow Fe$
MnO_2/Mn_2O_3	487	$MnO_2 \rightarrow Mn_2O_3$
	652	$Mn_2O_3 \rightarrow MnO$
5% Mn on Fe	240	$MnO_2 \rightarrow Mn_2O_3$
	340	$Mn_2O_3 \rightarrow MnO$
	480	$Fe_2O_3 \rightarrow Fe_3O_4$
	633	$Fe_3O_4 \rightarrow Fe$

TPR profiles were also recorded for Mn loadings on the Fe_2O_3 of 10%, 20% and 50%. (Figure 3.11) and the data from the profiles have been tabulated in Table 3.5. The data are consistent with the suggestions as described for the 5% loaded material. Thus, as the manganese content is increased the Mn peaks move to higher temperature. This arises since there is less iron (i.e. the Mn/Fe ratio has increased) to assist with the

reduction process. Table 3.5 shows how the peaks for the iron and manganese shift with manganese loading. The data suggests little intimate interaction between the iron and manganese components, but the ability of the hydrogen transfer is clearly evident.

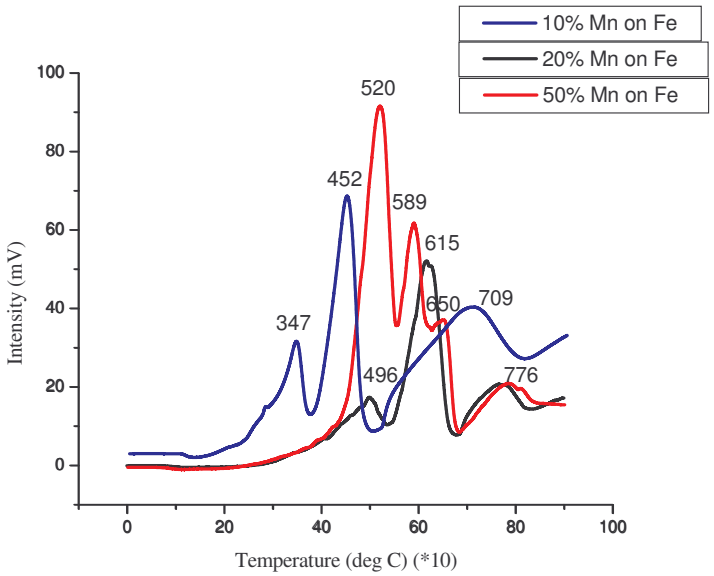


Figure 3.11: TPR profiles of 10% (blue), 20% (black) and 50% (red) Mn/Fe_2O_3.

Table 3.5: Results showing temperature at which reduction occurs for catalysts shown in Figure 3.11.

Catalyst	Temperature/ °C	Reduction
10% Mn on Fe	280, 347	$MnO_2 \rightarrow Mn_2O_3 \rightarrow MnO$
	452	$Fe_2O_3 \rightarrow Fe_3O_4$
	709	$Fe_3O_4 \rightarrow Fe$
20% Mn on Fe	400, 496	$MnO_2 \rightarrow Mn_2O_3 \rightarrow MnO$
	615	$Fe_2O_3 \rightarrow Fe_3O_4$
	770	$Fe_3O_4 \rightarrow Fe$
50% Mn on Fe	520	$MnO_2 \rightarrow Mn_2O_3$
	589	$Mn_2O_3 \rightarrow MnO$
	650	$Fe_2O_3 \rightarrow Fe_3O_4$
	776	$Fe_3O_4 \rightarrow Fe/$

3.3 FT performance of impregnated catalysts

The FT performances of all of the (5%, 10% and 20% Mn/Fe_2O_3) catalysts (1 g) were studied using a stainless steel fixed bed reactor. All catalysts were reduced in pure hydrogen at 350 °C for 20 hours. The FTS reaction was carried out at 270 °C at a pressure of 10 bar, flow rate of 30 ml/min and a H_2:CO ratio equal to 2. The FTS calculations i.e. the activity and selectivity calculations commenced after 24 hours and the time on stream of the catalyst was approximately 120 – 140 hours. Even after 140 hours on line the catalysts were still showing minor deactivation.

3.3.1 Effect of Mn loading on the activity of impregnated catalysts

The activities of the catalysts with 5%, 10% and 20% Mn loading, expressed as the percentage of CO conversion during the time on stream, is shown in Figure 3.12. All three catalysts showed a rapid change in conversion during the first 10 hours on stream, typical of FT catalysts. The activity then stabilised. As can be seen all three catalysts stabilised at about 60-70% CO conversion. Thereafter the catalyst activity kept reasonably stable for another 50 hours before all three catalysts showed slow deactivation. There is a dip in CO conversion at approximately 75 hours. This is due to the draining of the oil and wax traps.

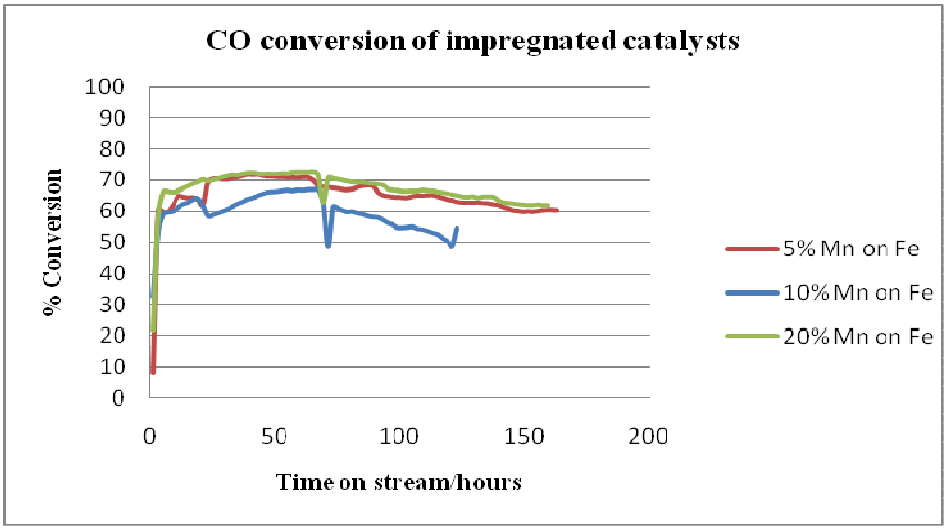


Figure 3.12: Activity of catalysts with varying loadings of manganese.

The remarkable feature is that the three catalysts with quite different iron content showed the same CO conversion abilities. Further they all deactivated at about the same rate. This initially is unexpected. There are two possible explanations for the data:

(1) In Fe_2O_3 most of the Fe is in the bulk and thus the 'active' Fe used in FT constitutes only a small proportion of the total Fe content. If the Mn acted as not to alter the surface area of the active iron, then the active iron content would remain constant even with increased Mn promotion.

(2) The Mn could act as a promoter to the iron. Thus addition of Mn would result in a higher activity of each Fe site. Thus less sites could generate the enhanced CO conversion.

These effects can be detected by various techniques. The surface Fe content could be detected by surface techniques. The promoter effect could be determined (possibly) by monitoring the catalyst selectivity. Das *et al.*[4] reported that Fe-Mn-K catalysts promoted with 17%-33% mol manganese can improve the activity of unsupported catalysts. However, they used the co-precipitation method to incorporate manganese into the catalyst.

3.3.2 FT selectivity of the impregnated catalysts

The effect of manganese loading on the product selectivity is shown in Table 3.6. The selectivity data has been calculated as the mass wt % in the total hydrocarbon product. The catalysts selectivities can be compared since the CO conversion of all three catalysts are similar.

For all the impregnated catalysts the most notable feature is the similarity of the selectivities. All the changes in selectivity are minimal. This must be due to the weak interaction between the iron and manganese since the impregnation method deposits

manganese onto the surface of the Fe_2O_3. Manganese is known to enrich the surface of the catalyst and increase the basicity allowing for chain growth to continue. It may be possible that even after the manganese loadings are increased considerably (5% to 20%) the basicity has not changed dramatically and therefore the shift in selectivity to heavier hydrocarbons is not very big.

Table 3.6: FTS performance of impregnated catalysts (IWIM) at iso-conversion of 67%

Mn loading (%)	**5**	**10**	**20**
CO conv. %	66.0	59.8	67.8
Rate CO (mol/min)	3.58×10^{-4}	3.21×10^{-4}	4.06×10^{-4}
Rate CO_2 (mol/min)	7.29×10^{-5}	5.12×10^{-5}	7.22×10^{-5}
Rate FT	2.84×10^{-4}	2.7×10^{-4}	3.34×10^{-4}
Activity/ µmol/min.g_{Fe}	357.8	321.4	406.7
α 1	0.51	0.56	0.53
HC distribution (mass %)			
C_1	16.1	13.9	13.9
$C_2 – C_4$	43.8	43.3	40.7
$C_5 – C_{11}$	21.5	27.6	27.7
C_{12} +	18.6	17.9	20.7
C_2 olefin % in $total_{HC}$	6.7	7.7	6.1
$(C_2 – C_4)^{=}/(C_2 - C_4)^0$ (mass %)	76.0	78.2	73.8
CO_2 %	6.2	4.7	6.1

Reaction conditions : T = 270 °C, 30 ml/min, P = 10 bar, H_2/CO = 2, 1 g catalyst

3.3.3 Methane selectivity

Figure 3.13 shows the effect of increasing manganese content on the selectivity to methane. As Mn content increased from 5% to 10% formation of methane was suppressed but changing from 10% to 20% Mn did not affect the methane selectivity. This effect has been reported in the literature previously.[7, 8] This is due to the decreased selectivity to lighter hydrocarbons and an increased selectivity to heavier hydrocarbons with increasing manganese content.

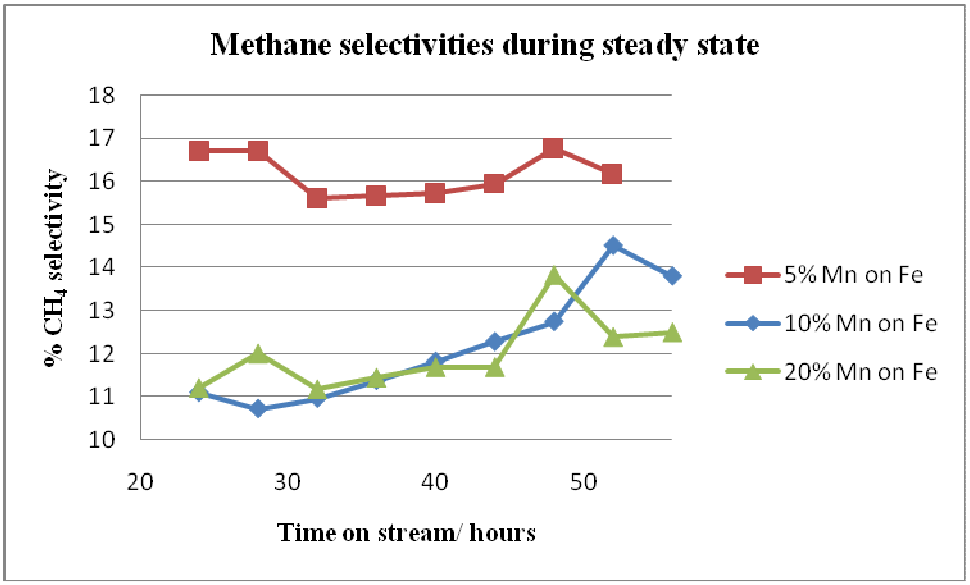


Figure 3.13: Effect of manganese content on methane formation for impregnated catalysts.

3.3.4 Olefin formation

The effect of manganese on the olefin selectivity of the catalysts are studied at the same CO conversion. The o/p ratios were calculated for the $C_2 - C_5$ hydrocarbons. The olefin selectivity increased with ascending carbon number for all loadings of manganese. In most cases the C_4 hydrocarbon showed the highest selectivity to olefins. The 10 wt% Mn/Fe_2O_3 catalyst has the highest selectivity to C_2 olefins with

60% compared to 50% for the 5 wt% and 20 wt% catalysts. For the C_3 – C_5 hydrocarbons the 5 wt% catalyst has the slightly higher selectivity.

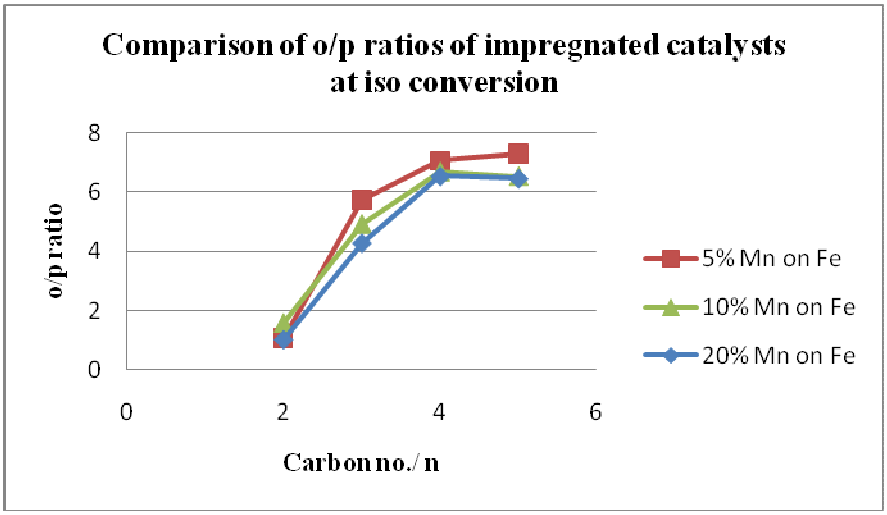


Figure 3.14: Effect of manganese content on olefin selectivity of impregnated catalysts.

3.4 Addition of Mn promoter - Co-precipitation (co-ppt) method

Catalysts with loadings of 5%, 10%, 20% and 50 wt% Mn on iron were prepared via the co-precipitation method. The catalysts were characterized using various techniques and the results are shown here.

3.4.1 Transmission electron microscopy

The TEM images shown in Figure 3.15 indicate the effect the manganese promoter has on the structure and morphology of the catalysts. The TEM images were recorded after calcination of the samples at 350 °C. From the TEM images it can be seen that as the manganese loading increases the particle size decreases. With a 5% Mn loading the particle size is approximately 15-20 nm. The TEM images show that as the manganese loading increases the particles coagulate. The clusters that form in the co-precipitated catalysts are made up of very tiny particles of approximately 5 – 7 nm [Figure 3.15(b) and (c)]. This indicates that the manganese plays a role as a structural promoter of iron. These results correspond well with the BET results which show a huge increase in the surface area due to the presence of these tiny particles [see 3.4.2].

For the 50% Mn catalyst calcined at 350 °C we notice a change in morphology. Figure 3.15d shows the presence of rod like structures. These rod-like structures may be due to an excess amount of manganese which has not interacted strongly with iron due to the low calcination temperature used. These rod–like structures are a common morphology of MnO_2 pyrolusite which may have formed.[9] An XRD powder pattern for this catalyst could not be obtained probably due to the poorly crystalline nature of the material or the crystallites being too small. The catalyst was then calcined at 650 °C and the image shown in figure 3.15e was obtained. The image shows that the catalyst now has a spherical morphology and that the particle size has increased to approximately 70 nm in size due to sintering of the particles.

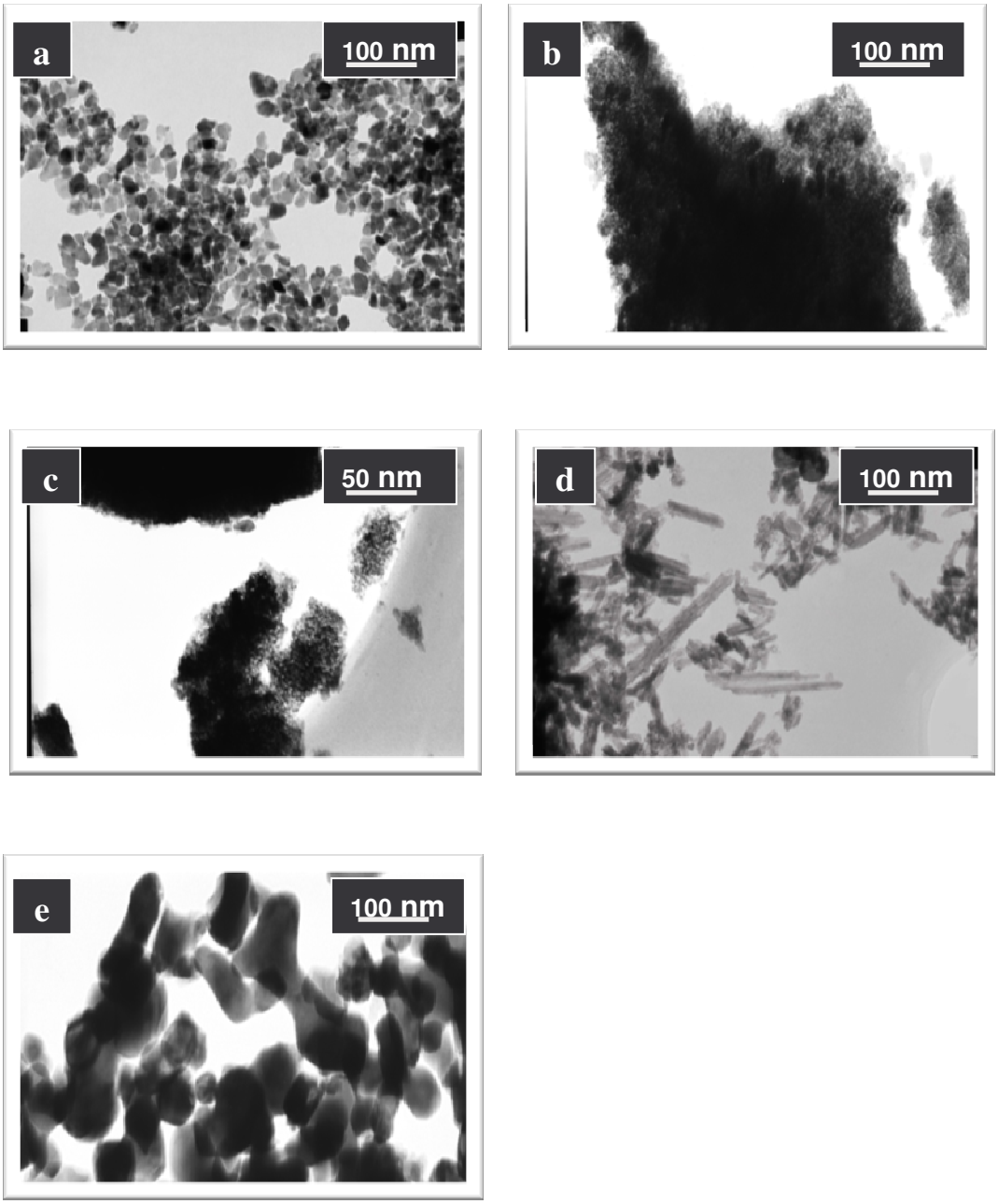


Figure 3.15: TEM images showing particle size and morphology of a) 5% Mn, b) 10% Mn, c) 20% Mn, d) 50% Mn calcined at 350 °C and e) 50% Mn calcined at 650 °C.

3.4.2 Surface area measurements (BET)

The results are shown in Table 3.7 and reveal the effect of manganese on the surface area and porosity of the catalyst when prepared by the co-precipitation method.

The general trend that we see from the table is that as the amount of manganese added becomes larger the surface area of the catalyst increases with the exception of the 50% Mn catalyst. Although the 50% catalyst has a high surface area there is a decrease in surface area when compared to the 20% catalyst. This may be due to the large amount of manganese which has not interacted with the iron and formed the rod like structures as seen in the TEM images. Therefore 20% Mn loading is the preferred loading for obtaining a Mn/Fe material with high surface area. There is also a large decrease in pore size and a significant increase in the pore volume as the manganese content is increased. The increased porosity leads to the increased surface area. According to Li *et al.*[2] the manganese promoter has a 'strong interaction' with the iron oxide and prevents agglomeration of the iron oxide particles during calcination thereby increasing dispersion of the iron particles. Manganese is also known to cause a decrease in the iron crystallite size which leads to an increase in surface area.[10] This means that manganese does not only act as a chemical promoter but as a structural promoter as well.

Table 3.7: Surface areas of co-precipitated FeMn catalysts.

Mn loading in Fe	Surface area (m^2/g)	Pore diameter (nm)	Pore volume (cm^3/g)
Fe_2O_3	24	12	0.074
5% FeMn	39	10	0.10
10% FeMn	114		
20% FeMn	160	4	0.17
50% FeMn	133	5	0.18
50% FeMn cal 650 °C	6	44	0.073

3.4.3 Powder X-ray diffraction

The powder patterns of the co-precipitated catalysts are compared in Figure 3.16 and the effects of manganese on the catalyst structure and types of phases present are shown.

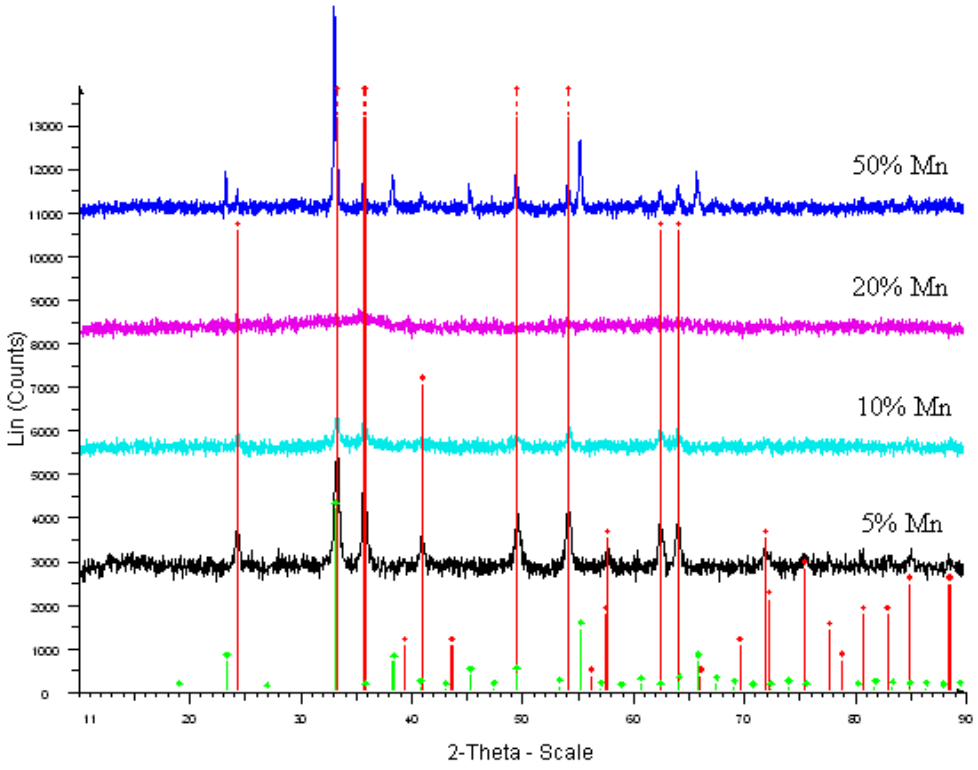


Figure 3.16: Powder patterns showing appearance of a Fe-Mn mixed oxide phase with increased loading of Mn (calcinations temperature = 350 °C; except for 50% Mn loaded sample calcined at 650 °C). The red lines represent the pure haematite pattern and the green lines a FeMn mixed oxide. These were obtained from the EVA software package database.

The powder pattern of the catalyst with 5% Mn has a single pure haematite phase present. No peaks due to MnO_x were observed. This catalyst has fairly broad peaks but they are much more intense than those peaks detected for the 10% Mn catalyst. The peaks broaden with increased manganese addition and this indicates that the manganese reduces the iron crystallite size. The powder pattern for the 20% Mn catalyst has no visible peaks which may be due to the iron crystallite size being too small for diffraction to occur. These results correlate with the BET results where a

large increase in surface area as manganese promotion increased was noticed. The powder pattern for the catalyst calcined at 350 °C could not be obtained as the crystallite size may be too small. The powder pattern obtained for the 50% Mn catalyst was that of the catalyst which had been calcined at 650 °C. The powder pattern shows the presence of two phases i.e. the iron haematite phase as well as a FeMn solid solution mixed oxide β–$(Mn_{1-x}Fe_x)_2O_3$ phase with x = 0.017. Similar results have been reported for samples in which the two phases exist in almost equal amounts.[4] The PXRD results clearly indicate the effect the preparation method has on the structure of the catalyst.

3.4.4 Temperature programmed reduction

Figure 3.17 compares the reduction behaviour of the co-precipitated catalysts with varying amounts of manganese. As the manganese amount is increased from 5% to 50 % the emergence of a peak at approximately 350 °C is noticed. The peak at 422 °C which is attributed to the reduction of Fe_2O_3 tends to get sharper as the manganese is increased from 5% to 50%. This suggests that the manganese may be acting as a structural promoter and thereby reducing the iron crystallite size. By reducing the iron crystallite size the reduction step is much faster therefore the reduction peak is much sharper. This also indicates that manganese may be incorporated into the iron lattice in co-precipitated catalysts and not just deposited on the surface of the iron. As mentioned before, the formation of a mixed oxide even at low loadings of manganese cannot be ruled out.

Although it is uncertain that a mixed oxide phase has been formed in the catalysts with 5% to 20% Mn loading, the effect of manganese on the reduction of the catalyst can be seen. For the 50% catalyst calcined at 650 °C we notice a shift of peaks to the right and the peaks become broad. The reduction now only occurs in two steps. This indicates that a mixed oxide has been formed and that the manganese suppressed the reduction of the iron. This may be due to a strong interaction between the manganese and iron particles which retards the adsorption of hydrogen. Therefore the calcination temperature affects the structure of the catalyst as well as its reduction behaviour.

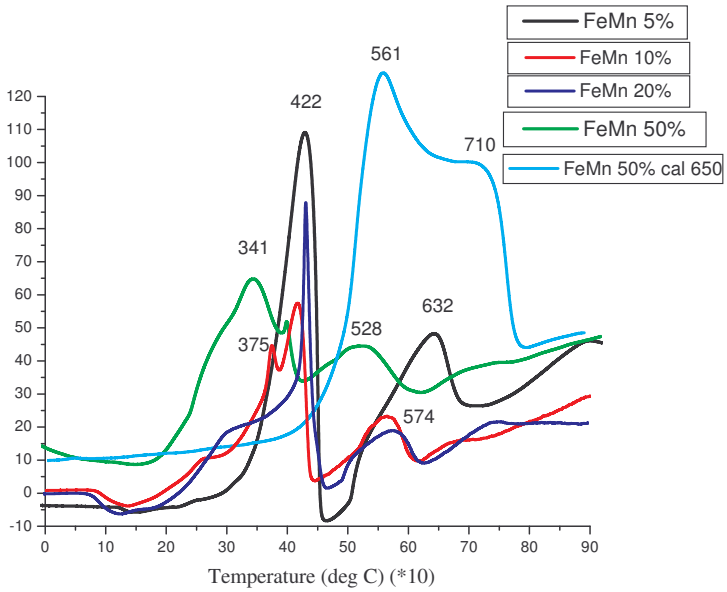


Figure 3.17: TPR profiles of the co-precipitated catalysts with Mn loadings of 5% to 50%.

Table 3.8: data showing temperatures at which reduction occurs for the TPR profiles shown in Figure 3.17

Catalyst	Temperature/ °C	Reduction
5% FeMn co-ppt	422	$Fe_2O_3 \rightarrow Fe_3O_4$
	632	$Fe_3O_4 \rightarrow Fe$
10% FeMn co-ppt	250, 375	$MnO_2 \rightarrow Mn_2O_3 \rightarrow MnO$
	422	$Fe_2O_3 \rightarrow Fe_3O_4$
	574	$Fe_3O_4 \rightarrow Fe$
20% FeMn co-ppt	422	$Fe_2O_3 \rightarrow Fe_3O_4$
	574	$Fe_3O_4 \rightarrow Fe$
50% FeMn co-ppt	341	$MnO_2 \rightarrow Mn_2O_3/MnO$
	400	$Fe_2O_3 \rightarrow Fe_3O_4$
	528	$Fe_3O_4 \rightarrow Fe$
50% FeMn cal 650 °C	561	$Fe_2O_3 \rightarrow Fe_3O_4$
	710	Reduction of β–$(Mn_{1-x}Fe_x)_2O_3$

3.5 FT performance of co-precipitated catalysts

3.5.1 Effect of Mn loading on the activity of co-precipitated catalysts

The activities of the co-precipitated catalysts with 5, 10, 20 and 50 wt% loadings of manganese are shown in Figure 3.18. The activity is expressed as the percentage of CO conversion during the time on stream.

In Figure 3.18 the CO conversions of the co-precipitated catalysts are compared. Figure 3.18 indicates that all the catalysts have a high and reasonably stable activity after 10 hours on stream. The CO conversions then remain moderately stable for approximately 79 hours (5%, 10% and 20% Mn loaded catalysts) before the CO conversion commences to decrease. It is clear that the catalysts are not stable with time. This suggests sintering or conversion of the active catalyst sites with time. Interestingly for the 50% Mn loaded catalyst the CO conversion increases with time.

It is noticed that as the manganese content is increased the activity of the catalyst decreases with the exception of the 10% FeMn catalyst which has the highest activity (80%). Thus 10% loading may be the optimum amount of Mn needed to increase the activity of the catalyst. Li *et al.*[7] also reported that an appropriate amount of manganese (Fe/Mn weight ratio of 100/7) could lead to an increase in activity but that excessive amounts (Fe/Mn weight ratio 100/20) reduce activity due to the enrichment of manganese at the surface of the catalyst which hinder the formation of iron carbides.

With the increase in manganese the deactivation becomes less severe i.e. the drop in percentage CO conversion is reduced. As the Mn content is increased to 50% the CO conversion decreases and catalyst has the lowest activity. However, the catalyst shows a steady increase in activity over the time period. Thus manganese decreases the activity but increases the stability of the catalysts.

Li *et al.*[7] have found similar results. The manganese has a strong interaction with iron and stabilises the iron carbides and prevents its reoxidation to Fe_3O_4 which may be responsible for the drop in activity. Thus the carburization of the catalyst is improved as the manganese content increases and this may cause stabilisation or even increase in activity.[7]

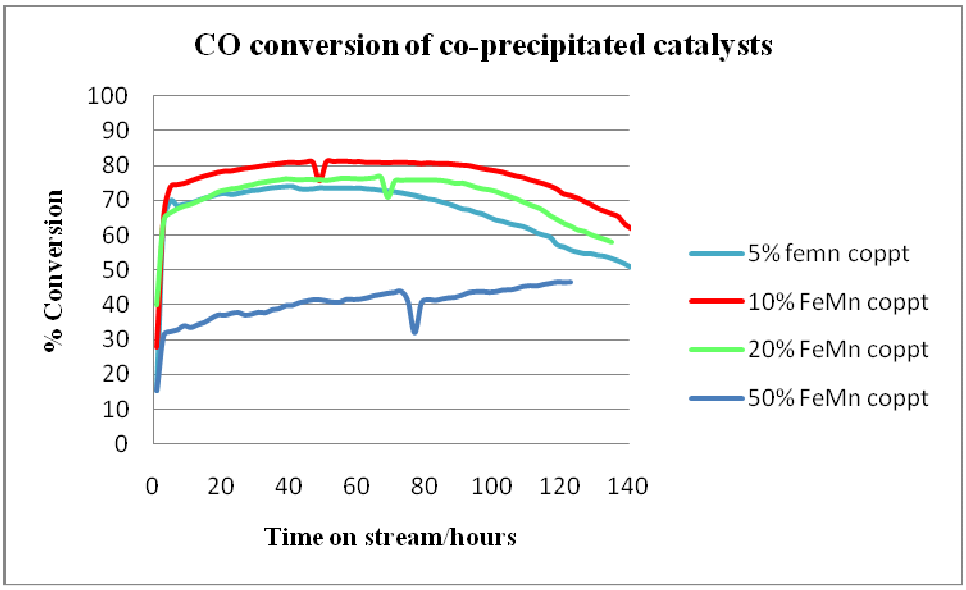


Figure 3.18: Activity of catalysts with varying loadings of manganese.

3.5.2 Selectivity of co-precipitated catalysts: effect of Mn loading

The CO conversion or activity of the catalyst affects the selectivity of the catalyst. The 5%, 10% and 20% loaded catalysts have similar CO conversion and hence their selectivities can be compared and the effect of the promoter on selectivity can be studied. For the co-precipitated catalysts, an increase in the alpha value as the manganese content increases from 5 wt% to 20 wt% i.e. from 0.46 to 0.6 is seen. As expected the selectivity to methane and $C_2 - C_4$ decreases whereas there is a increase in selectivity to slightly heavier hydrocarbons in particular the oil fraction $C_5 - C_{11}$. This occurs because the Fe-Mn interaction is much stronger in the co-precipitated catalyst and as the loading of manganese increases the basicity at the surface of the catalyst increases leading to more dissociative adsorption of CO and increased

selectivity to longer hydrocarbon chains. The 50% loaded catalyst has a much lower activity compared to the 5%, 10% and 20% catalysts and this may be due to it having the lowest iron content.

Table 3.9: FTS performance of co-precipitated catalysts (CO-PPT) at iso-conversion of 74 %

Mn loading (%)	**5**	**10**	**20**	**50**
CO conv. %	66.4	76.9	72.1	41.9
Rate CO (mol/min)	3.87×10^{-4}	4.7×10^{-4}	4.7×10^{-4}	2.2×10^{-4}
Rate CO_2 (mol/min)	8.45×10^{-5}	9.23×10^{-5}	8.24×10^{-5}	2.74×10^{-5}
Rate FT	3.0×10^{-4}	3.8×10^{-4}	3.9×10^{-4}	2.0×10^{-4}
Activity/ µmol/min.g_{Fe}	387.0	470.7	474.6	224.2
α 1	0.49	0.47	0.60	0.63
HC distribution (mass %)				
C_1	16.4	15.7	12.7	14.4
$C_2 - C_4$	47.7	50.3	41.0	40.9
$C_5 - C_{11}$	19.4	20.8	32.4	30.1
C_{12} +	16.4	13.1	16.2	17.8
C_2 olefin % in $total_{HC}$	7.9	8.4	7.0	3.8
$(C_2 - C_4)^{=}/(C_2 - C_4)^{0}$ (mass %)	76	79.3	78.2	62.7
CO_2 %	7.22	7.83	6.85	2.28

Reaction conditions : T = 270 °C, 30 ml/min, P = 10 bar, H_2/CO = 2, 1 g catalyst

3.5.3 Methane selectivity

Figure 3.19 shows the effect of increasing manganese content on the selectivity to methane. As Mn content increases from 5 wt% Mn to 20 wt% Mn the formation of methane is suppressed. Similar effect for Mn added to Fe catalysts have been reported in the literature.[8, 12] This is due to the decreased selectivity to lighter hydrocarbons and increased selectivity to heavier hydrocarbons with increasing manganese content.

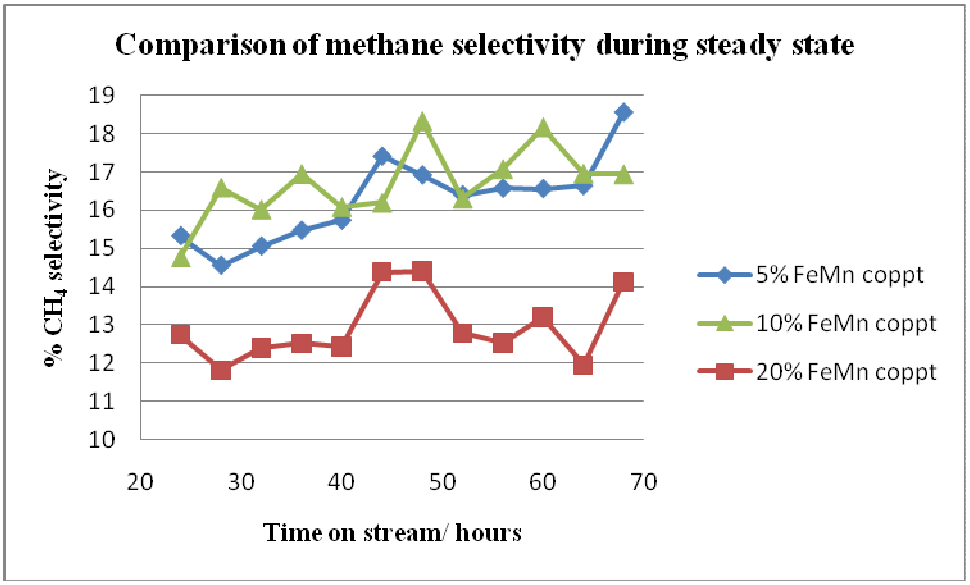


Figure 3.19: Effect of manganese content on methane formation for co-precipitated catalysts.

3.5.4 Olefin formation

The co-precipitated catalysts show that as the carbon number increases the olefin /paraffin ratio hardly changes. The C_4 hydrocarbon has the highest olefin selectivity. In this case the 10 wt% Mn catalyst has the highest selectivity to olefins for the C_2 – C_5 range. There is not much difference in the olefin selectivities of the 5 wt% and 20 wt% catalysts. This again indicates that there is an optimum loading of manganese needed to achieve the highest activity and best selectivity to lower molecular weight olefins in the C_2 – C_5 range. An increased amount of manganese (20%) may lead to

lower selectivity to the $C_2 - C_5$ due to its increased selectivity to heavier molecular weight hydrocarbons. .

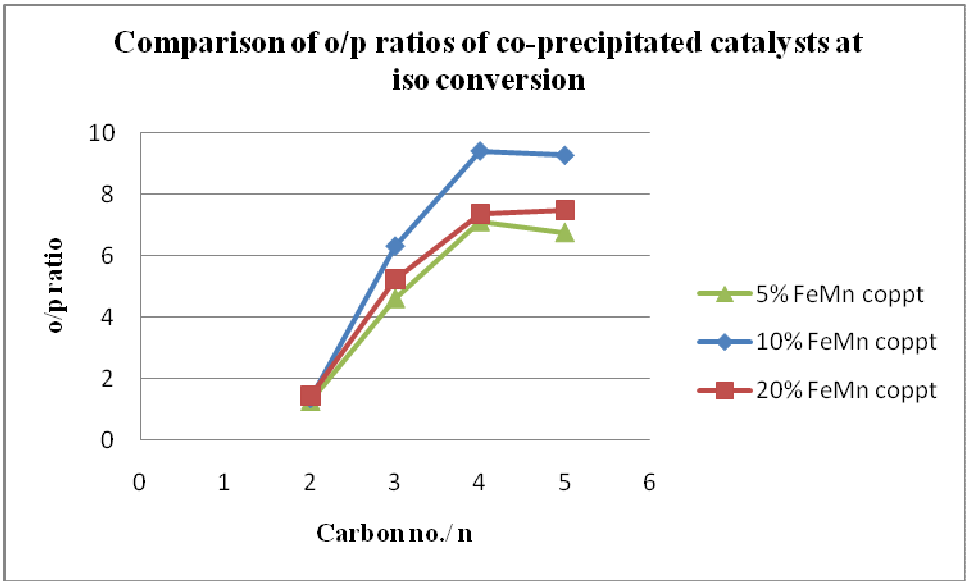


Figure 3.20: Effect of manganese content on olefin selectivity of co-precipitated catalysts.

3.6 Effect of preparation method: Comparison of impregnated and co-precipitated catalysts

This section gives a summary of the results presented in chapters 3.2 to 3.5 and discusses the effect that the preparation method has on the structure and morphology of the catalyst and its effect on the FT performance of the catalyst. The effect of Mn loading on the catalyst structure when prepared by the two methods and its effect on the activity and selectivity in the FT reaction is also compared.

The effect of the Mn loading on the structure and morphology of the catalyst can be seen in the TEM images. The impregnated catalysts with low loadings of manganese (5 wt%) have particles sizes of approximately 30-35 nm. As the Mn loading is increased (20 and 50 wt%) clusters form. The co-precipitated catalysts also form clusters as the Mn loading increases but these clusters are made up of much smaller particles (5-7 nm). Thus in the co-precipitated method the manganese acts as a structural promoter and decreases the iron crystallite size and increases dispersion. This can be confirmed by the surface area measurements which show a huge increase in surface area. This result is in contrast to the results obtained for the impregnated catalysts in which increased manganese promotion caused a decrease in the surface area of the catalysts. This technique clearly indicates the effect of the preparation method on the structure of the catalyst. The XRD patterns obtained also suggest that different phases of iron and manganese can be present in the catalyst when a particular preparation method is used. A mixed oxide is formed in addition to the haematite phase in the co-precipitated catalyst and a manganese oxide phase is present together with the iron phase in the impregnated catalyst. However, these phases are only present in the 50 wt% Mn catalyst when prepared by both methods. The TPR results indicate that the reduction of iron is suppressed (i.e. peaks shift to higher temperatures) as the manganese loading is increased for the impregnated catalysts. However, for the co-precipitated catalyst it is noticed that the reduction of the haematite remains at 422 °C but as the Mn loading increases the reduction peak gets sharper i.e. the iron is reduced quickly due to the decreased crystallite size of the iron.

The incipient wetness impregnation method and the co-precipitation method also affect the activity and selectivity of the Fe-Mn catalysts in different ways. The activities of the catalysts prepared by the co-precipitated and impregnated methods are compared in Figure 3.21. Only those with 5% and 10% Mn loadings are shown. The co-precipitated catalysts have a higher activity than the impregnated catalysts with the 10% FeMn co-precipitated catalyst having the highest activity. These results are as expected and have been previously reported in the literature.[2] This is because the manganese has a stronger interaction with the iron when prepared by the co-precipitation method. The addition of Mn decreases the crystallite size of the iron and increases dispersion thus increasing the surface area and creating more active sites for the FTS reaction. The co-precipitated catalyst, after an increase in Mn content, is stable for a longer period before deactivation begins when compared to data for the impregnated catalysts. However, the 5% impregnated catalyst has a smaller drop in CO conversion when deactivation begins and seems to become more stable than the co-precipitated catalysts after 140 hours of time on stream.

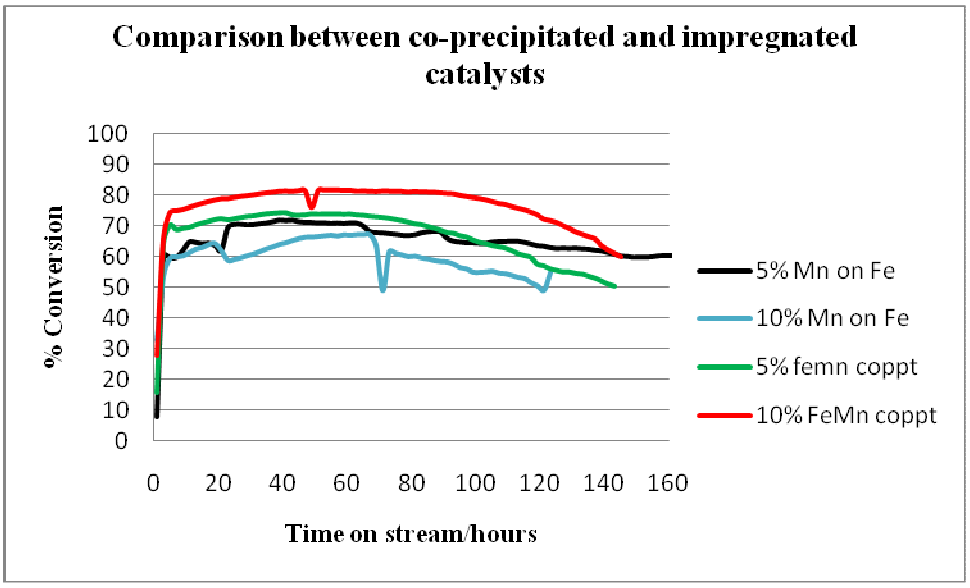


Figure 3.21: Activities of the catalysts prepared via the co-precipitation and impregnation methods with 5% and 10% Mn loading.

Comparing the selectivities of impregnated and co-precipitated catalyst with Mn 5 wt% and 10 wt% loadings the shift towards heavier hydrocarbons (i.e. C_5+ oils and waxes) is bigger in the impregnated catalysts than in the co-precipitated catalysts. This is because the manganese enriches the surface of the catalyst in impregnated catalysts which makes the surface basicity much greater than in co-precipitated catalysts. In the latter samples the manganese is acting more as a structural promoter. With excessive Mn loadings (20 wt% and 50 wt%) the selectivity to C_5+ hydrocarbons are similar for both preparation methods since manganese enriches the surface in both cases and therefore the basicity is also similar.

3.7 Characterization of microwave heated catalysts

The effect of microwave heating on the Mn/Fe catalysts was studied using characterization techniques such as TEM, BET, H_2 – TPR and PXRD. The results have been compared with the non-microwaved catalysts. From our previous study on the effect of preparation method on the structure and FT performance of Fe-Mn catalysts, it was found that the Fe-Mn catalyst with a 5 wt% loading of manganese prepared by the incipient wetness impregnation method and the Fe-Mn co-precipitated catalyst with a 10 wt% loading of Mn gave the best FT results. The best activity and selectivity to lower molecular weight hydrocarbons (C_2 – C_4), the highest selectivity to olefins and the least selectivity to heavier molecular weight hydrocarbons was noted for the catalysts. Therefore these catalysts were chosen to study the effect of microwave heating on the Mn/Fe catalysts and whether the microwave effect would enhance the catalyst selectivities. This was the main objective of this study.

3.7.1 Characterization of microwave heated impregnated catalysts

The 5 wt% Mn/Fe_2O_3 catalyst was heated in a commercial microwave oven with a power level setting of 450 W. The catalyst was heated for 10 s. The catalyst was characterized and data compared with the non-microwave heated catalyst.

Transmission electron microscopy

The TEM images of the catalyst before and after microwave heating are shown in Figure 3.22 (a) and (b) respectively. The particles have the same morphology and size. It can be seen from these TEM images that there is no change in particle size after microwave heating. Previous work done by Linganiso[11] showed that microwave heating at 540 W for 8 s caused a growth in particle size of an unsupported iron catalyst and a potassium promoted iron catalyst. This was attributed to agglomeration of particles, however, this did not occur in this case i.e. in the presence of Mn. It is

possible that the power level may be too low to have had any effect on the size of the catalyst particles.

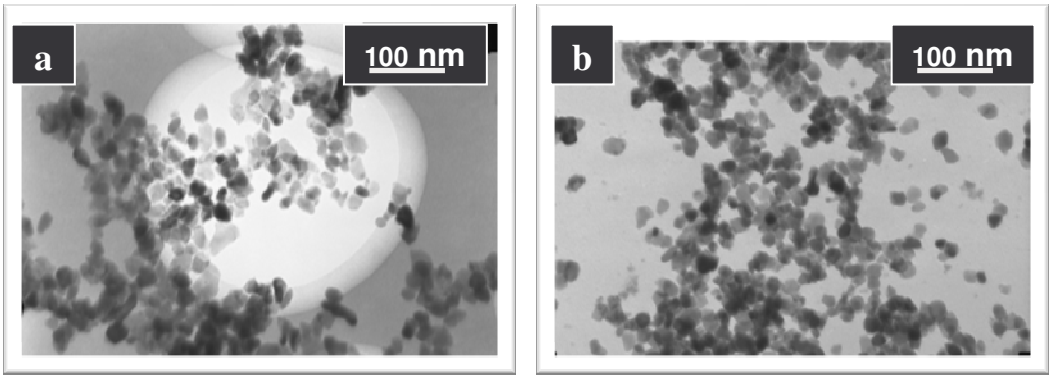


Figure 3.22: TEM images comparing the 5 wt% Mn impregnated catalysts a) before microwave heating, b) after microwave heating at 450 W for 10 s.

Surface area measurements (BET)

The surface area, pore sizes and pore volumes were studied before and after microwave treatment. The results are compared in Table 3.10. From the table it is seen that the surface areas of the 5% Mn/Fe_2O_3 catalyst remains the same after microwave heating indicating that the heating did not have any effect on the surface area nor the pore size of the catalyst. This result correlates with the TEM results where there is no change in particle size. Linganiso[11] reported a small decrease (43 m^2/g to 37 m^2/g) in surface area after microwave heating due to agglomeration of iron particles.

Table 3.10: Data showing BET measurements before and after microwave heating

Mn loading in Fe	Surface area (m^2/g)	Pore diameter (nm)	Pore volume (cm^3/g)
5% Mn/ Fe_2O_3	21.4	7.8	0.051
5% Mn/Fe_2O_3 MW (450 W)	20.5	7.5	0.040

Powder X-ray diffraction

The powder patterns before and after microwave heating were compared. Figure 3.23 shows the powder patterns of 5% Mn/Fe_2O_3 (a) before microwave heating and (b) after microwave heating. It is noted that the patterns show the presence of the haematite phase and are very similar. It seems as if the microwave heating did not have any effect on the structure of the catalyst. The crystallite sizes were measured and are similar (Table 3.11) for the microwaved and non-microwaved catalysts. Therefore microwave heating did not cause a growth in the crystallite size of the iron.

Table 3.11: Crystallite sizes of the catalyst before and after microwave heating.

Catalyst	Peak position/ 2θ	Crystallite size/ nm
5% Mn/ Fe_2O_3	33.2	19
	35.8	30
5% Mn/ Fe_2O_3 - MW	33.3	19
	35.8	33

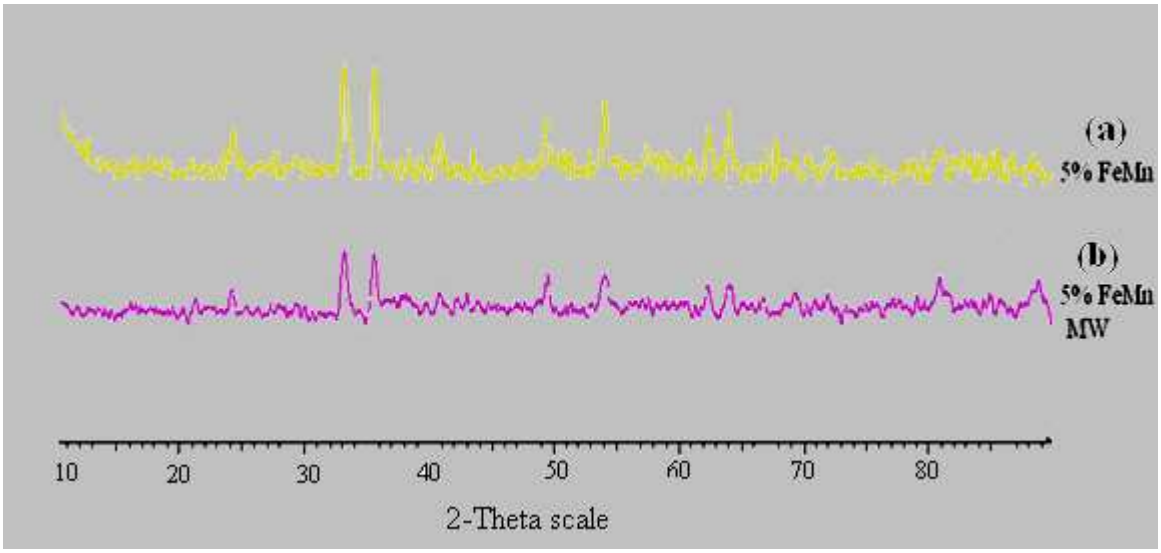


Figure 3.23: Powder patterns of the impregnated catalysts (a) before and (b) after microwave heating. Note that these patterns were background subtracted and smoothed to remove noise due to the fluorescence of the iron. This was done using the EVA software package.

Temperature programmed reduction

The reduction behaviour of the impregnated catalysts before and after microwave heating is shown in Figure 3.24. The reduction occurs in four steps for the microwaved and non-microwaved catalysts. Both samples show very similar reduction temperatures with the reduction of manganese occurring at 240℃ and 341 °C and the reduction of Fe_2O_3 and Fe_3O_4 taking place at 460 °C and 630 °C respectively. It can be seen that the microwave did not have any significant effect on the reduction behaviour of the catalyst.

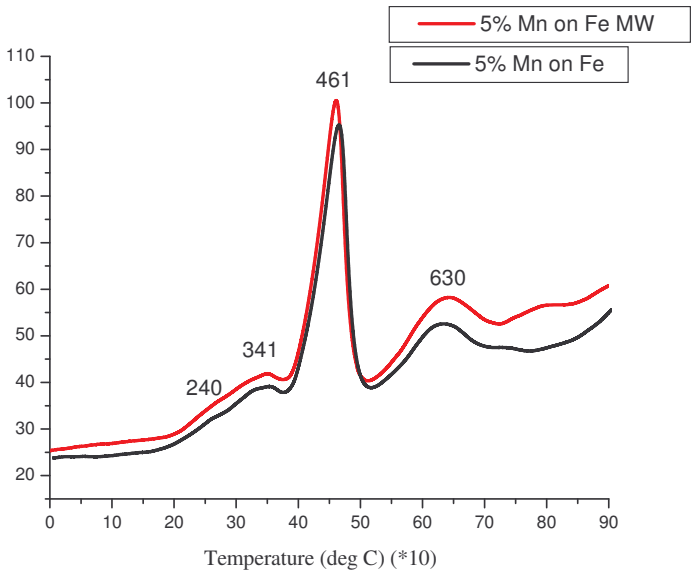


Figure 3.24: Profile of 5% Mn/Fe_2O_3 impregnated catalyst before and after microwave heating.

3.7.2 FT performance of the microwave heated impregnated catalysts

Effect of microwave heating on the activity of catalysts

Catalysts with a 5 wt% loading of manganese prepared by the impregnation were heated in a microwave oven at 450 W for 10 s. The activity of the catalysts was compared before and after microwave heating (Figure 3.25). From the plot it is seen that there is a slight decrease in activity after microwave heating. Linganiso[11] reported a drop in activity (by ~5%) after microwave heating of a supported iron catalyst and attributed the effect to an increase in iron particle size. From the characterization results however, there was no increase in particle size for these particular catalysts. Calcination is known to cause manganese to migrate to the surface of the catalyst.[13] Thus it is possible that after microwave heating manganese migrates and enriches the surface of the catalyst, reducing the amount of iron at the surface and this can suppress carburization of the iron catalyst causing a slight drop in activity with time as seen in Figure 3.25.[7]

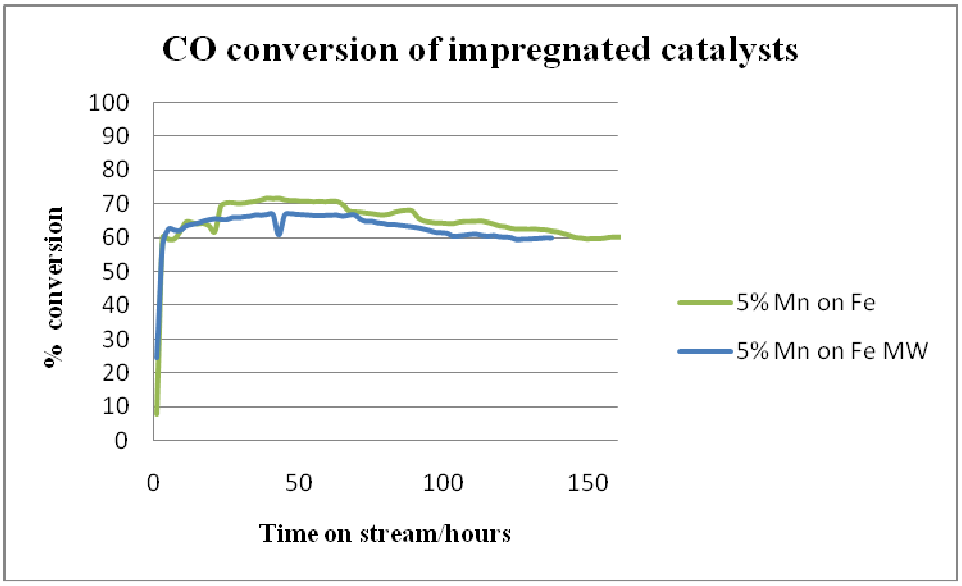


Figure 3.25: Activity of 5 wt% Mn impregnated catalysts before and after microwave heating.

Effect of microwave heating on selectivity of impregnated catalysts

The microwave heating caused a little change in the selectivity in the impregnated catalysts (Table 3.12). The non–microwave heated catalyst can be compared to the microwave heated catalyst as the CO conversions were similar.

After microwave heating of the catalyst there is no change in the alpha value and it remains as 0.51. Microwave heating led to no change in methane formation, but a slightly greater selectivity to lower molecular weight hydrocarbons in particular the C_2 – C_4 range and lower selectivity to heavier molecular weight hydrocarbons i.e. C_{12}+ hydrocarbons. The microwave heated catalysts also showed a slight increase in olefin formation particularly the C_2 hydrocarbon. It is possible that these minor changes in selectivity for the impregnated 5% Mn/Fe_2O_3 catalyst occur due to the higher concentration of manganese at the surface of the catalyst which may be further enhanced due to migration of manganese to the surface after microwave heating.

Table 3.12: Comparison of FTS performance between microwaved and non-microwaved catalysts at iso-conversion.

Mn loading (%) IWIM	**5% Mn/ Fe_2O_3**	**5% Mn/ Fe_2O_3 MW**
CO conv. %	66.0	63.6
Rate CO (mol/min)	3.58×10^{-4}	3.51×10^{-4}
Rate CO_2 (mol/min)	7.29×10^{-5}	7.3×10^{-5}
Rate FT	2.84×10^{-4}	2.78×10^{-4}
Activity/ µmol/min.g_{Fe}	357.8	351.3
α 1	0.51	0.51
HC distribution (mass %)		
C_1	16.1	15.3
$C_2 – C_4$	43.8	47.7
$C_5 – C_{11}$	21.5	22.8
C_{12} +	18.6	14.1
C_2 olefin % in $total_{HC}$	6.7	8.8
$(C_2 – C_4)^{=}/(C_2 - C_4)^{0}$ (mass %)	76.0	80.1
CO_2 %	6.2	6.0

Reaction conditions: T = 270 °C, 30 ml/min, P = 10 bar, H_2/CO = 2, 1 g catalyst

Effect of microwave heating on methane formation

The effects of microwave heating on methane selectivity during the steady state are shown for the impregnated catalysts in Figure 3.26.

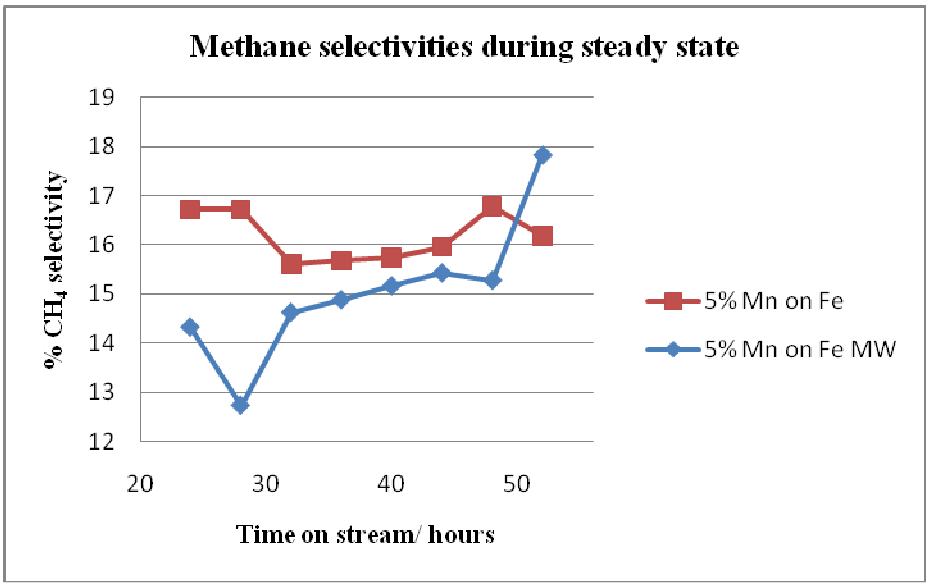


Figure 3.26: Effect of microwave heating on methane selectivity for impregnated catalysts with 5 wt% Mn loading.

A very minor decrease in methane selectivity which is quite low occurs after the catalyst has been microwave heated is noted. Manganese is known to cause the suppression of methane formation[14] and this has been proposed to be enhanced due to the microwave effect. Linganiso[11] reported a decrease in methane selectivity due to an increase in iron crystallite size after microwave heating. The catalysts used in this study showed no change in the size of the iron crystallites after microwave heating. Any changes in selectivity must be due to a stronger interaction of the microwave with the manganese promoter and stronger Fe-Mn interaction.

Olefin formation

The olefin/paraffin ratios of low molecular weight hydrocarbons (C_2 – C_5) before and after microwave heating of the impregnated catalysts are shown in Figure 3.27. The o/p ratios were compared at iso-conversion.

The catalyst showed little change in olefin selectivity after microwave heating. There is a slight increase in selectivity for the C_2 hydrocarbon. Selectivity is increased from approximately 52% to 62% after microwave heating. The olefin/paraffin ratios of the C_3 – C_5 hydrocarbons are very similar.

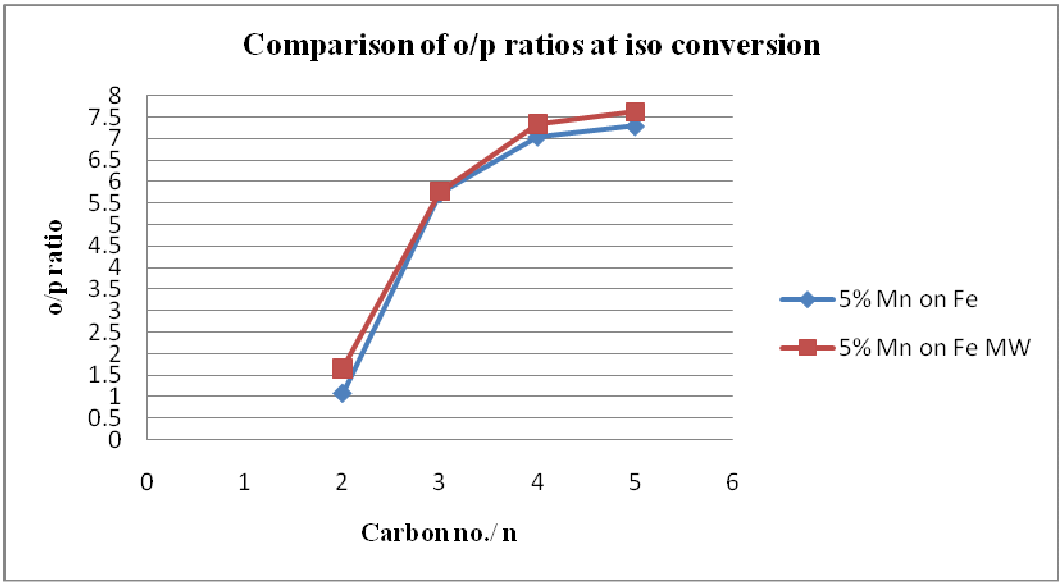


Figure 3.27: Effect of microwave heating on olefin formation for impregnated catalysts with 5 wt% Mn loading on Fe_2O_3.

3.7.3 Characterization of microwave heated co-precipitated catalysts

The effect of microwave heating was also studied on the 10 wt% FeMn co-precipitated catalyst. From the study on the impregnated catalyst it was shown that microwave heating the catalyst at 450 W for 10 s had no effect on the structure of the catalyst but some minor microwave effects were seen in the FT performance of the catalyst. Therefore, to investigate whether microwave heating had any significant effect on MnFe catalysts, the FeMn co-precipitated catalyst was studied. The catalyst was heated at a higher power level of 900 W and for a longer period of time i.e. 30 s. The results are presented below.

Transmission electron microscopy

The catalyst prepared by the co-precipitation method with a 10% Mn loading is shown in Figure 3.28 (a) before microwave heating and (b) after microwave heating. From the TEM images it is seen that the catalysts tends to form clusters. However, these clusters are made up of very tiny particles (approximately 4 – 7 nm) as well as larger spheres, most of them approximately 15-17 nm in size (figure 3.28 a). After microwave heating the clusters containing the tiny particles are still present but a slight increase in particle size of the larger spheres to approximately 25-30 nm in size (figure 3.28 b) is noted. There are many more of the larger spheres present in the microwave treated samples than in the non-microwave heated catalyst. Therefore in the case of the co-precipitated catalyst we see that microwave heating at higher power and longer periods may cause some agglomeration of the particles and a possible increase in iron particle size in some of the catalyst particles.

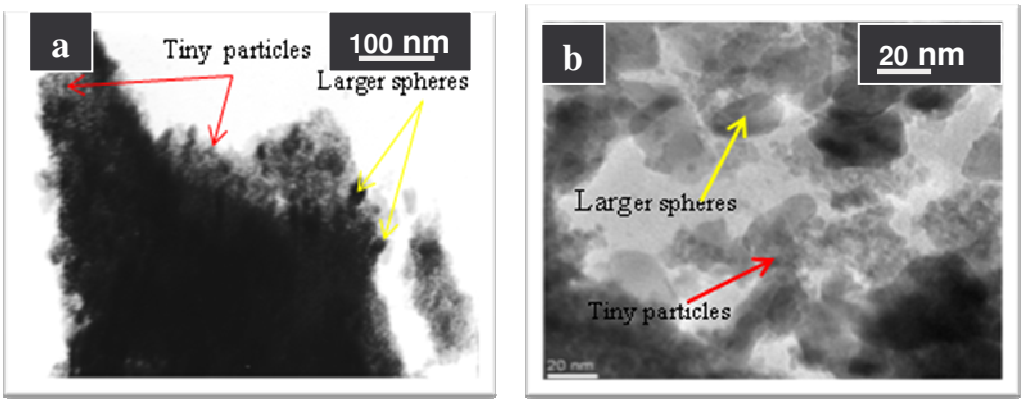


Figure 3.28: a) 10% FeMn coppt before microwave heating and b) 10% FeMn coppt microwave heated at 900 W for 30s.

Surface area measurements (BET)

The results in Table 3.13 show the effect of microwave heating on the surface area of the catalyst. For the co-precipitated catalyst there is a decrease in surface area after microwave heating. This may be due to the growth in particle size of the catalysts. The particles which then form larger ones also reduce the number of pores present. This leads to the decreased surface area. When compared to the impregnated Mn/Fe_2O_3 catalysts results obtained here may be due to the increase in power level and time at which the catalyst was microwave heated. This result correlates well with the TEM data.

Table 3.13: Surface area measurements before and after microwave heating.

Mn loading in Fe	Surface area (m^2/g)	Pore diameter (nm)	Pore volume (cm^3/g)
10% coppt	114.4		
10% coppt MW (900 W)	95	5.5	0.13

Powder X-ray diffraction

The powder patterns of the non-microwave heated and microwave heated co-precipitated catalysts are shown in Figure 3.29 (a) and (b) respectively. It seems that there is no difference in the two patterns and they both have very similar crystallite sizes (Table 3.14). This may be due to the change in particle size being too small to be detected by XRD and therefore there is not much difference in the crystallite sizes responsible for diffraction since this is a bulk characterization technique.

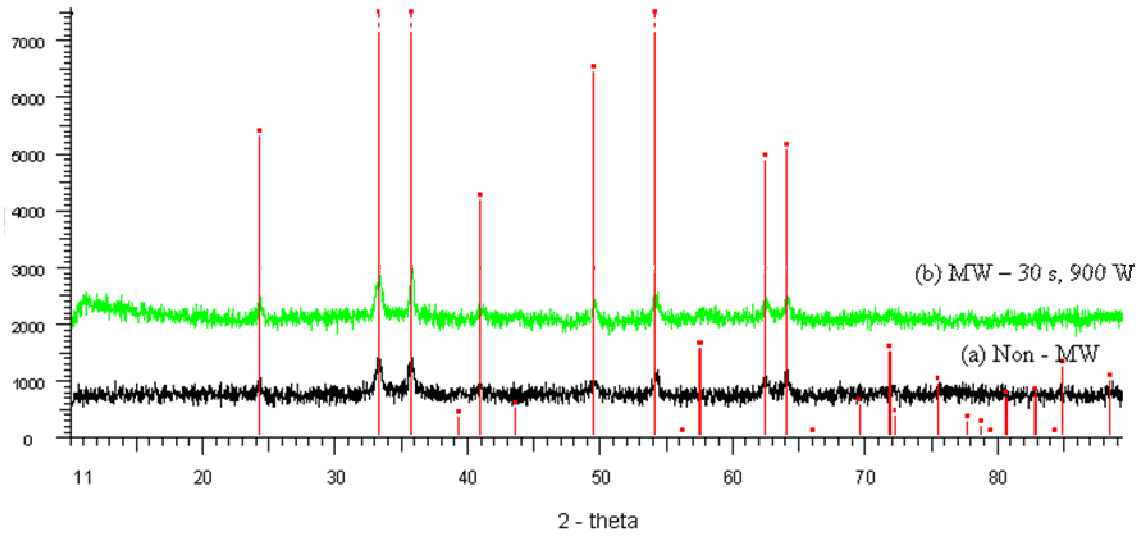


Figure 3.29: Powder patterns of the 10% FeMn co-precipitated catalysts (a) before and (b) after microwave heating.

Table 3.14: Crystallite sizes of certain peaks of catalysts before and after microwave heating.

Catalyst	Peak position/ 2θ	Crystallite size/ nm
10% FeMn co-ppt	24.1	26
	33.2	20
10% FeMn co-ppt MW	24.2	22
	33.2	20

Temperature programmed reduction

The TPR profiles for the co-precipitated microwaved and non-microwaved catalysts (Figure 3.30) are almost identical and show that microwave heating does not have an effect on the reduction behaviour of the catalyst.

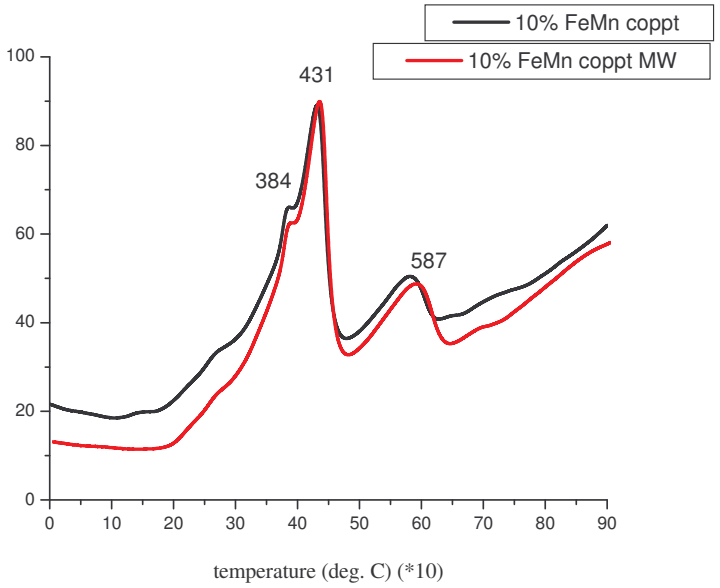


Figure 3.30: Profile of co-precipitated catalyst before and after microwave heating.

Temperature programmed surface reaction (TPSR)

The effect of microwave heating on the adsorption of CO molecules onto the surface of the catalyst was studied using the TPSR. The TPSR profiles of the 10% FeMn co-precipitated catalyst before and after microwave heating are compared in Figure 3.31.

Both the non-microwave heated and microwave heated catalyst show 2 peaks below 250 °C which are due to weakly adsorbed CO that has been desorbed. The peaks at higher temperatures are due to more strongly adsorbed CO. The non-microwaved catalyst shows a greater amount of weakly adsorbed CO than the microwave heated catalyst. There also seems to be a shift towards higher temperatures (peak at 465 °C and 584 °C) for the strongly adsorbed CO in the microwave heated catalyst. This

would suggest that the microwave heating causes the CO to bind more strongly to the surface of the catalyst. This may be the reason for the microwave heated catalyst showing a slightly higher selectivity to longer hydrocarbon chains i.e. microwave heating enriches manganese at the surface of the catalyst thereby increasing the basicity, allowing for CO adsorption and hence facilitating chain growth.

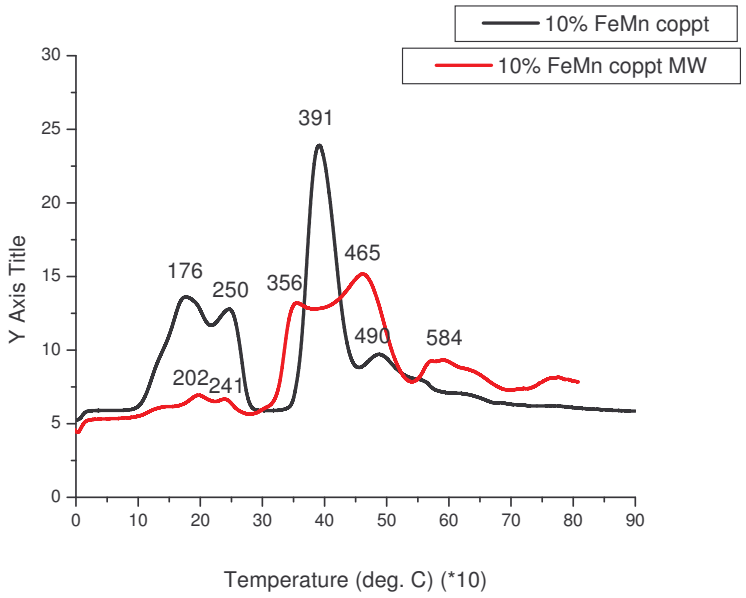


Figure 3.31: TPSR profiles of the 10% FeMn co-precipitated catalyst before and after microwave heating.

3.7.4 FT performance of microwave heated co-precipitated catalysts

Effect of microwave heating on the activity of catalysts

The activity plot for the 10 wt% FeMn coppt catalyst shows a similar trend to the 5 wt% Mn/Fe_2O_3 impregnated catalysts described in chapter 3.7.2. The microwave heated catalyst also shows a decrease in activity; the drop in CO conversion is approximately 7-8 %. The microwave heated catalyst also is more stable over the 150 hour period than the non-microwaved catalyst. The deactivation of the co-precipitated catalyst is more rapid and drops approximately by 20% in 150 hours whereas the deactivation of the microwave heated catalyst is less than 10% in 150 hours.

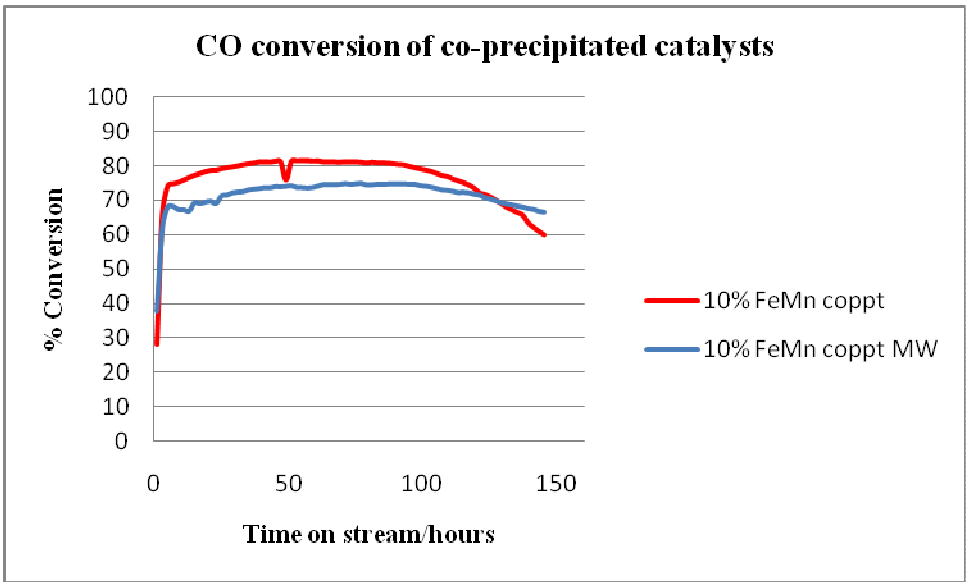


Figure 3.32: Activity of 10 wt% Mn co-precipitated catalysts before and after microwave heating at 900 W for 30 s.

From the characterization results for the 10% co-precipitated catalyst it is known that the microwave heated catalyst showed an increase in particle size of the FeMn co-precipitated catalyst. It is possible that this increase in particle size as well as the possible enrichment of manganese at the surface of the catalyst leads to the decreased activity of the microwave heated catalyst. The increase in power level and time period

for microwave pre-treatment may be responsible for the substantial increase in particle size of the catalyst and therefore the larger decrease in activity.

Effect of microwave heating on selectivity of catalysts

The selectivity data are presented in Table 3.15 and an increase in the alpha value after microwave heating is noted. The hydrocarbon distribution results show a minor change in methane production and a slightly lower selectivity to lighter molecular weight hydrocarbons (C_2 – C_4) for the microwave heated catalyst. The microwave heated catalyst shows a slight increase in selectivity to the (C_5 – C_{11}) fraction which is a mixture between the lighter and heavier molecular weight hydrocarbons. The selectivity to heavier hydrocarbons C_{12}+ remains the same after microwave heating.

The results for this catalyst are slightly different to those catalysts that were microwave heated at a lower power level and shorter time span. Microwave heating at 450 W for 10 s led to no change in the alpha value of the 5% Mn/Fe_2O_3 catalyst which is in contrast to the 10 wt% co-precipitated FeMn catalyst heated at 900 W for 30 s which increased the alpha value as well as a minor shift in selectivity to slightly longer chains (C_5 – C_{11}) is noted.

Table 3.15: Comparison of FTS performance between microwave heated and non-microwave heated catalysts at iso-conversion.

Mn loading (%)	FeMn 10% coppt	FeMn 10% coppt MW
CO conv. %	76.9	
Rate CO (mol/min)	4.7×10^{-4}	4.9×10^{-4}
Rate CO_2 (mol/min)	9.23×10^{-5}	7.34×10^{-5}
Rate FT	3.8×10^{-4}	4.25×10^{-4}
Activity/ µmol/min.g_{Fe}	470.7	498.2
α 1	0.48	0.58
HC distribution (mass %)		
C_1	15.7	14.2
$C_2 – C_4$	50.3	44.5
$C_5 – C_{11}$	20.8	30.3
C_{12} +	13.1	13.0
C_2 olefin % in total$_{HC}$	8.4	7.4
$(C_2 – C_4)^{=}/(C_2 - C_4)^0$ (mass %)	79.3	78.3
CO_2 %	7.8	6.1

Reaction conditions: T = 270 °C, 30 ml/min, P = 10 bar, H_2/CO = 2, 1 g catalyst

Effect of microwave heating on methane formation

The plot of the methane formation during the reaction is shown in Figure 3.33. The microwave heated catalyst has a slightly lower methane selectivity. This may be due to the increase in iron crystallite size after microwave heating which is said to suppress methane formation as well as the increase in manganese at the surface of the catalyst after microwave heating. The larger decrease in methane selectivity when compared to the 5 wt% Mn catalyst may be due to the increased manganese loading and power level and time period of microwave pre-treatment.

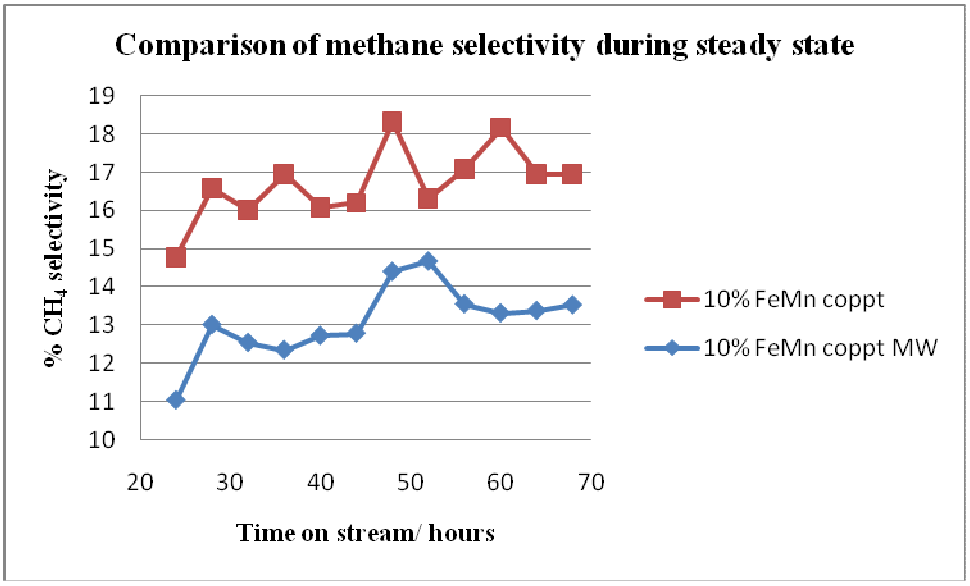


Figure 3.33: Effect of microwave heating on methane selectivity for co-precipitated catalysts with 10 wt% Mn loading.

Olefin formation

The olefin paraffin ratios of the $C_2 – C_5$ and $C_6 – C_{11}$ fraction of the microwave heated and non-microwave heated catalyst are shown in Figures 3.34 and 3.35 respectively. The o/p ratios are compared at iso conversion.

Figure 3.33 shows for the $C_2 – C_5$ hydrocarbons that there is no change in the olefin paraffin ratio after microwave heating. The o/p ratio of the microwave heated catalyst continues to increase as the chain grows whereas there is a drop in o/p ratio from the C_4 to C_5 hydrocarbon for the non-microwave heated catalyst.

In the $C_6 – C_{11}$ fraction however (Figure 3.35) the o/p ratios for the C_6 and C_7 hydrocarbons are much lower than the o/p ratio for C_5. This may be due to loss of sample as the oil was analysed on an offline GC. The microwave heated catalyst shows a slight increase in olefin paraffin ratio for the $C_6 – C_8$ hydrocarbons when compared to the non-microwaved catalyst. This may be due to the microwave heated

catalysts slight increase in selectivity to the $C_5 - C_{11}$ fraction as shown in Table 3.15.

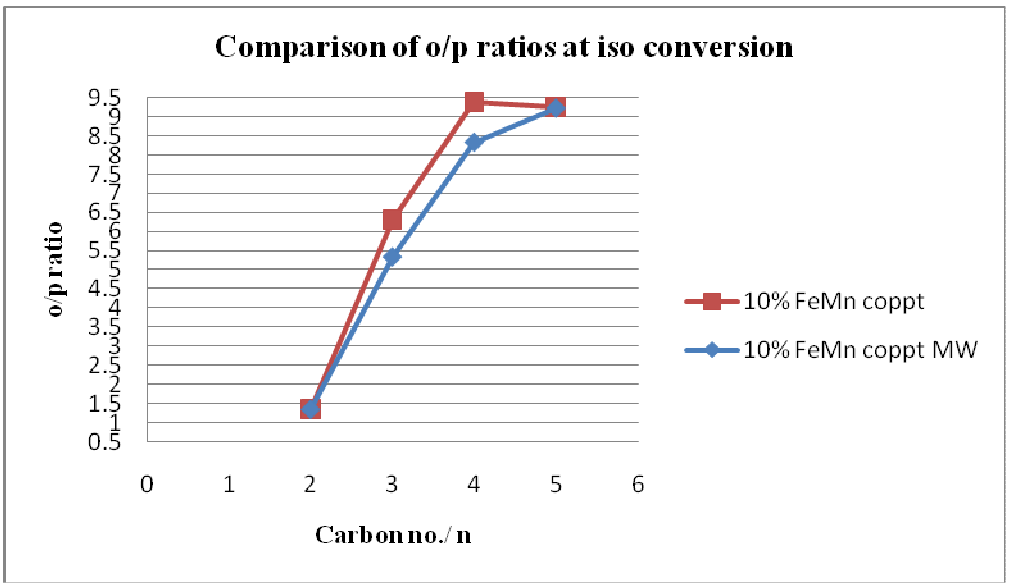


Figure 3.34: Effect of microwave heating on olefin formation in the $C_2 - C_5$ range for co-precipitated catalysts with 10 wt% Mn loading.

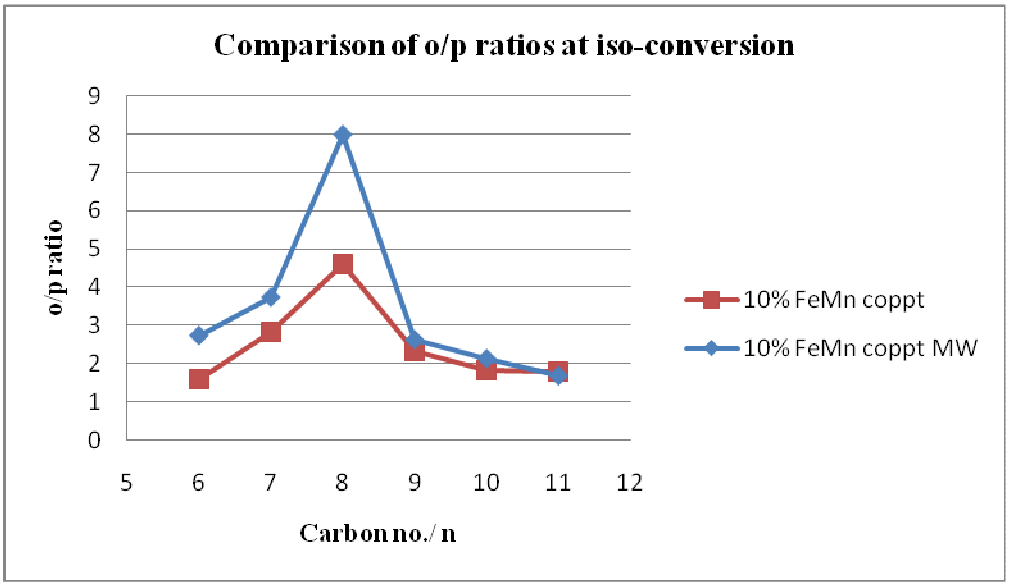


Figure 3.35: Effect of microwave heating on olefin formation in the $C_6 - C_{11}$ range for co-precipitated catalysts with 10 wt% Mn loading.

3.8 Effect of microwave heating on manganese and potassium promoted iron catalysts

The effects of potassium have been studied extensively and the results well documented. It is a well known fact that potassium increases the selectivity of iron catalysts to lighter olefins and heavier molecular weight hydrocarbons. Potassium functions similarly to manganese in that it suppresses hydrogen adsorption and favours CO adsorption. Therefore the effects of promoting the Fe-Mn catalyst with potassium and the effect of microwave heating as well was studied using a 0.1%K/5%Mn/Fe_2O_3 catalyst. The K/Mn/Fe catalysts were microwave heated at 450 W for 10 s.

3.8.1 Characterization of catalysts

Transmission and scanning electron microscopy

The TEM images of the potassium promoted Fe-Mn catalyst before and after microwave heating are shown in Figure 3.36 (a) and (b) respectively.

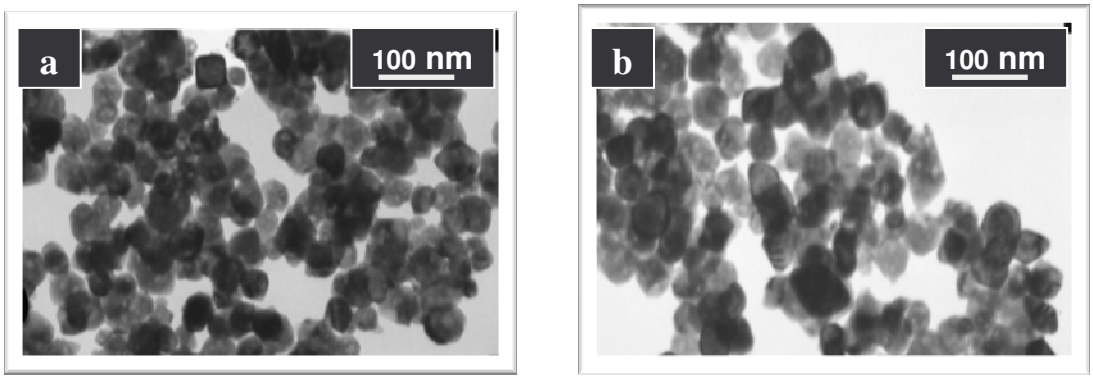


Figure 3.36: TEM images of iron particles in a) before microwave heating and b) after microwave heating.

The TEM images show that the particles appear to have a spherical shape. Compared to the Fe-Mn particles (Figure 3.6a) we notice a large increase in the particle size after potassium promotion typically in the range of 80-100 nm. The particle size

distribution is shown in Figure 3.38. It indicates that the particle size distribution has a wide range. A similar result has been reported for the growth in iron crystallite size after promotion with potassium.[11, 15] This effect has been explained to be due to potassium enhancing agglomeration of the FeOOH precursor thus increasing the crystallite size after calcination at 350 ℃. Tiny lighter spots can be seen on the iron particles and these are thought to be due to the particles becoming more porous. The SEM images do not show any pores on the iron particles but confirm that the morphology of the catalyst particles was spherical (Figure 3.37). The microwave heating had no effect on the size of the particles. This is the same as was found for the Mn/Fe_2O_3 catalysts made without promoters. Other researchers[11] have reported an increase in particle size after microwave heating of catalysts promoted with potassium. It is possible that in this case that the power level and heating time may have been too low to see any effects on the structure of the catalyst.

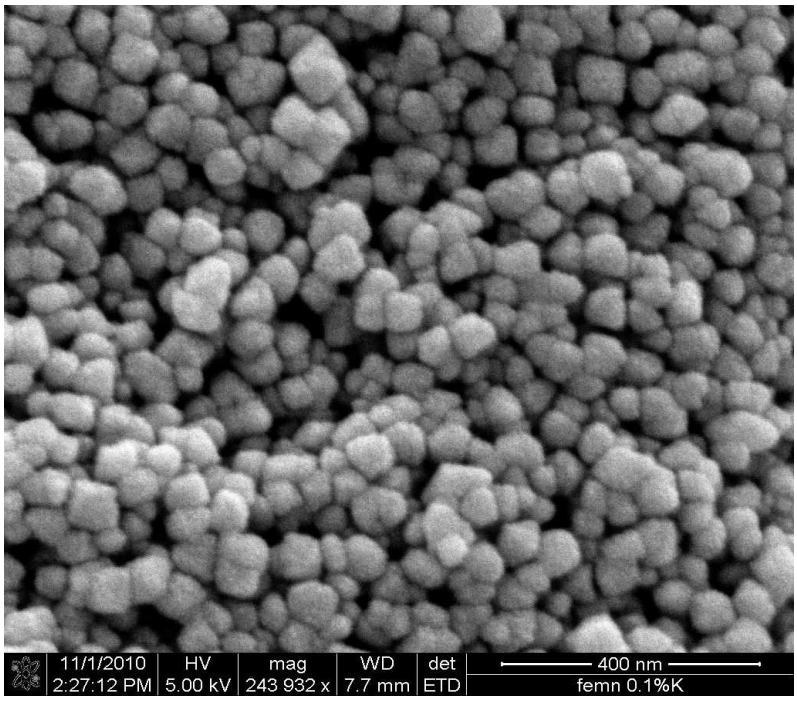


Figure 3.37: SEM image showing morphology of iron particles at 240 000× magnification.

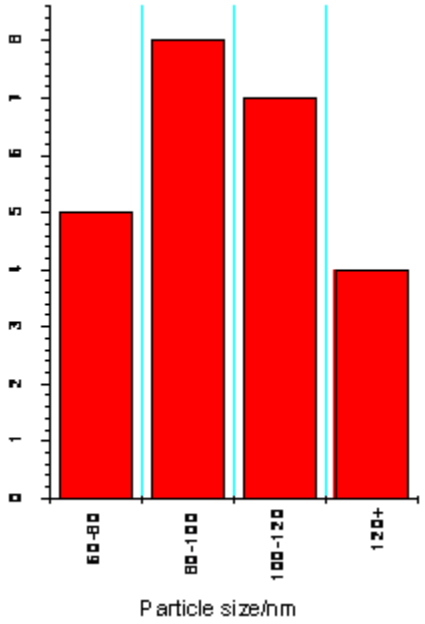


Figure 3.38: Graph showing particle size distribution of Fe-Mn catalyst promoted with potassium.

Surface area measurements (BET)

The surface areas of the Mn/Fe_2O_3 catalyst and Mn/Fe_2O_3 promoted with potassium before and after microwave heating are compared in Table 3.16 below:

Table 3.16: Surface area measurements of Fe-Mn and Fe-Mn-K catalysts

	Surface area (m^2/g)	Pore diameter (nm)	Pore volume (cm^3/g)
5% Mn on Fe	21.5	9.6	0.052
5% Mn on Fe 0.1% K	15	9.0	
5% Mn on Fe 0.1% K MW	14	12.6	0.04

The results indicate that the addition of potassium causes a decrease in the surface area of the catalyst. This is probably due to the the growth of the iron particles which

reduce the surface area of the catalyst. Yang *et al.*[15] and Dry[16] also reported a decrease in surface area of Fe/Mn[15] catalysts after promotion with potassium. After microwave heating there is no change in the surface area of the catalyst.

Powder X-ray diffraction

The powder patterns of the microwave heated and non-microwave heated catalysts are shown in Figure 3.39

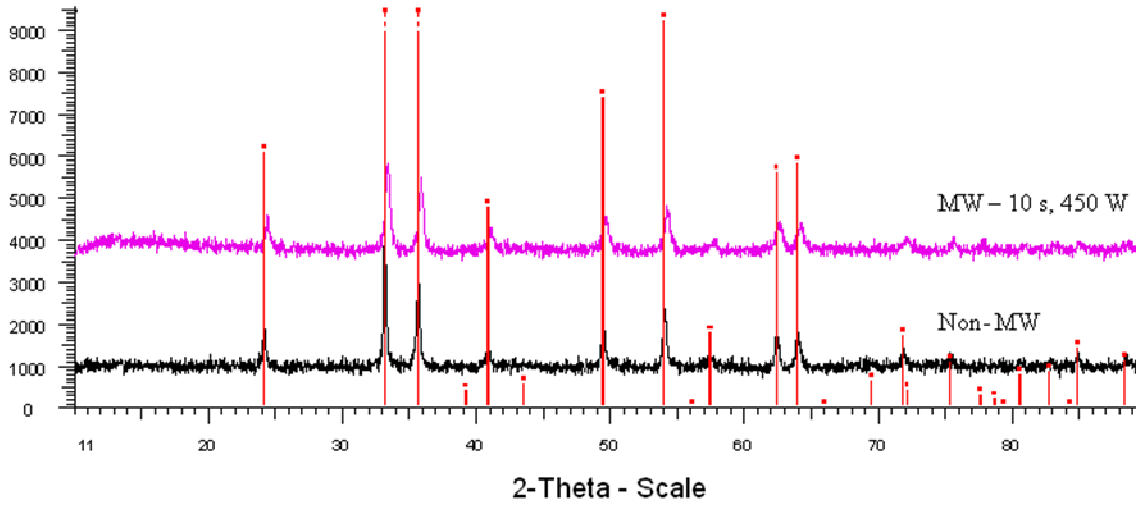


Figure 3.39: Comparison of the 0.1%K/5%Mn/Fe_2O_3 impregnated catalysts before and after microwave heating.

The powder pattern shows that the catalyst is in the haematite iron phase. After promotion with potassium the intensity of the peaks increase and become sharper. This is due to the increase in crystallite size of the iron catalyst. These results correlate well with those from TEM and BET surface area measurements. The Scherrer equation was used to determine the sizes of the iron crystallites. They were determined for the peaks with the 2θ positions shown in table 3.17. Potassium promotion caused a large increase in crystallite size when compared to the catalyst without potassium. Therefore potassium promotes agglomeration of the iron crystallites.[15] The powder pattern for the microwave heated catalyst showed no significant change and therefore it indicates

that microwave heating did not have any effect on the structure of the catalyst. The same result was obtained for the catalyst without potassium promotion.

Table 3.17: Crystallite sizes obtained using the Scherrer equation for the given peak positions.

Peak position/ 2θ	Crystallite size/ nm 5% Mn/Fe_2O_3	Crystallite size/ nm 0.1%K/ 5%Mn/Fe_2O_3	Crystallite size/ nm 0.1%K/ 5%Mn/Fe_2O_3 MW
24.1	32	39	34
33.1	19	52	52
35.6	30	52	53
40.8		78	64

Temperature programmed reduction

The effects of potassium and microwave heating on the reduction behaviour of the catalyst are shown in Figure 3.40.

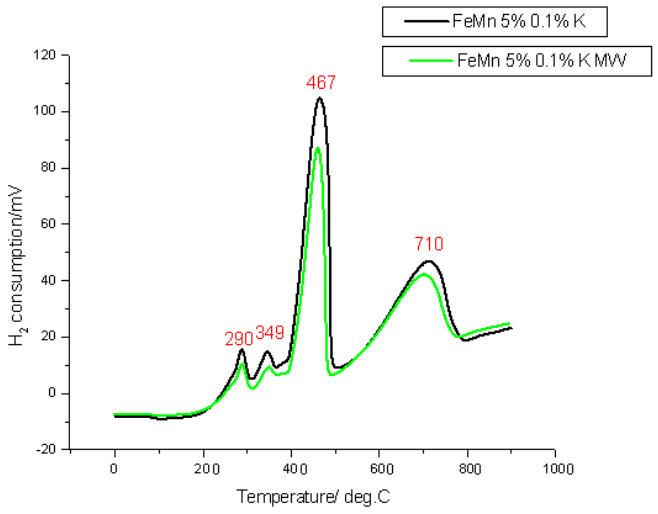


Figure 3.40: TPR profiles of 0.1%K/5%Mn/Fe_2O_3 impregnated catalysts before and after microwave heating.

There is not much difference in the TPR profiles of the potassium promoted and un-promoted catalyst (Figure 3.10) with the reduction of iron occurring at approximately the same temperatures. There is a slight shift of the last reduction peak to a higher temperature. There is also an emergence of a new peak at 290 °C. This may be due the reduction of MnO_2 at the surface of the catalyst. Miller and Moskovits[17] and Rankin and Bartholomew[18] have found that potassium suppresses the reduction of iron. In contrast Jiang *et al*.[19] indicated that potassium promoted the reduction of iron oxide by interacting strongly with the iron species at the surface of the catalyst. Therefore it is possible with a small loading of 0.1 wt% K that the reduction of iron is not severely suppressed because the potassium interacts with the manganese oxide which is concentrated at the surface of the catalyst. The reduction of manganese is actually promoted, hence the observation of the peak emerging at 290 °C.

Comparing the microwave heated catalyst to the non-microwave heated catalyst in Figure 3.40 it is seen that the microwave heating has no effect on the reduction behaviour of the potassium promoted catalyst. Similar results were observed by Linganiso[9] on catalysts promoted with potassium.

Table 3.18: Results showing the temperatures at which reduction occurs.

	Temperature/ °C	Reduction
Peak 1	290	$MnO_2 \rightarrow Mn_2O_3$
Peak 2	349	$Mn_2O_3 \rightarrow MnO$
Peak 3	467	$Fe_2O_3 \rightarrow Fe_3O_4$
Peak 4	710	$Fe_3O_4 \rightarrow Fe$

3.8.2 FT performance of potassium promoted catalysts

Effect of microwave heating on activity of catalysts

The 5 wt% Mn/Fe_2O_3 catalyst promoted with potassium (Figure 3.41) has a lower activity (steady state CO conversion – 60%) than the un-promoted catalyst (steady state CO conversion 70% as shown in figure 3.12). The addition of potassium gives a large increase in the initial activity of the catalyst (90%) after which it drops drastically to approximately 60%. The catalyst also reaches a steady state after a longer period than the un-promoted catalyst. There have been contrasting reports of potassium promotion on the effect on activity of a catalyst. Some have reported that potassium increases activity in FTS reactions[19, 20] while others have reported that it has no effect or decreases activity.[17, 21] What is noticed in this catalyst is that initially potassium increases the activity dramatically. This may be due to the increased basicity at the surface of the catalyst which leads to increased CO adsorption and carburization of the iron catalyst. Many researchers have reported that the iron carbides formed are the active phase for the FTS reaction.[1] However, after a longer time on stream the activity decreases which may be caused by the increased CO adsorption which facilitates carbon deposition and can lead to deactivation of the catalyst.[15] The lower activity for potassium promoted catalysts may also be due to the increase in iron crystallite size.

When comparing the microwave heated and non-microwave heated K containing catalysts a slight decrease in the activity of the microwave heated catalyst is noted. The same result was obtained for the microwave heated unpromoted Mn/Fe_2O_3 catalysts. This trend is observed for all microwave heated catalysts. This occurs for the same reasons as explained earlier for the Fe-Mn microwave heated catalyst. Another trend that is observed for microwave heated catalysts is that microwave heating increases the stability of the catalysts. This can be seen in the microwave heated catalyst (Figure 3.41) which reaches steady state more quickly and is stable with no deactivation after 30 hours on stream. Potassium is also known to increase the stability

of a catalyst.[1] Therefore it is possible that the microwave heating enhanced the potassium's ability to stabilise the catalyst.

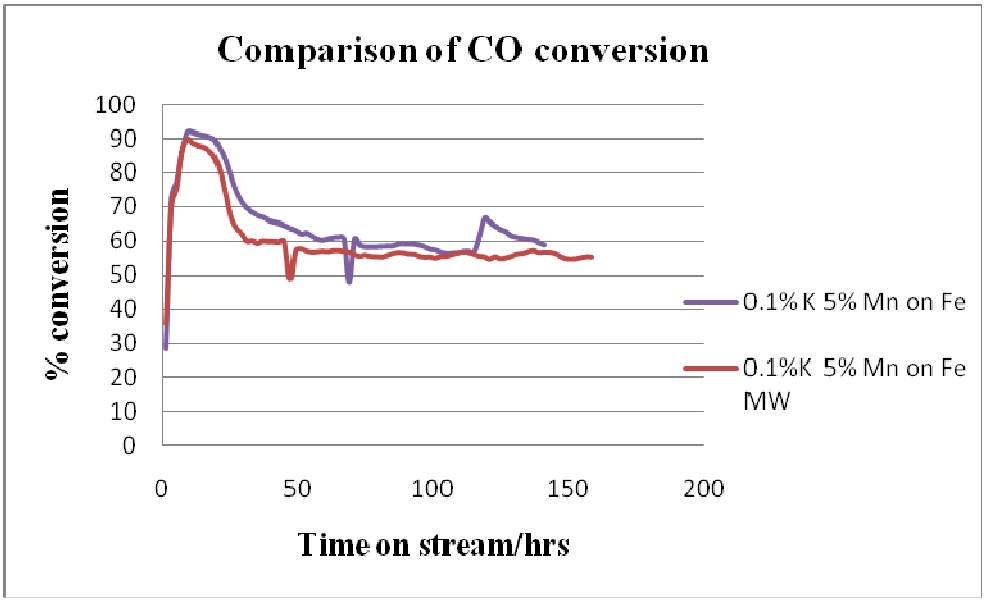


Figure 3.41: Activity of catalysts before and after microwave heating.

Effect of microwave heating on selectivity

The selectivity data for the microwave heated and non-microwave heated catalysts are presented in Table 3.19. It is seen that after microwave heating the alpha value increases to some extent. There is a decrease in methane formation, a lower selectivity to the lighter molecular weight hydrocarbons in particular $C_2 - C_4$ and a large increase in selectivity to the heavier molecular weight hydrocarbons i.e. $C_{12}+$. There is also a slight increase in selectivity to lower olefins. Potassium is known to increase selectivity to heavy hydrocarbons and lower olefins but after microwave heating selectivity increases dramatically. There may be an interaction between the microwave and potassium promoter which further enhances its ability. It is possible that microwave heating causes potassium enrichment at the surface of the catalyst which increases the basicity and facilitates CO dissociation and therefore chain growth. Similar results were observed for the microwave heated Mn/Fe_2O_3 catalysts where the

there was a slight increase in selectivity to longer growing chains as the manganese content and hence the basicity increased.

Table 3.19: Comparison of FTS performance between microwave heated and non-microwave heated Fe-Mn-K catalysts at iso-conversion.

Mn loading (%)	FeMn 5% 0.1% K	FeMn 5% 0.1% K MW
CO conv. %	59.6	56.3
Rate CO (mol/min)	3.5×10^{-4}	3.2×10^{-4}
Rate CO_2 (mol/min)	8.33×10^{-5}	7.2×10^{-5}
Rate FT	2.7×10^{-4}	2.5×10^{-4}
Activity/ µmol/min.g_{Fe}	348.2	318
α 1	0.64	0.68
HC distribution (mass %)		
C_1	12.9	9.6
$C_2 – C_4$	37.9	32.7
$C_5 – C_{11}$	32.6	33.1
C_{12} +	16.6	30.4
C_2 olefin % in total$_{HC}$	5.9	6.0
$(C_2 – C_4)^{=}/(C_2 - C_4)^0$ (mass %)	78.3	80.6
CO_2 %	6.9	6.0

Reaction conditions : T = 270 °C, 30 ml/min, P = 10 bar, H_2/CO = 2, 1 g catalyst

Effect of microwave heating on methane selectivity

The plots of the methane selectivity during the steady state for K/Mn/Fe catalysts are shown in Figure 3.42. As seen in the plots of methane selectivity for the Mn/Fe_2O_3 catalysts, microwave heating leads to the suppression of methane formation. There is approximately a 5% drop in methane formation. This may occur for similar reasons that have been explained for the Mn/Fe_2O_3 catalysts. It is known that manganese and potassium decrease methane selectivity and this property is enhanced after microwave heating. Thus the microwave heating has an effect on the nature of the promoters functioning. The increase in methane selectivity at approximately 50 hours may be due to a change in flow rate as the oil and wax traps were drained.

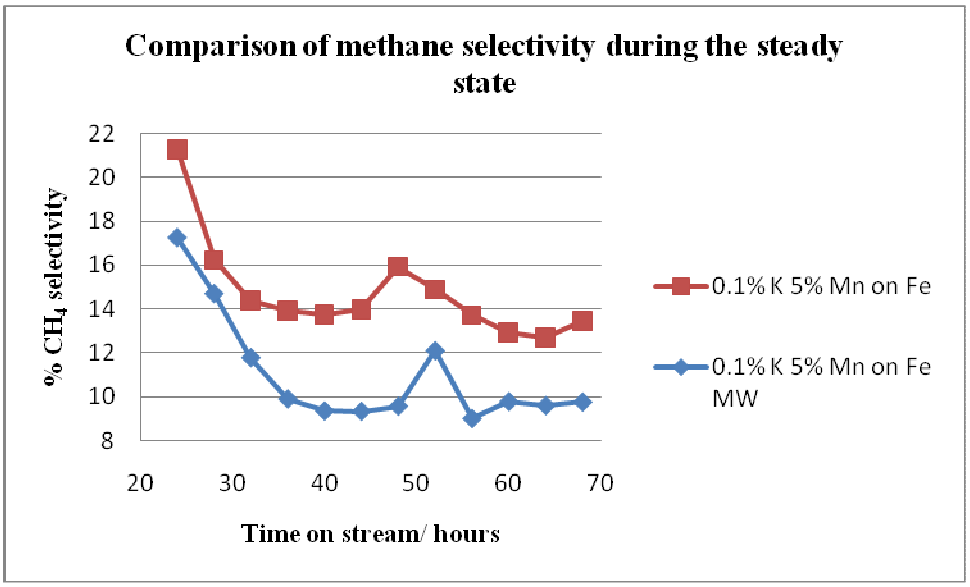


Figure 3.42: Comparison of methane selectivity before and after microwave heating.

Olefin formation

The effect of microwave heating on selectivity to olefins in the $C_2 - C_5$ range is shown in Figure 3.43. it is noted that the microwave heated catalyst has a slightly higher olefin-paraffin ratio for the C_2 hydrocarbon than the non-microwave heated catalyst. The $C_3 - C_5$ hydrocarbons have very similar o/p ratios before and after microwave

heating. Similar results have been found for microwave heated catalysts without potassium as well. Linganiso[11] reported an increase to olefin selectivity after microwave heating at 450 W for 8 s and attributed this to the way in which the iron and potassium interact.

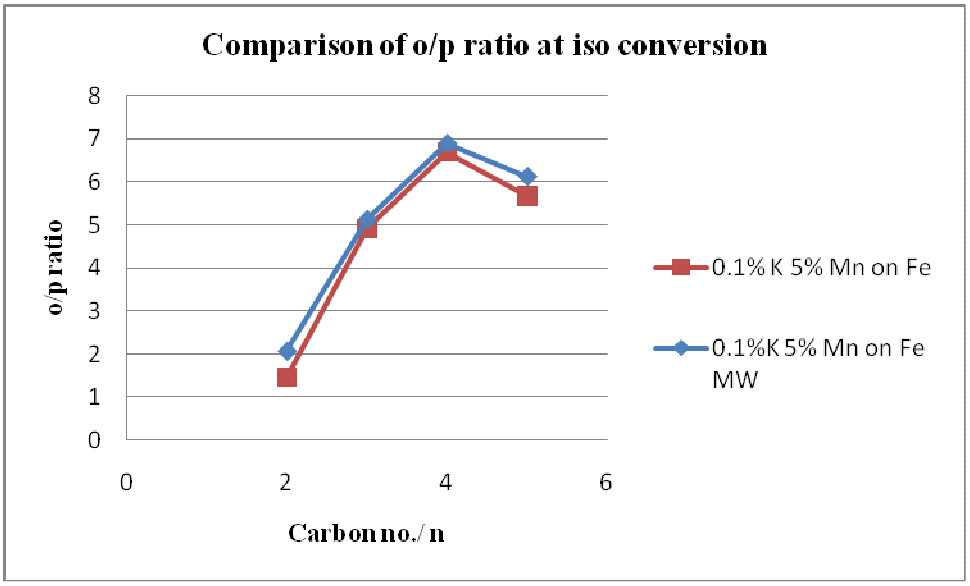


Figure 3.43: Effect of microwave heating on olefin selectivity.

3.9 References

1. H. Wan, B. Wu, C. Zhang, H. Xiang, Y. Li, *Journal of Molecular Catalysis A: Chemical* 283 (2008) 33-42.
2. T. Li, Y. Yang, C. Zhang, Z. Tao, H. Wan, X. An, H. Xiang, Y. Li, *Journal of Natural Gas Chemistry* 16 (2007) 244-250.
3. G. C. Maiti, R. Malessa, U. Lochner, H. Papp, M. Baerns, *Appl. Catal* 16 (1985) 215.
4. D. Das, G. Ravichandran, D. K. Chakrabarty, *Catal. Today* 36 (1997) 285-293.
5. J. Villasenor, P. Reyes, G. Pecchi, *Catal. Today* 76 (2002) 121-131.
6. E. R. Stobbe, B. A. de Boer, J. W. Geus, *Catal. Today* 47 (1999) 161-167.
7. T. Li, Y. Yang, C. Zhang, Z. Tao, H. Wan, X. An, H. Xiang, Y. Li, *Journal of Natural Gas Chemistry* 16(2007) 278-282.
8. T. Li, Y. Yang, C. Zhang, X. An, H. Wan, Z. Tao, H. Xiang, Y. Li, F. Yi, B. Xu, *fuel* 86 (2007) 921-927.
9. B. Tang, G. Wang, L. H. Zhuo, J. Ge, *Nanotechnology* 17(2006) 947-951.
10. J. Abbott, N. J. Clark, B. G. Baker, *Appl. Catal.* 26, (1986), 141.
11. L. Z. Linganiso, Microwave induced solid-state interactions for the synthesis of Fischer-Tropsch catalysts, PhD Thesis, University of the Witwatersrand, Johannesburg, 2008.
12. J. Barrault, C. Forquy, V. Perrichon, *Appl Catal* 16 (1983) 119–125.
13. T. Grzybek, H. Papp, M. Baerns, *Appl. Catal.*, 29 (1987) 335-336.
14. J. Barrault, C. Forquy, J. Menezo, R. Maurel, *Reac. Kinet. Catal. Lett.*15 (1980) 153.
15. Y. Yang, H-W. Xiang, Y-Y. Xu, L. Bai, Y-W. Li, *Appl. Catal.,A* 266 (2004) 181-194.
16. M. E. Dry, G. J. Oosthuizen, *J. Catal.* 11 (1968) 18.
17. D. G. Miller, M. Moskovits, *J. Phys. Chem.* 92 (1988) 6081-6085.
18. J. L. Rankin, C. H. Bartholomew, *J. Catal.* 100 (1986) 533.
19. D. B. Bukur, D. S. Mukesh, A. Patal, *Ind. Eng. Chem. Res.*29 (1990) 194.

20. R. B. Anderson, B. Sekigman, J. F. Schulz, M. A. Elliot, *Ind. Eng. Chem.*44 (1952) 391.
21. R. A. Dictor, A. T. Bell, *J. Catal.*97 (1986) 121.

4. Conclusions

The structure of a catalyst is related to its function. The main objectives of this study were to investigate the effect of preparation method on the physicochemical properties of a series of Mn/Fe catalysts and to determine whether microwave heating would enhance catalyst performance in terms of activity and selectivity.

The results obtained in this study showed that the Mn that was loaded onto Fe_2O_3 formed different phases of manganese oxides which were enriched at the surface of the Fe_2O_3 catalyst. This caused a decrease in the surface area of the catalyst as the manganese loading increased. The manganese present at the surface of the catalyst suppressed the reduction of iron as the manganese loading increased. The FT performance of the impregnated catalysts 5, 10 and 20 wt% Mn were suprisingly similar. Even with an increase in manganese loading up to 20 wt% Mn, the activity of the Fe_2O_3 catalyst remained the same as that observed with a 5 wt% loading of Mn. This suggested that the manganese may promote the activity of the catalyst by enhancing the activity of each Fe site. Minimal changes in selectivity were seen with the increase in manganese content.

The co-precipitated catalysts increased in surface area with an increase in manganese loading. This suggested that Mn acted as a structural promoter. It was suggested that this resulted in a decrease in iron crystallite size thereby dispersing the iron. This was confirmed by TPR results which showed the rate of reduction of Fe_2O_3 increased (peaks get sharper) as the manganese content increased for catalysts calcined at 350 °C. After calcination at 650 °C the manganese suppressed the reduction of iron. This was due to the stronger Fe-Mn interaction as a new Fe-Mn solid solution was formed. The FT performance of the Mn/Fe catalyst showed that the activity increased with Mn loading up to 10 wt% but then decreased with Mn loadings of 20 wt% and 50 wt% Mn. Therefore 10 wt% Mn may be the appropriate amount to increase activity. The 10 wt% Mn/Fe catalyst also showed the best selectivity to lower molecular weight hydrocarbons and olefins ($C_2 - C_4$). However, manganese loadings greater than 10%

led to a slight increase in selectivity to heavier molecular weight hydrocarbons in particular $C_5 – C_{11}$ products.

The study on the effect of microwave heating of the impregnated Mn/Fe catalysts showed that the microwave heating did not have any effect on the structure of the catalysts studied. The activities and selectivities of the microwaved and non-microwaved catalyst were very similar. A minor shift in selectivity to lower molecular weight hydrocarbons, in particular the C_2 olefin can be seen. It is possible that microwave heating at 450 W for 10 s may have been too low a power setting and period of time to have had any effect on the catalyst.

The co-precipitated Mn/Fe catalyst microwave heated at 900 W for 30 s showed some change to the catalyst structure. An increase in particle size after microwave heating was noted. This is due to the agglomeration of iron particles. The increase in particle size of the catalyst led to a decrease in surface area. TPSR results showed that CO adsorption is stronger in the microwave heated catalyst. This may be due to the microwave heating causing migration of the Mn to the surface of the catalyst thereby increasing the basicity and leading to more CO adsorption. The FT performance of the catalysts showed a decrease in activity after microwave heating although it appeared to be slightly more stable. This may also be due to the increase in particle size of the catalyst as well as enrichment of manganese at the surface of the catalyst. The microwave heated catalyst showed a slight increase in selectivity towards heavier hydrocarbons and a minor decrease in selectivity towards $C_2 – C_4$ hydrocarbons. Therefore it seems that microwave heating at a higher power level and for a longer period of time leads to more significant changes in the physicochemical properties of a catalyst and its activity and selectivity.

Microwave heating of 0.1 wt% loaded potssium promoted Mn/Fe_2O_3 catalysts showed no significant changes to the structure of the catalyst. The activity of the microwave heated catalyst was slightly lower than the non-microwave heated catalyst but a slight increase to heavier molecular weight hydrocarbons was noted. This may be due to the

enhancement of the manganese and potassium promoters which are known to increase selectivity trowards heavier hydrocarbons.

Future Work

- It will be necessary to study the effect of microwave heating on the activity and stability of the catalysts for periods greater than 150+ hours on stream.

- To study the effect of the microwave heating power level and period of time used to pre-treat the catalyst on the structure and activity and selectivity of the catalysts.

- To carry out an XPS study to confirm the amounts of manganese and potassium present at the surface of the catalysts both before and after microwave heating.

- Further TPSR studies to investigate the CO adsorption/desorption on the Mn/Fe catalyst before and after microwave heating.